Fluctuation Relations for Stochastic Systems far from Equilibrium

Sven Dorosz

Dissertation submitted to the Faculty of the
Virginia Polytechnic Institute and State University
in partial fulfillment of the requirements for the degree of

Doctor of Philosophy
in
Physics

Michel J. Pleimling, Chair
Giti Khodaparast
Tatsu Takeuchi
Uwe C. Täuber

March 26, 2010
Blacksburg, Virginia

Keywords: Fluctuation Relations, Entropy Production, Large Deviation Functions

Fluctuation Relations for Stochastic Systems far from Equilibrium

Sven Dorosz

Fluctuations are of great importance in systems of small length and energy scales. Measuring the pulling of single molecules or the stationary flow of microspheres dragged through a viscous media enables the direct analysis of work and entropy distributions. These probability distributions are the result of a large number of repetitions of the same experiment. Due to the small scale of these experiments, the outcome can vary significantly from one realization to the next. Strong theoretical predictions exist, collectively called Fluctuation Theorems, that restrict the shape of these distributions due to an underlying time reversal symmetry of the microscopic dynamics. Fluctuation Theorems are the strongest existing statements on the entropy production of systems that are out of equilibrium.
Being the most important ingredient for the Fluctuation Theorems, the probability distribution of the entropy change is itself of great interest. Using numerically exact methods we characterize entropy distributions for various stochastic reaction-diffusion systems that present different properties in their underlying dynamics. We investigate these systems in their steady states and in cases where time dependent forces act on them. This study allows us to clarify the connection between the microscopic rules and the resulting entropy production. The present work also adds to the discussion of the steady state properties of stationary probabilities and discusses a non-equilibrium current amplitude that allows us to quantify the distance from equilibrium. The presented results are part of a greater endeavor to find common rules that will eventually lead to a general understanding of non-equilibrium systems.

This work is supported by the PHD 2010 scholarship program of the Virginia Tech Graduate School and by the NSF Grant DMR-0904999.

Dedication

To my parents Helga and Peter Dorosz

Acknowledgments

Let me take this opportunity to thank my advisor Michel Pleimling and my committee members Giti Khodaparast, Tatsu Takeuchi, and Uwe Täuber. The last four years were a great experience for my forthcoming as a researcher. Thank you for your ongoing support and encouragement that allowed me to partially continue the topic of my Master thesis [41]. Through Michel I had the chance to meet a great number of scientists in my field. He sent me to participate in various conferences, summer schools and workshops, as for example the Trimester at the Institut Henri Poincare in Paris in the fall of 2007, the international workshop at the MPI in Dresden in spring 2009 and the summer school in Boulder, CO in the summer of 2009. Michel, you are a great advisor that always treated me as a team mate rather than a student. I am looking forward to keep working with you in the years to come.
My great friends Sayak Mukherjee, Thierry Platini and Kevin Pond that are an important part in my life here in Blacksburg. Especially Sayak was the person to discuss physics and to spend time outside of the office for the last 4 years. I am very proud of the work that was done in collaboration with Thierry and Sayak. You three were also important to keep me focused until the end of my PhD.
I would also like to thank George Daquila, Marc Palm, and Qian He. It was a great time we had here in Blacksburg working together. I wish you all the best for the future. I enjoyed my life in the US and I made a lot of friends. I want to thank Julia Bartens, Franziska Hinkelmann, Christian Wernz, and Amanda Rohm-Daquila as well as Binh Nguyen, Kamal Idrisi, Thananart Klongcheongsan, and Abhishek Mukhopadhyay. The Stammtisch and the Doppelkopf nights were definitely fun. I also enjoyed the many events that were organized through the Graduate School.
My parents are outstanding. Everything I achieved so far was possible because of you. I am very lucky to have you.

Contents

List of Figures

List of Tables

Chapter 1

Introduction

The understanding of systems far from equilibrium is one of the most important challenges of our time. Phenomena on very different length and energy scales exhibit constant change, from biology and chemistry to geosciences and meteorology, see figure 1.1. Understanding these systems and their time evolution far from equilibrium has yet to be fully accomplished. Our experience tells us that a system not exposed to external forces will ultimately relax to its state of thermodynamic equilibrium. A cup of water, for example, will adapt to the surrounding room temperature after a certain amount of time. A robust theory based on a statistical description exists today that can successfully explain systems in their equilibrium state. It enables us to characterize systems with only a handful of parameters, mainly temperature and pressure. The theory allows us in principle to calculate any system in equilibrium. Now that research of equilibrium systems has reached a mature state we can use it to go beyond its limitations.

Despite its usefulness, equilibrium statistical mechanics quickly breaks down if external forces act upon the system. Most natural systems behave this way. In fact, life can only exist far from equilibrium. Living organisms will not reach an equilibrium state because there is a steady energy conversion of ATP to ADP that keeps the cellular processes out of equilibrium. Only in the organism's death will the equilibrium state be achieved.

Properties of materials change drastically out of equilibrium. A simple illustration would be a metallic rod that is connected at its ends to two different temperatures. After the system reached a steady state, we observe a constant heat flux through the system. Even though in this case the current of energy through the system is homogeneous and time independent, we cannot apply the theory of systems in equilibrium. We call this state a non-equilibrium steady state. Extreme conditions produce materials with new and interesting properties. Diamonds and impurities in crystals are interesting examples. Another class of materials are glasses. Once quickly cooled from a melting to a solid phase, the supercooled liquid will relax so slowly that it will never reach equilibrium. The examples given above are very diverse. The dynamics out of equilibrium can reveal a very rich and complex behavior, beautiful patterns, and structural self organization that are only possible far from equilibrium.

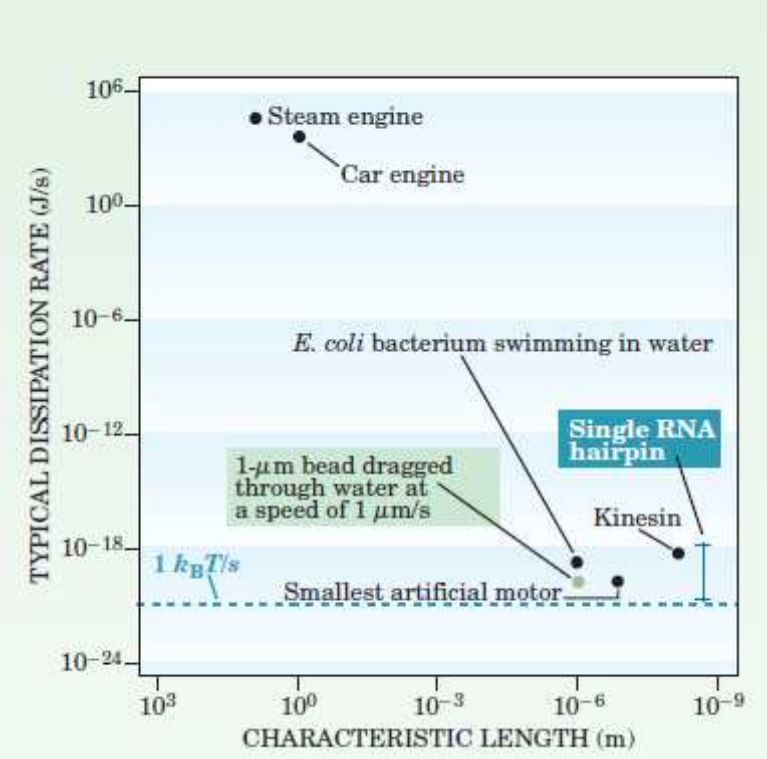

Figure 1.1: Thermodynamic systems of different length and energy scales. The focus of the work is set to small length and energy scales. Reprinted with permission from C. Bustamante, J. Liphardt, and F. Ritort. The nonequilibrium thermodynamics of small systems. Physics Today, 58(7):4348, 2005. Copyright 2005, American Institute of Physics.

A general theory that could explain the behavior of matter far from equilibrium is therefore essential. If we were able to manipulate matter in a predictive way far from equilibrium we could optimize a variety of processes in engineering. Harder, more flexible or completely new materials could be designed. Even conversion and storage of energy could be made more efficient. Therefore, it is crucial to advance our knowledge further in this field of research. Much progress has been made in recent years but it is still patch work trailing a general theory [115, 156, 95].

In the last twenty years, important advances were made in the understanding of non-equilibrium processes through the study of work and entropy relations. These mathematical exact results were collectively labeled *Fluctuation Theorems*. We will exploit different stochastic systems that we can treat with numerically exact methods in order to analyze their dynamics far from equilibrium and discuss their change in entropy. Either systems are in a steady state or are forced out of a steady state by time dependent system parameters. The microscopic rules of each system permits us to point out important features and relate them to abstract properties of their configuration space. This allows us to investigate the stationary states and the transient behavior on an abstract level and to draw general con-

clusions that are adding to our understanding of systems far from equilibrium.
The thesis is organized in the following way. In chapter 2 we are going to introduce the most prominent Fluctuation Relations and focus on their application in experiments. In chapter 3 we describe the mathematical description of the stochastic dynamics and define equilibrium systems and non-equilibrium systems. Chapter 3 also covers the definition of the different stochastic models and discusses different aspects in their individual dynamics, important for the study of entropy production that will follow. Stationary properties that characterize the stationary states are presented and discussed. In chapter 4 we start with the discussion of single steady states. We exploit exact results to characterize the distributions of entropy change in time for non-equilibrium systems. This will be done for short measurement times as well as in the long time limit. These two regimes will give us different information about our systems. In the chapter 5 we investigate transient properties of our systems. With a given rate of change the systems are driven away from their stationary state and we analyze the immediate response of the systems. This will lead to new results in the extreme case of irreversible dynamics that can be realized in our systems. In the last chapter we give our conclusion.

Chapter 2

Theoretical Background

This chapter presents the relevant fluctuation relations. We start out with the demonstrations of the Jarzynski relation based on Hamiltonian dynamics [77]. In the second part we present the derivation of the Crooks relation [29]. The second part ends with the discussion of the experimental results by Colin et al. [27] that verified the Crooks as well as the Jarzynski relations. The third section discusses the steady state fluctuation relation for stochastic dynamics that was presented by Lebowitz and Spohn [96]. We finish the discussion of established fluctuation relations with the Hatano Sasa relation for systems driven out of a non-equilibrium steady state [66] and the Seifert entropy relation [139] as well as its experimental verification by Tietz et al. [133].
The first reported symmetry of the entropy production was by Evans et al. [54] in 1993. In this work, computer simulations were performed for a two dimensional sheared liquid and the entropy production was calculated over small time intervals while the system was in its steady state. Interestingly, with small probabilities, negative entropy changes were detected on these time scales. By repeating this measurement a large number of times, they were able to produce and analyze a histogram of entropy change. The surprising feature was a symmetry that related the probability of an increase of the entropy ($P(\Delta S)$) to the probability of a decrease of the entropy ($P(-\Delta S)$), by a simple exponential

$$\frac{P(\Delta S)}{P(-\Delta S)} = e^{\Delta S}, \tag{2.1}$$

where we set $k_B = 1$. Relation (2.1) shows that the probability to see a trajectories of the system with negative entropy change decreases exponentially fast. This result was extended in [14, 55, 57] into a theory for dynamical systems. For dynamical systems the SRB measure [125, 126, 127], named after Sinai, Ruelle, and Bowen, represents the steady state of the system in phase space. It was possible to prove the fluctuation symmetry (2.1) as a consequence of the SRB measure if one assumes the chaotic hypothesis [57] which is the analog to the ergodic hypothesis for equilibrium systems. This relation is asymptotically exact for large times compared to the microscopic timescales of the system.

Motivated by these results for dynamical systems, Kurchan demonstrated the fluctuation relation for a stochastic system in 1998 [90]. For a stochastic system, the chaotic hypothesis is not a requirement due to the coupling of the system to the environment which introduces randomness. As a result, the trajectories cover the entire phase space and the fluctuation symmetry holds. A more general result was established by Lebowitz and Spohn for Markov systems in a single stationary non-equilibrium state [96]. In addition to the asymptotic symmetry relation (2.1), the Lebowitz Spohn fluctuation symmetry is exact for stochastic systems for arbitrary times. For an overview of different aspects of fluctuation relations, see [3, 17, 64, 75, 101, 122, 142, 158]. Following the theoretical predictions experimental verifications of steady state fluctuation relations [7, 11, 19, 26, 134, 146, 153, 133, 159] and theoretical extension and applications to a variety of systems [4, 5, 6, 23, 24, 22, 43, 63, 58, 74, 86, 130, 129, 137, 138, 139, 140, 142, 145] were published.
A different fluctuation relation was established by Jarzynski [77, 76]. Here a system initially in equilibrium is forced out of stationarity by an external mechanical force in a finite time. If the experiment, i.e. same initial equilibrium state and same time dependent force, is repeated a large number of times, information about the free energy difference of the initial and final states can be obtained by analyzing the histogram of the mechanical work. A variety of different experiments [27, 47, 85] confirmed the theoretical predictions. The Jarzynski relation is stated as

$$\langle e^{-\beta W} \rangle = e^{-\beta \Delta F} \quad \forall \lambda(t) \ , \tag{2.2}$$

where $\lambda(t)$ is a time varying parameter of the system. The average is calculated with respect to the probability distribution of mechanical work and the free energy difference ΔF is calculated between the initial and final states of the system. Following Jarzynski's result, Crooks discovered a more general statement that underlies Jarzynski's result [29, 30, 31, 100]. This statement is based on time reversal symmetry of the microscopic dynamics. The trajectory in phase space during the time dependent process has a corresponding reversed trajectory that results from time inverting the external process. The comparison of a given trajectory and its time reversed trajectory allows the calculation of increase in entropy during the process, see [80, 81, 92] for an overview.
Both results were first proven for Hamiltonian dynamics, and have since been extended to different classical as well as quantum systems [2, 8, 18, 25, 53, 91, 109] and illustrated explicitly for various models [32, 43, 52, 84, 107, 152, 157]. The Crooks relation was experimentally verified in [9, 47, 98].
For systems that are initially in a non-equilibrium steady state, more general results exist, namely the Hatano Sasa relation [66] and the Seifert entropy relation [139, 142]. Trepagnier et al. performed the first experimental verification of the Hatano Sasa relation [155] by analyzing a trapped bead that is dragged through a liquid with varying velocity. The Hatano-Sasa relation as well as the Seifert entropy relation reduce to the Jarzynski relation in the case of detailed balance, see [64, 80, 142].

2.1 Jarzynski Relation

The Jarzynski relation is a mathematically exact statement about the probability distribution of applied mechanical work on a system during a non-equilibrium process that allows access to equilibrium properties of the system under consideration. As already mentioned in the previous section, the Jarzynski relation formulated in [77] received great attention. Since then, the relation was demonstrated for different dynamics including Hamiltonian dynamics, Master equations, and Langevin dynamics for classical systems [21, 64, 100, 116]. The Jarzynski relation is stated as follows:
The system S is initially in an equilibrium state described by an inverse temperature β

$$P_s(C) \propto e^{-\beta H(C,\lambda)}, \tag{2.3}$$

where $P_s(C)$ is the probability for the system to be in state C described by the Hamiltonian H. During a finite time interval τ a parameter of the system λ is varied from an initial to a final value at an arbitrary rate. The external parameter λ defines the non-equilibrium process. During the time interval τ, work W is performed on the system due to the change in λ.

Now, the work W must be defined. Jarzynski himself uses the following illustration,

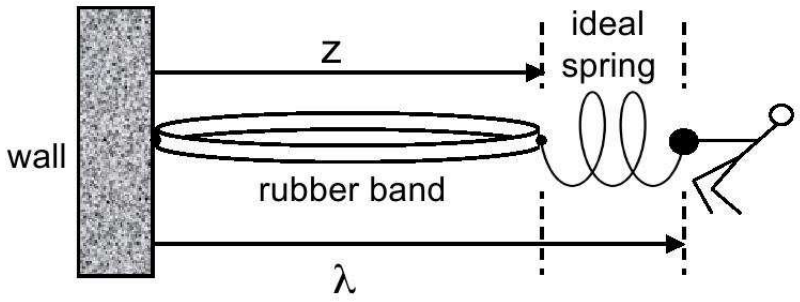

Figure 2.1: Illustration of the definition of work that enters the Jarzynski relation. Reprinted with permission from C. Jarzynski, Nonequilibrium work relations, Boulder Lecture Notes-Nonequilibrium Statistical Mechanics: Fundamental Problems and Applications, 2009.

see figure 2.1. At fixed parameter value λ, the rubber band is in equilibrium with the environment at inverse temperature β. If we change the parameter in a finite time interval τ from a position λ_A to a final value λ_B we perform work on the system. In order to calculate the work one needs to define the system of interest. Considering only the rubber band, the work performed on the rubber band is the force acting on the rubber band times its displacement, given by

$$W_M = \int F_{Spring} dz, \tag{2.4}$$

but if we include the change in the spring as well, we consider the force to be a result of the change in λ and the force on the rubber band is not directly controlled from the outside,

$$W = \int F_{Spring} d\lambda. \tag{2.5}$$

It is the second definition that allows us to access the free energy difference ΔF. The first definition leads to an earlier result derived by Bochkov and Kuzovlev [13, 12],

$$\langle e^{-\beta W_M} \rangle = 1. \tag{2.6}$$

This relation restricts the possible shapes of the distribution but does not relate to equilibrium quantities. For a more thorough discussion of the two work statements, we refer to [71, 142].

The Jarzynski relation as demonstrated here comes from [77] and is based on Hamiltonian dynamics. Consider a system S described by a Hamiltonian $H(\lambda)$. The external parameter λ is varied in time during a time interval τ. During this process, the amount of work recorded is defined by

$$W = \int_0^\tau dt \frac{\partial \lambda}{\partial t} \frac{\partial H}{\partial \lambda}. \tag{2.7}$$

Here W depends on the initial configuration and its trajectory. If the same process is repeated a large number of times, starting in the same initial equilibrium state, one obtains the probability distribution of work done on the system. The distribution depends strongly on the way the parameter λ is varied during the process. Independently of how the parameter is varied during the process, the average value of the exponentiated work is a constant for the same initial and final values of λ,

$$\langle e^{-\beta W} \rangle = e^{-\beta \Delta F} \quad \forall \lambda(t). \tag{2.8}$$

The free energy difference, $\Delta F = F(\lambda_f) - F(\lambda_i)$, of the system is considered between the initial and final values of λ and the average is calculated using the distribution of possible work values W. Therefore the Jarzynski relation permits the measurement of equilibrium properties of the system by performing a non-equilibrium process. Measuring equilibrium properties was, up to this point, only possible if the system was assumed to be in intermediate equilibrium states throughout the process. This constraint is due to the second law of thermodynamics,

$$W \geq \Delta F, \tag{2.9}$$

with equality only in the case of an infinitely slow change in λ. For this reason the Jarzynski relation is an important alternative for measurements of free energy differences.

We are going to discuss the proof of the Jarzynski relation and its implications. Starting from an initial equilibrium distribution, we calculate the average value $\langle e^{-\beta W} \rangle$ for this process. The average is taken over all possible trajectories $\int dX$ in phase space. In addition it is assumed that the system is weakly coupled to the temperature reservoir, thus that over the

time period τ no heat can be exchanged with the environment. As a result the work done on the system is equal to the change in internal energy,

$$W = \Delta H. \tag{2.10}$$

With these assumptions the proof of the Jarzynski relation is as follows:

$$\begin{aligned} \langle e^{-\beta W} \rangle &= \int dX \; P_s(x_0, \lambda_0) e^{-\beta W} \\ &= \int dx_0 \frac{e^{-\beta H(x_0,\lambda_0)}}{Z_{\lambda_0}} e^{-\beta(H(x_\tau,\lambda_\tau)-H(x_0,\lambda_0))} \\ &= \frac{1}{Z_{\lambda_0}} \int dx_0 e^{-\beta H(x_\tau,\lambda_\tau)} = \frac{Z_{\lambda_\tau}}{Z_{\lambda_0}} = e^{-\beta \Delta F}. \end{aligned} \tag{2.11}$$

If we use Jensen's inequality [83] because ΔF is a convex function, the exact result includes the second principle of thermodynamics,

$$\langle W \rangle \geq \Delta F.$$

Since the average value of the exponentiated work observable has to be computed, it is important to have a detailed sampling of rare events. When calculating the average value of $e^{-\beta W}$, rare events with negative work values are amplified and carry important information to the average value. A large sampling size is therefore necessary to obtain the rare events of the work probability distribution in experiments and in computer simulations. Important algorithms were developed to overcome this obstacle [10, 59, 61, 73, 111, 144, 166]. Since the Jarzynski relation is a statement about the average value of the exponentiated work, it is called an integral fluctuation theorem.

2.2 Crooks Fluctuation Theorem

The Crooks Fluctuation Theorem is a statement about an underlying symmetry of the Jarzynski relation [29, 78], based on time reversal symmetry. Imagine a system S initially in equilibrium with a temperature reservoir described by an inverse temperature β. The system parameter λ is varied in time according to the sequence

$$\lambda_F(t) = \{\lambda_0, \lambda_1, ..., \lambda_{M-1}, \lambda_M\}.$$

This process is called the forward process. The probability distribution $P_F(W)$ is obtained for the total amount of work during the time interval τ. Now imagine the system being in equilibrium at the final value of $\lambda = \lambda_M$ at the same inverse temperature β. The reversed process is defined by the time inverted sequence of the parameter λ ending at λ_0. For the

reversed process we obtain a second distribution of work, $P_R(W)$. With these distributions the Crooks fluctuation relation states

$$P_F(W) \;=\; P_R(-W)e^{\beta(W-\Delta F)}. \tag{2.12}$$

The free energy difference ΔF is obtained by comparing the distributions of the forward and time reversed process of a non-equilibrium process. We denote with X a trajectory in configuration space and with $X^\dagger$ its time reversed trajectory. $P_s(x,\lambda)$ is the stationary probability for the system to be in configuration x while the external parameter is at a value λ. For the proof of the Crooks relation we note, assuming the process is Markovian that,

$$P_F(X) \;=\; P_s(x_0,\lambda_0)\prod_{i=0}^{M-1}\omega(x_i\to x_{i+1},\lambda_{i+1}) \tag{2.13}$$

where $\omega(x_i\to x_{i+1},\lambda_{i+1})$ is the transition rate to jump from configuration C_i to configuration C_j while the external parameter is at value λ_{i+1}. It follows that we can rewrite the forward trajectory as

$$\begin{aligned} P_F(X) &= P_R(X^\dagger)\left[\frac{P_s(x_0,\lambda_0)}{P_s(x_\tau,\lambda_\tau)}\prod_{i=0}^{M-1}\frac{\omega(x_i\to x_{i+1},\lambda_{i+1})}{\omega(x_{i+1}\to x_i,\lambda_{i+1})}\right] \\ &= P_R(X^\dagger)\prod_{i=0}^{M-1}\frac{P_s(x_i,\lambda_i)}{P_s(x_i,\lambda_{i+1})}. \end{aligned} \tag{2.14}$$

In the last equality we are exploiting the fact that the system fulfills detailed balance,

$$\frac{\omega(x_i\to x_{i+1},\lambda_i)}{\omega(x_{i+1}\to x_i,\lambda_i)} = \frac{P_s(x_{i+1},\lambda_i)}{P_s(x_i,\lambda_i)},$$

for all values of the parameter λ. This allows us to rewrite the ratio of transition rates as a ratio of stationary probabilities. If we further use the Boltzmann distribution for the stationary probabilities,

$$\ln P_s(x,\lambda) = -\beta(H(x,\lambda)-F(\lambda)), \tag{2.15}$$

we obtain Jarzynski's definition of work during the discrete time process,

$$\prod_{i=0}^{M-1}\frac{P_s(x_i,\lambda_i)}{P_s(x_i,\lambda_{i+1})} = \exp\left(\beta\sum_i\left[H(x_i,\lambda_{i+1})-(H(x_i,\lambda_i)\right]-\beta\Delta F(\lambda)\right) = e^{\beta[W_F(X)-\Delta F]}.$$

The expression,

$$P_F(X) = P_R(X^\dagger)e^{\beta[W_F(X)-\Delta F]} \tag{2.16}$$

represents the symmetry on the level of single trajectories. In order to obtain the Crooks relation on the level of work values, we need to integrate expression (2.16) over all possible trajectories with a constraint on the value W:

$$\begin{aligned} P_F(W) &= \int dX P_F(X)\delta(W_F(X) - W) \\ &= \int dX P_R(X^\dagger)\delta(W_F(X) - W)e^{\beta[W_F(X)-\Delta F]} \\ &= \int dX^\dagger P_R(X^\dagger)\delta(W_R(X^\dagger) + W)e^{-\beta[W_R(X^\dagger)+\Delta F]} \\ &= P_R(-W)e^{\beta(W-\Delta F)}. \end{aligned} \tag{2.17}$$

If we integrate the Crooks relation (2.17) over all possible values of W, the Jarzynski relation is recovered:

$$\begin{aligned} \int dW P_F(W) &= \int dW P_R(-W)e^{\beta(W-\Delta F)} \\ \int dW e^{-\beta W} P_F(W) &= e^{-\beta\Delta F}\int dW P_R(-W) \\ \left\langle e^{-\beta W}\right\rangle &= e^{-\beta\Delta F}\,. \end{aligned} \tag{2.18}$$

The power of the non-equilibrium work relations is best illustrated by a recent experiment of mechanically pulling MRNA molecules by Collin et al. [27]. On the level of single MRNA (Messenger RNA) molecules, the free energy landscape is dominated by two configurations, the folded state and the unfolded state. The manipulation of a single molecule is realized by chemically attaching the molecule between two plastic beads. Holding one of the plastic beads fixed with the help of a micro pipette, the second plastic bead is displaced with the help of a laser tweezer. An induced dipole moment pulls the plastic bead into the point of strongest gradient of light intensity of the laser. For more information on how to realize single molecule experiments, see [87, 124]. Changing the distance between the micro pipette and the center of the laser tweezer, the molecule experiences different amounts of tension. At a sufficiently large tension the molecule spontaneously unfolds, resulting in a drop in the tension on the molecule. In the reversed process the distance between the two beads is reduced, allowing the molecule to refold. Since this cyclic process shows hysteresis, we know that the system is driven out of equilibrium. Different realizations show that the unfolding and refolding process is stochastic, resulting in a distribution of work values for both the forward and reversed processes.The experiment was done for two different types of MRNA. The Crooks relation 2.12 was shown to hold and we can read off the free energy difference at the intersection of forward and reversed distributions, i.e. $W = -W = 0$. The ratio of the two distributions validates the exponential relation predicted by the Crooks relation. The experimental results can be found in [27]. This experiment is a successful confirmation of the non-equilibrium work relations and the results for the free energy differences ΔF agree with formerly obtained results from the quasi stationary process by $\pm 4\%$.

2.3 Lebowitz Spohn Relation

In this section the steady state fluctuation theorem, first proven for dynamical systems [57], is presented as a symmetry of the entropy generating function for a Markov process. The outline of the proof follows [96].
The dynamics is based on transition rates $\omega(C_i \to C_j)$ to jump from configuration C_i to C_j. As a necessary condition of the proof, it has to be assumed that the reversed transition is always possible, i.e. if $\omega(C_i \to C_j) > 0$ then $\omega(C_j \to C_i) > 0$. The probabilities evolve according to the Master equation

$$\frac{\partial P(C_i,t)}{\partial t} = \sum_{C_j} \omega(C_j \to C_i)P(C_j,t) - \sum_{C_j} \omega(C_i \to C_j)P(C_i,t) = L^* P(C_i,t), \tag{2.19}$$

where L is the Liouville operator. Let $X = \{C_0, C_1, .., C_M\}$ be a trajectory of the stochastic process in configuration space during a finite amount of time t with M transitions happening. Along the trajectory we evaluate the quantity

$$\Delta s_{\mathrm{m}}(t, \{X, 0 \leq t\}) = \ln\left[\frac{\omega(C_0,C_1)}{\omega(C_1,C_0)} \cdots \frac{\omega(C_{M-1},C_M)}{\omega(C_M,C_{M-1})}\right]. \tag{2.20}$$

Here the assumption of reversible transitions is crucial in order to have Δs_{m} well defined. Observable (2.20) is called an action functional in [96] or medium entropy Δs_{m} in [142]. The fluctuation theorem is stated in the following way:
Consider the expectation value $\langle \exp[-\lambda \Delta s_{\mathrm{m}}(t)] \rangle$ of $\Delta s_{\mathrm{m}}(t)$ and define

$$\lim_{t\to\infty} -\frac{1}{t} \ln \langle e^{-\lambda \Delta s_{\mathrm{m}}(t)} \rangle = e(\lambda). \tag{2.21}$$

The fluctuation theorem states that the limit (2.21) exists with $e(\lambda)$ convex, where $e(\lambda)$ obeys the symmetry

$$e(\lambda) = e(1-\lambda). \tag{2.22}$$

To prove the fluctuation theorem, one defines the following function

$$g(C_i,t) = \left\langle e^{-\lambda \Delta s_{\mathrm{m}}(t)} \right\rangle_{C_i}. \tag{2.23}$$

The expectation value restricts the system to be in configuration C_i at time $t = 0$. The time evolution of $g(C_i,t)$ is given by

$$\begin{aligned}
\frac{d}{dt} g(C_i,t) &= \sum_{C_j} \omega(C_i \to C_j) e^{-\lambda \ln \frac{\omega(C_i \to C_j)}{\omega(C_j \to C_i)}} g(C_j,t) - \sum_{C_j} \omega(C_i \to C_j) g(C_i,t) \\
&= \sum_{C_j} \omega(C_i \to C_j)^{1-\lambda} \omega(C_j \to C_i)^{\lambda} g(C_j,t) - \sum_{C_j} \omega(C_i \to C_j) g(C_i,t) \\
&= (L_\lambda)_{i,j} g(C_j,t).
\end{aligned} \tag{2.24}$$

At $t = 0$ the generating function has the initial condition $g(C_i, 0) = 1$. The general solution can be written as

$$\langle e^{-\lambda \Delta s_{\mathrm{m}}(t)} \rangle = \sum_{C_i} P_s(C_i) g(C_i, t) = \sum_{C_i, C_j} P_s(C_i) (e^{L_\lambda t})_{C_i C_j}. \tag{2.25}$$

The Perron-Frobenius theorem [56, 117] states that L_λ has a unique maximal eigenvalue $e(\lambda)$ that satisfies

$$L_\lambda v_\lambda(C_i) = -e(\lambda) v_\lambda(C_i) \tag{2.26}$$

with $v_\lambda(C_i)$ being the corresponding eigenvector to $e(\lambda)$. Due to the existence of the greatest eigenvalue, the limit in (2.21) exists. The two linear operators L_λ and L_λ^* have the same largest eigenvalue. Using now the definition of the Liouville operator, we see that

$$L_\lambda^* = L_{1-\lambda}. \tag{2.27}$$

Hence the maximal eigenvector w_λ of $e(\lambda)$ of L_λ^* satisfies

$$L_\lambda^* w_\lambda(C_i) = -e(\lambda) w_\lambda(C_i) = L_{1-\lambda} w_\lambda(C_i). \tag{2.28}$$

Since $L_{1-\lambda} v_{1-\lambda}(C_i) = -e(1-\lambda) v_{1-\lambda}(C_i)$, we conclude by uniqueness that $w_\lambda = v_{1-\lambda}$ and $e(\lambda) = e(1-\lambda)$. Equation (2.22) implies a large deviation property for the probability distribution $p_t(\sigma)$ with $\sigma = \Delta s_{\mathrm{m}}(t)/t$, i.e.

$$p_t(\sigma) \cong e^{-t\chi(\sigma)}, \tag{2.29}$$

where $\chi(\sigma)$ is the Legendre transform of $e(\lambda)$. $\chi(\sigma)$ is called the rate function of entropy production. It is convex, $\chi(\sigma) \geq 0$, and satisfies

$$\chi(\sigma) - \chi(-\sigma) = \sigma. \tag{2.30}$$

It was shown in [3, 96] that this general result reduces to the Green-Kubo relation [62, 89] and the Onsager reciprocity relation [114] for small driving forces.
This fluctuation symmetry can be extended to finite time intervals t. The trajectory in configuration space is given by the following sequence

$$X(t) = \{C_1, ..., C_M\}, \tag{2.31}$$

with M the number of transitions during a fixed amount of measurement time t. The trajectory has the following probability of occurrence

$$P(X) = P_s(C_0, 0) \prod_{i=0}^{M-1} \omega(C_i \to C_{i+1}). \tag{2.32}$$

The corresponding reversed trajectory $X^\dagger$ exists if all transitions are reversible, given by,

$$P(X^\dagger) = P_s(C_M) \prod_{i=M-1}^{0} \omega(C_{i+1} \to C_i). \tag{2.33}$$

Therefore the forward and reversed trajectories are related by

$$P(X) = P(X^\dagger) \exp\left(\Delta s_m(X) + \ln \frac{P_s(C_0)}{P_s(C_M)}\right). \tag{2.34}$$

Thus for $\Delta s_m(X) + \ln \frac{P_s(C_0)}{P_s(C_M)}$ the fluctuation theorem holds even for finite M in the steady state. In the long time limit the additional boundary term, $\ln \frac{P_s(C_0)}{P_s(C_M)}$, can be neglected.

2.4 Hatano Sasa Relation

The Hatano Sasa relation is an integral fluctuation relation that measures the lag or excess heat. Oono and Paniconi introduced the term excess heat [115]. Excess heat is dissipated as the result of driving the system at a finite rate of change of the external parameter $\lambda(t)$. At $t = 0$ the system is in its non-equilibrium steady state, given by the stationary probability $P_s(C_i)$, where C_i is a configuration of the system. If we slowly vary the parameter λ, the system evolves through a continuous sequence of stationary states and the dissipated work is at a minimum. If the parameter is varied at a greater rate of change, the system is not able to stay in intermediate stationary states. If we are considering transitions between equilibrium states, the lag is measured by the total entropy increase since no entropy is generated in the steady state. For transitions between non-equilibrium steady states, Hatano and Sasa [66] defined the observable ϕ, which measures the additional entropy increase due to the rate of change in λ. The excess heat ϕ is defined in the following way

$$\phi = \int_0^\tau dt \dot{\lambda}(t) \frac{\partial P_s}{\partial \lambda}(C(t), \lambda(t)). \tag{2.35}$$

In the case of a discrete change in λ and a discrete configuration space this translates into

$$\phi = \sum_{i=0}^{M-1} (P_s(C_i, \lambda_{i+1}) - P_s(C_i, \lambda_i)). \tag{2.36}$$

The value of ϕ for a single trajectory depends on both the external process $\lambda(t)$ and the system's trajectory in configuration space. Because of the stochastic nature of the time evolution, each realization of the process has a different value for ϕ. The probability distribution of ϕ obeys the following relation

$$\left\langle e^{-\phi} \right\rangle = 1. \tag{2.37}$$

The average is taken over the complete set of possible trajectories. We are not going to prove the Hatano Sasa relation in this section since we are presenting the proof for the discrete case in chapter 4. Relation (2.37) implies

$$\langle \phi \rangle \geq 1, \tag{2.38}$$

if we apply Jensen's inequality [83]. If the dynamics obeys detailed balance, the Hatano Sasa relation reduces to the Jarzynski relation and $\phi = W$. We also want to mention that the Hatano Sasa relation does not rely on reversible dynamics, since it is not comparing a forward to its reversed trajectory. For a more detailed discussion, see [66, 64, 79, 113]. The Hatano Sasa relation was successfully tested experimentally in [155].

2.5 Seifert Entropy

The Seifert entropy theorem [139] is a fluctuation symmetry for the total entropy change Δs_{tot}. Because entropy change is a trajectory dependent observable, Seifert promotes the terminology of *stochastic thermodynamics* [141]. The total entropy produced in a process is divided into two contributions, the entropy change in the surrounding medium Δs_{m} and the entropy change of the system Δs under consideration,

$$\Delta s_{\mathrm{tot}} = \Delta s_m + \Delta s. \tag{2.39}$$

Maes showed [101] that a more general way of writing the Jarzynski integral fluctuation theorem exists. If the dynamics are reversible, we can define the observable R to be

$$R = \sum_{i=0}^{M-1} \ln \frac{\omega(C_i \to C_{i+1}, \lambda_{i+1})}{\omega(C_{i+1} \to C_i, \lambda_{i+1})} + \ln \frac{P_0(C_0, \lambda_0)}{P_1(C_M, \lambda_M)}. \tag{2.40}$$

P_0 and P_1 are two unspecified, normalized distributions and a system parameter λ is varied during a finite time interval τ at arbitrary rate. In this case a general integral fluctuation relation exists for the observable R, stated as

$$\begin{aligned} \left\langle e^{-R} \right\rangle &= \sum_{C_0,\ldots C_M} P_0(C_0, \lambda_0) \prod_{i=0}^{M-1} \omega(C_i \to C_{i+1}, \lambda_{i+1}) e^{-R} \\ &= \sum_{C_0,\ldots C_M} P_1(C_M, \lambda_M) \prod_{i=0}^{M-1} \omega(C_{i+1} \to C_i, \lambda_{i+1}) = 1. \end{aligned} \tag{2.41}$$

This relation implies that

$$\langle R \rangle \geq 0 \ . \tag{2.42}$$

The conclusion drawn in [139] is that infinitely many integral fluctuation relations exist that imply an analog of the Clausius inequality $\langle \Delta S \rangle \geq 0$.
Seifert proposes $P_1(C)$ to be the solution of the time dependent process for the normalized probability distribution, obtained from the Master equation or for continuous configuration space, from the Fokker Planck equation [123].

For this choice of $P_1(C)$ the observable R is identical to Δs_{tot} and its integral fluctuation relation is stated as

$$\left\langle e^{-\Delta s_{\mathrm{tot}}} \right\rangle = 1. \tag{2.43}$$

The stated integral fluctuation relation is valid for arbitrary initial conditions as well as arbitrary length and strength of the driving out of equilibrium. If we are investigating the system in its steady state, the observable Δs_{tot} reduces to the finite time fluctuation relation established in [96], see equation (2.34). In this case the observable Δs_{tot} obeys in addition to the integral fluctuation relation a detailed fluctuation relation

$$\frac{P(\Delta s_{\mathrm{tot}})}{P(-\Delta s_{\mathrm{tot}})} = e^{\Delta s_{\mathrm{tot}}}. \tag{2.44}$$

As it was stated in [139] the steady state detailed fluctuation theorem applies even for periodic driving once the system settles in the steady state. Experiments in the context of stochastic thermodynamics were performed by Tietz et al. [133, 153] in order to test the Seifert entropy relation.
The system considered in the experiment is an optically driven defect center in natural IIa-type diamond. Two states of the defect exist. One of the two states results in an emitted photon and is therefore called the bright state. The second one is called the dark state. Stimulated by two different laser wavelengths, transitions occur between the bright and the dark state with rate a resp. rate b:

$$0(\text{dark}) \underset{a}{\overset{b}{\rightleftharpoons}} 1(\text{bright}). \tag{2.45}$$

Transition rate a is modulated in time $a(t) = a_0[1+\gamma \sin(2\pi t/t_m)]$ due to a varying intensity of green laser light. Transition rate b is held constant given by red laser light. After the system settles into a steady state, single trajectories of the system are analyzed. This allows the analysis of the entire distribution of total entropy change by measuring a large number of realizations. With the distribution of the total entropy production the corresponding detailed fluctuation theorem has been verified. The experimental results can be found in [153].

Chapter 3

Interacting Many Body Systems

This chapter introduces the stochastic dynamics and the models under investigation. In the first part we start with the definition of the stochastic dynamics that is used and define stationary probabilities and non-equilibrium currents. Furthermore we characterize non-equilibrium steady states through their stationary probabilities and non-equilibrium currents [164]. Two possible definitions of the amplitude of the probability current K are discussed that allow to quantify the distance from equilibrium. In the second part of this chapter, we introduce the dynamic rules for different reaction-diffusion models and transport processes. Differences in their dynamic properties are highlighted and their individual importance for our general analysis is motivated. Their stationary probabilities $P_s(C)$ and non-equilibrium currents are discussed as a function of the system parameters. This allows us to interpret in the following chapters signatures of entropy production.

3.1 General Setup of Markov Processes

The stochastic processes that are studied here are Markov processes [72]. Being a Markov process, the evolution to a new state of the system is only function of the system's current state and is independent of its history. The underlying mathematical formalism that is used to describe the time evolution of the stochastic systems is the Master equation. The Master equation is a deterministic equation that allows us to calculate the time evolution of the system of interest. To be more precise, we calculate the time evolution of the set of probabilities to find the system in one of its possible states (configuration), denoted as C. The systems we are considering are realized on a discrete lattice of finite size. The occupation number is restricted to at most one particle per site. This allows us to calculate the properties of the system based on a finite number of configurations. The total number of configurations is 2^N, where N is the number of sites in our system.
By the definition of the dynamic rules of the system, transitions occur with a certain prob-

ability per time interval. For example, radioactive decay with a given half life evolves in continuous time because a deterministic firing does not exist. In general, the transition rate to go from configuration C_i to C_j is denoted by $\omega(C_i \to C_j)$. Such a transition is called reversible if the reversed transition rate is $\omega(C_j \to C_i) > 0$. As a result every trajectory in configuration space has a time reversed trajectory. Later on we shall see that the existence of the reversed trajectory is important to define entropy change. We talk about irreversible processes if trajectories exist without the existence of the reversed trajectory.
Since the set of probabilities is calculated as a function of time, the Master equation has to satisfy the conservation of probability at all times. This has implications onto the time evolution operator that we will discuss. The discrete time evolution is given by

$$P(C_i, t + \Delta t) - P(C_i, t) = \sum_j \left[\omega(C_j \to C_i)P(C_j, t) - \omega(C_i \to C_j)P(C_i, t)\right]. \tag{3.1}$$

In the present form, the Master equation is expressing the conservation of probability in the form of a continuity equation. Therefore it is natural to talk about the right part of the equation being the gradient of a current. In the long time limit, the system, if allowed to relax, ends up in a final state where time translation invariance is present. In general, this final state is called a stationary state and is conveniently subdivided in two separate groups of system - equilibrium systems and non-equilibrium steady states. The left hand side of equation (3.1) is zero then and we obtain

$$\sum_j \left[\omega(C_j \to C_i)P_s(C_j) - \omega(C_i \to C_j)P_s(C_i)\right] = 0. \tag{3.2}$$

For later purposes, we are introducing the definition of the local probability current

$$K_s(C_i, C_j) = \omega(C_j \to C_i)P_s(C_j) - \omega(C_i \to C_j)P_s(C_i). \tag{3.3}$$

The expression *local probability currents* refers to currents across single bonds in configuration space connecting a pair of configurations of the system. $\mathbf{K_s}$ is an antisymmetric matrix. Expression (3.2) can be satisfied in two possible ways. If $\omega(C_j \to C_i)P_s(C_j) - \omega(C_i \to C_j)P_s(C_i)$ is equal to zero for every state C_i and C_j, the system is satisfying detailed balance. One can also use the Kolmogorov criterion of closed loops in configuration space to prove detailed balance and to construct the hamiltonian H [88]. For each pair of configurations the net probability flow across their bond in configuration space is zero. In this case the stationary state is an equilibrium state. This is not the case if non zero probability flow exists across bonds and only the sum of all individual currents cancels to zero. In this case the system is in a non-equilibrium stationary state. Notice that the condition for detailed balance is very strong. It does not suffice to demand reversibility for every possible transition as we have previously defined. Even though reversibility is present, the system might still be in a non-equilibrium steady state.
As can be seen in equation (3.1), the Master equation is linear. This allows us to define a

linear operator for the time evolution. The vector of probabilities ($\mathbf{P}(t)$) has components given by $\mathbf{P}(t)_i = P(C_i, t)$ and we write

$$\mathbf{P}(t + \Delta t) = \mathbf{W}\mathbf{P}(t), \tag{3.4}$$

with $\mathbf{W}$ being the transition matrix. Due to the conservation of probability, every column in the transition matrix adds up to 1. The time evolution of the vector of probabilities is expressed by the Liouville operator, defined as

$$\mathbf{L} = \mathbf{W} - \mathbf{1}. \tag{3.5}$$

As a consequence the Liouville operator adds up to zero in each column. The Perron-Frobenius theorem [70] states at this point that all eigenvalues of the Liouville operator are smaller or equal to zero and the zero eigenvalue is unique if the system is ergodic.
Before we go on with the discussion, we want to sum up the important points. The systems that are analyzed throughout this work are defined by a transition matrix $\mathbf{W}$. The elements of the transition matrix are given by the reaction and diffusion rates connecting configurations. This defines the reaction network. In the matrix representation the individual configurations are identified with the basis vectors of the system. If the system is realized on a lattice, each configuration is an ordered string of site occupation numbers η_i, where $i = 1, .., N$. In our case the site occupation is restricted to at most one particle per site $\eta_i = \{1, 0\}$. The eigenvector of the Liouville operator that corresponds to the zero eigenvalue is then a linear combination of the basis elements. If detailed balance is satisfied for all possible transitions, the system is in equilibrium and the set of stationary probabilities fully determines the one time quantities in the steady state. This is not the case for systems in a non-equilibrium steady state. If detailed balance is not satisfied, the stationary probabilities are not sufficient to fully characterize the system because macroscopic particle or energy currents might exist. A conjecture for a general characterization of the non-equilibrium steady states was proposed in [164, 165]. It is not the stationary probabilities alone but the stationary probabilities plus the information about the non-equilibrium currents that should be taken into account to describe the steady state of the system.

3.2 Full Characterization by P_s and K_s

Zia and Schmittmann [164, 165] conjectured that one can fully characterize the dynamic properties of a system described by a Master equation through the knowledge of the set of stationary probabilities $P_s(C_i)$ and the set of stationary probability currents between two configurations C_i and C_j, defined as

$$K_s(C_i, C_j) = \omega(C_j \to C_i)\, P_s(C_j) - \omega(C_i \to C_j) P_s(C_i). \tag{3.6}$$

One can illustrate for a very simple model, that the sole knowledge of the stationary probabilities is not sufficient to determine whether the system is in equilibrium or out of equilibrium.

The model we are considering is the asymmetric simple exclusion process (ASEP) with periodic boundary conditions. The system is realized on a discrete lattice with N sites on a ring with n particles. A randomly chosen particle hops with probability p to the right and probability q to the left as long as no particle is occupying the neighboring site. This type of interaction is called hardcore repulsion. In the case of biased hopping rates, i.e. $p > q$, the system has a non zero macroscopic current running along the ring. In the case of equal hopping rates the system satisfies detailed balance. Independent of the actual values of p and q, the stationary probabilities are uniform. Therefore the knowledge of just the stationary probabilities is not sufficient.
In order to distinguish the two cases in a microscopic description, one needs to consider the stationary probabilities $P_s(C_i)$ and the non-equilibrium currents $K_s(C_i, C_j)$. The conjecture, given in [164, 165] is even stronger and discusses possible transformations that leave the pair $\{P_s, K_s\}$ invariant. This idea is in analogy to equilibrium systems. In order to calculate a physical observable of a system that is independent of time and time differences, various simulation techniques can be used. These techniques are very sophisticated and adapted to different situations. For example, a spin system might be calculated with a Metropolis [104] dynamics, heat bath [105] or even with the help of cluster algorithms as the Swendsen-Wang [160] or Wolff algorithms [162], see [94] for a general review on Monte Carlo algorithms. These different simulation algorithms all satisfy the detailed balance relation with the same stationary probabilities. But since the dynamics are different, a meaningful physical time is not possible to assign to the update scheme. Autocorrelation functions thus depend explicitly on the simulation technique used.
The claim for non-equilibrium systems in their steady state is analogous. The configuration space can be represented as a tree structure [132] to discuss the non-equilibrium current flow. The transformations keep the stationary probabilities and the non-equilibrium currents invariant but as a result, the timescales of the dynamics change and two time quantities like correlation functions change with these transformations. Even though this is a very important ansatz, this aspect of the conjecture is not pursued in this work. The more important point for our purposes is the idea of a distance from equilibrium. We use information given by the non-equilibrium currents to characterize our systems. As discussed in the following, the norm of the matrix $\mathbf{K_s}$ can serve as a metric to describe the distance to equilibrium.
Different ways to define a positive metric for the matrix $\mathbf{K_s}$ can be imagined. The euclidian norm of the matrix $\mathbf{K_s}$ was proposed in [165], defined as

$$K_E^2 = \sum_{i,j} \left(\omega(C_j \to C_i)\, P_s(C_j) - \omega(C_i \to C_j) P_s(C_i)\right)^2 . \tag{3.7}$$

An alternative would be to define a metric by summing the absolute values of the individual currents across bonds,

$$K = \sum_{i,j} \left|\omega(C_j \to C_i)\, P_s(C_j) - \omega(C_i \to C_j) P_s(C_i)\right| . \tag{3.8}$$

It was shown [118] that the latter choice can directly be related to macroscopic currents in the system and scales linear with the system size. We illustrate the two norms for the totally

asymmetric exclusion process (TASEP) on a periodic ring. This system is the extreme case of the ASEP with hopping rate $p = 1$ to the right and hopping rate $q = 0$ to the left. A characteristic current of particles exists due to the unidirectional hopping on the ring. For any number of particles the stationary probabilities are uniform as it was mentioned before. Let us start out with the calculation of the euclidian distance:

$$\begin{aligned} K_E^2 &= \sum_{i,j} (K_s(C_i, C_j))^2 \\ &= 2 \sum_{i,j} \left[P_s(C_j) \omega(C_j \to C_i) \right]^2 . \end{aligned} \tag{3.9}$$

We thereby use the fact that the transition rate $\omega(C_j \to C_i)$ are only equal to 0 or 1 such that $\omega(C_j \to C_i)^2 = \omega(C_j \to C_i)$ and $\sum_i \omega(C_j \to C_i) = \mathcal{N}_{10}(C_j)$, where $\mathcal{N}_{10}(C_j)$ is the number of particle-hole pairs in the state C_j. So one has

$$K_E^2 = 2 \sum_j (P_s(C_j))^2 \mathcal{N}_{10}(C_j). \tag{3.10}$$

On a ring, every configuration has the same probability, $P_s(C_j) = P_s(C_i) = 1/\Omega_n^N$ for all C_i and C_j. We calculate the total number of possible configurations Ω_n^N for N sites with n particles to be

$$\Omega_n^N = \frac{N!}{n!(N-n)!}. \tag{3.11}$$

Finally, the expression (3.10) can be written as

$$K_E = \sqrt{\frac{2}{\Omega_n^N} \sum_j P_s(C_j) \mathcal{N}_{10}(C_j)} = \sqrt{\frac{2}{\Omega_n^N} J} = \sqrt{\frac{2\mathrm{j}N}{\Omega_n^N}}, \tag{3.12}$$

with j being the current density on the ring. When taking the infinite volume limit the quantity K in the euclidean norm vanishes exponentially fast.
The absolute value norm is calculated in the same way and leads to the following expression for the probability current,

$$\begin{aligned} K &= \sum_{i,j} |K_s(C_i, C_j| \\ &= 2 \sum_{i,j} P_s(C_j) \omega(C_j \to C_i) \\ &= 2 \sum_j (P_s(C_j)) \mathcal{N}_{10}(C_j) \\ &= 2J = 2N\mathrm{j}. \end{aligned} \tag{3.13}$$

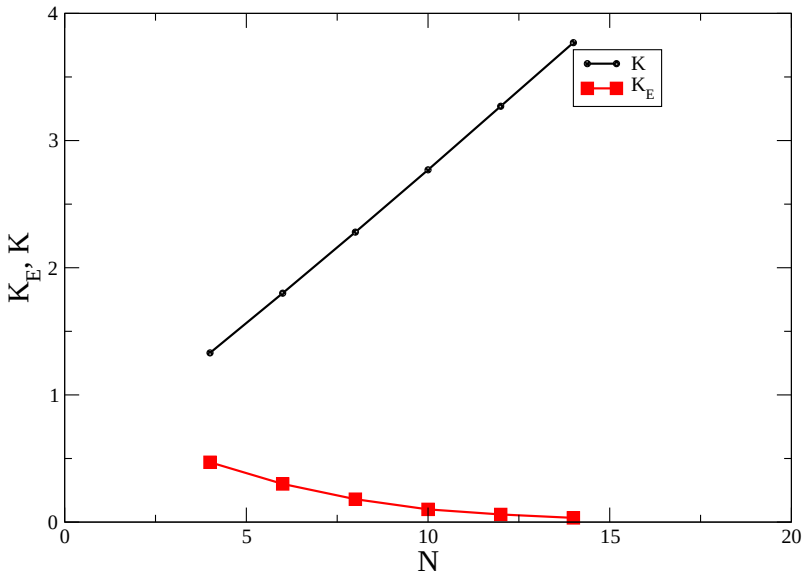

Figure 3.1: The non-equilibrium probability current amplitude calculated for the closed TASEP on a one dimensional ring for the two quantities, K_E and K. The dependence on the system size N is shown. The system considered, has a constant density of particles, $\rho = 1/2$.

This suggests dealing with the absolute value defined as $K = \sum_{i,j} |K_s(C_j, C_j)| \propto N\mathrm{j}$. The two quantities, K and K_E, are presented in figure 3.1 as a function of the system size N with a fixed number of particles $n = N/2$.

It can be shown even for more complicated systems, for example reaction-diffusion systems, that the quantity K is extensive, i.e. growing linearly with the system size [118]. By construction, K only vanishes in the case of detailed balance. We follow the idea of [164] and characterize the stationary probabilities and their distances from equilibrium K for different stochastic models.

3.3 Definition of the Stochastic Models

Reaction-diffusion models are a large family of models with different properties in their dynamics. They are used in a wide range of research areas, for example the study of chemical reactions or aging phenomena [49, 68], as well as in problems in percolation [20, 69] and in cell biology [16, 102]. The general setup includes at least one creation reaction that increases the number of particles and a second reaction that decreases the number of particles. But more complex reaction networks exist. The reaction rates, in the simplest case, are uniform throughout the lattice. However the study of disordered systems is of great interest [39]. Particles might also be allowed to diffuse across the lattice. Since no preferred

direction exists, there is no net particle current in the steady state across the system that could be associated to a net probability current. Nevertheless reaction-diffusion models are paradigmatic models to study properties far from equilibrium. The intention of the present analysis is to understand the steady state properties of various systems. Therefore we are not including reaction schemes that possess a dynamical transition to an absorbing state. The study of dynamical phase transitions to an absorbing state is drawing a lot of attention [67, 112, 151, 106] but is not of concern in this work.
Another group of models under investigation are transport models in one dimension. In the study of non-equilibrium systems transport models are of great importance [108, 135, 131, 136]. These systems possess a directed current of particles or energy through the system. Exact results for the stationary probabilities were obtained for closed systems [35, 36, 51] as well as for open systems [34]. Here, the current can be induced at the boundaries with homogeneous diffusion in the bulk [119, 148] or may result from biased hopping rates inside the bulk that enhance the total current [128]. A large number of variations of this model exists with additional features, for example inhomogeneous hopping rates at different sites [65], multiple lane systems [48, 161], slow sites [40], extended objects [93, 143] and systems coupled to finite resources [1, 28]. Even extensions to systems with varying length are based on this model [42, 110, 149, 150].
In the following two subsections we are going to define the dynamics of the models. The stationary probabilities and amplitudes of non-equilibrium currents are discussed as a function of the system parameters. The individual probability currents across single bonds are not presented explicitly but instead the absolute value norm of the $\mathbf{K_s}$ matrix is discussed.

3.3.1 Reaction-Diffusion Models

We consider one-dimensional systems made up of N sites with periodic boundary conditions. Excluding multiple occupancy of a given lattice site, particles A jump to unoccupied nearest neighbor sites with a diffusion rate D and undergo various reactions of creation and annihilation. Therefore a total of 2^N configurations exists. We present in the following four different reaction schemes, see Table 3.1, that are labeled model 1, 2, 3, and 4. For all four models the number of configurations is the same at constant system size, the models have different properties in their connectedness of configurations, i.e. the topological properties of the corresponding configuration space. The reaction schemes are set up to lack an absorbing state. Possessing non trivial stationary probabilities the models vary in the way configurations are connected by possible transitions defined by the chemical reactions. This property should play an important role if we look at the dynamics on short time intervals with a small number of occurring transitions. Different flow patterns and closed loops of probability currents between groups of configurations are the result. The time evolution of the models is calculated by the Master equation, given by their transition matrix $\mathbf{W}$.

For future discussions of entropy change it is essential to establish reversibility of all transitions which is not the case for model 2, 3, and 4. For this reason we are going to define a

Table 3.1: The four reaction schemes. A new particle A can only be created at an empty lattice site. Reactions are taking place on adjacent sites.

model 1	model 2	model 3	model 4
$A+A \underset{h}{\overset{\lambda}{\rightleftharpoons}} 0+A$	$A+A \xrightarrow{\lambda} 0+A$	$A+A \xrightarrow{\lambda} 0+0$	$A+A+A \xrightarrow{\lambda} 0+0+0$
	$0 \xrightarrow{h} A$	$0 \xrightarrow{h} A$	$0 \xrightarrow{h} A$

reversibility parameter $0 < \varepsilon \leq 1$. The parameter ε sets the amplitude of the reversed transition rate. The reader should remember that reversibility of the reactions is not sufficient for detailed balance to be satisfied. Only in the case of a single pair of conjugate reactions, detailed balance holds for any non zero value of the reaction rates.

Let us highlight the differences in the dynamic properties of the four models. For model

Table 3.2: The four reversible reaction schemes discussed in this thesis. A new particle can only be created at an empty lattice site. For the purpose of the discussion we introduce reversed reactions with rates εh and $\varepsilon\lambda$

model 1	model 2	model 3	model 4
$A+A \underset{h}{\overset{\lambda}{\rightleftharpoons}} 0+A$	$A+A \underset{\varepsilon\lambda}{\overset{\lambda}{\rightleftharpoons}} 0+A$	$A+A \underset{\varepsilon\lambda}{\overset{\lambda}{\rightleftharpoons}} 0+0$	$A+A+A \underset{\varepsilon\lambda}{\overset{\lambda}{\rightleftharpoons}} 0+0+0$
	$0 \underset{\varepsilon h}{\overset{h}{\rightleftharpoons}} A$	$0 \underset{\varepsilon h}{\overset{h}{\rightleftharpoons}} A$	$0 \underset{\varepsilon h}{\overset{h}{\rightleftharpoons}} A$

1 and model 2, every transition increases or decreases the total number of particles by one. In fact, the annihilation reaction is the same in both models. The difference between the two models is the creation process with reaction rate h. For model 1, the creation rate is actually the reversed, conjugate transition to the annihilation reaction. The system does obey detailed balance and is therefore an equilibrium system. Model 2 is a non-equilibrium system that possesses a non zero probability current K. Non reversible transitions exist for configurations containing a small number of particles. For example, a new particle can be created in the middle of three empty sites, $000 \longrightarrow 0A0$ with rate h, but to go back to the configuration with three empty sites by destroying this isolated A particle is not allowed, as we need to have one neighboring A particle for the annihilation process to take place. As we discuss later, the limit of very large creation rate favors configuration of high density and the distinction of the two reaction mechanisms $A \to 2A$ and $0 \to A$ vanishes. In this limit model 2 effectively reduces to an equilibrium system.

In model 3 and model 4, as long as $\varepsilon = 0$, microscopic reversibility is broken for all reactions. The number of particles created in a single transition is not equal to the number of particles annihilated in a single transition. The system is out of equilibrium as long as $\varepsilon \neq 1$,

because the system possesses two different reversible, conjugate, pairs of reactions instead of one. In the case of model 1 and model 2, two reactions were needed to return to the initial configuration. In the case of model 3, the return to the initial configuration requires three and in the case of model 4, four reactions. This has an important implication on the current structure in configuration space, see illustration 3.2. This is one of the main reasons we are

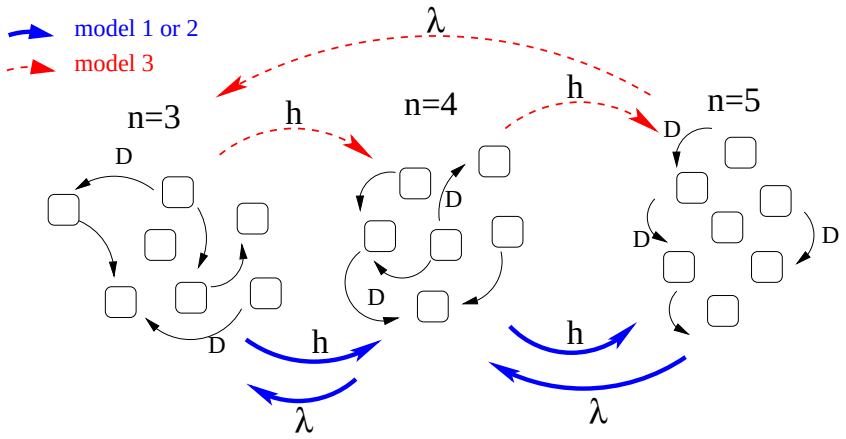

Figure 3.2: Schematic plot of the configuration space for models 1, 2, and 3 where configurations are grouped by the number of particles in the system n. In a diffusion step the system goes from one configuration to another in the same unit without changing the particle number. Passages between different units are due to reaction processes. For models 1 and 2, $\Delta n = \pm 1$. This is different for model 3 (and 4) where different changes in the number of particles in the system is possible, $\Delta n = +1, -2$ ($\Delta n = +1, -3$).

including the four models in the further discussion. To investigate the consequences for the entropy production of these models in a single steady state, see chapter 4, and in transient processes, see chapter 5.

3.3.2 Driven-Diffusive Systems

We are also investigating one dimensional transport models. The two relevant cases we will study are the symmetric simple exclusion process (SSEP) [148] and the totally asymmetric simple exclusion process (TASEP) [99, 147]. Both models are realized on a finite one dimensional lattice with N sites and open boundary conditions. Open boundary conditions describe the interaction of the system's boundaries with external particle reservoirs. For our case, a one dimensional system, we are considering the first site of the system being in contact with a particle bath **A** and the last site to the right being in contact with a particle reservoir **B**. As a result, particles enter and leave at both sides with different probabilities and a current of particles runs through the system. The boundary induced current can be

enhanced by an external driving that biases the hopping rate in the bulk from pure diffusion, equal probability to hop to the left or the right, to the extreme case of complete bias with probability one to hop to the right. This is the case of infinite forcing due to the external field. The complete dynamics is illustrated in figure 3.3. A parameter ε is introduced to guarantee reversibility at the boundaries. The reversibility in the bulk is assured by the hopping rates $p, q > 0$.

We shall discuss in more detail the case $p = 1$ in this part. In this case we are going to

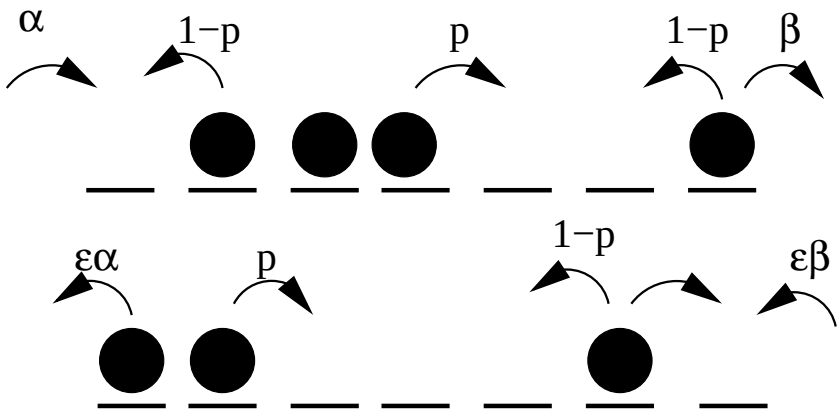

Figure 3.3: Illustration of the dynamical rules for the general setup of the transport processes. Particles are allowed to hop the right with probability p and to the left with probability $q = 1 - p$, respecting exclusion. At the boundary particles can enter on the left with probability α and leave with $\varepsilon\alpha$. On the right, particles leave with probability β and enter with probability $\varepsilon\beta$.

present the phase diagram for $\varepsilon = 0$ as a function of the entrance rate on the left α and exit rate at the right β, see figure 3.4. Three different regimes are identified. The low density phase (LD) where the density is equal to α, the high density phase (HD) with a mean density equal to $1-\beta$, and the max current phase (MC) where the mean density in the bulk is equal to $1/2$.

For more details of the general properties of the TASEP model, please refer to [34]. The reason to discuss transport models in addition to the reaction-diffusion models is the fact that we can distinguish in this model bulk and boundary properties. This was not the case for reaction diffusion models since reactions were allowed to take place anywhere across the system and no macroscopic current of particles exists in the system.

We investigate in the next section how the dynamical rules of the dynamics for the different models influence the stationary probabilities and stationary currents.

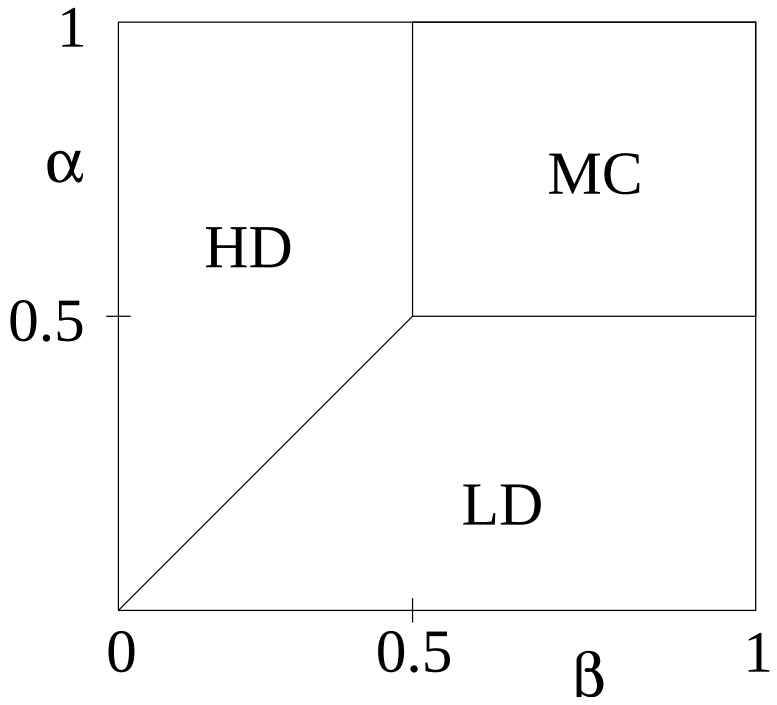

Figure 3.4: Phase diagram of the TASEP model as a function of the entrance rate to the left α and the exit rate to the right β. The hopping rate to the right is $p = 1$. HD is the high density, LD is the low density, and MC is the max current phase.

3.4 Stationary Probabilities and Currents

In the remainder of this chapter, we are discussing the properties of the stationary probabilities and current amplitudes of the models in table 3.2 and in figure 3.3, see also [46]. This discussion will allow us to characterize the steady states resulting from the fixed reaction rates of the different models. In addition, this prepares the reader for the discussion of entropy production in the coming chapters.
The analysis is organized as follows. We start with the discussion of the stationary probabilities of the reaction-diffusion models to understand the influence of the different reaction schemes. The data is presented in the following form. We calculate, for a fixed number of sites N, the complete set of probabilities for 2^N configurations. In the figures, the configurations are grouped by their total number of particles. On the left we present the probability of the empty configuration and on the right the configuration that is fully occupied. Afterwards, the stationary probability currents K are discussed as a function of the reaction rates. After the discussion of stationary probabilities and currents for the reaction diffusion models, we repeat the analysis for the transport models. At the end of the section, we are going to summarize our results.

3.4.1 Reaction-Diffusion Models

The discussion is organized in the following way. In figure 3.5 the stationary probabilities for all four models are discussed simultaneously for different sets of the reaction rates at constant system size $N = 8$. The annihilation rate is fixed to be $\lambda = 1$ and the stationary probabilities are calculated for two different creation rates $h = 0.2$ and $h = 1.4$. The reversibility parameter ε is set to zero in this calculation.

The data for the two different values of the creation parameter shows qualitatively similar

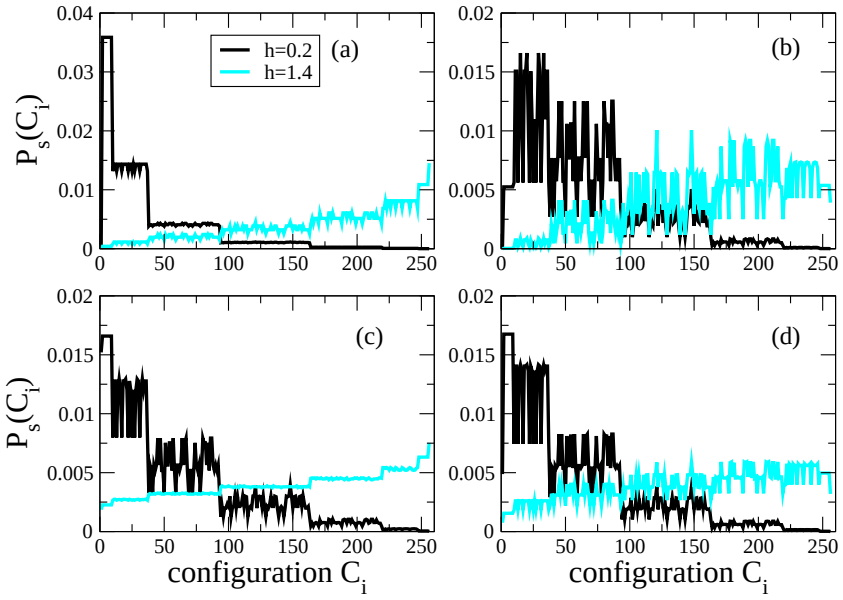

Figure 3.5: The stationary probabilities for (a) model 1, (b) model 2, (c) model 3, and (d) model 4 for a fixed annihilation rate $\lambda = 1$. The creation rate is set to $h = 0.2$ (black) and $h = 1.4$ (cyan). The data is calculated for systems with $N = 8$ lattice sites. The reversibility parameter is $\varepsilon = 0$ and the diffusion constant is set to $D = 1$. Reprinted with permission from S. Dorosz and M. Pleimling. Characterizing steady-state and transient properties of reaction-diffusion systems. Phys. Rev. E, 80(6):061114, Dec 2009. Copyright 2009, American Physical Society.

behavior for the four models. We see that groups of configurations with equal numbers of particles have approximately the same stationary probability. In fact for model 1, satisfying detailed balance, we notice very similar behavior as for model 2, 3, and 4. For the parameter values investigated, the variation of probability seems to be the most important for model 1. Model 2 has a larger variation than model 3, which is counter intuitive because at these parameter values, as we see later, model 3 has a larger amplitude of probability current than model 2 and therefore is further away from equilibrium. We conclude that the stationary probabilities are not sufficient to distinguish an equilibrium system from a non-equilibrium

system.
A second analysis that takes place at this point concerns the influence of the reversibility parameter ε onto the stationary probabilities. Since the entropy compares the probability of a given sequence of configurations to the probability of the reversed sequence, shown later, ε is directly related to the magnitude of entropy change in the system. We present in figure 3.6 the influence on stationary probabilities of model 2 and model 3 for a given set of reaction rates.

The stationary probabilities are marginally modified by the small parameter ε. Only for

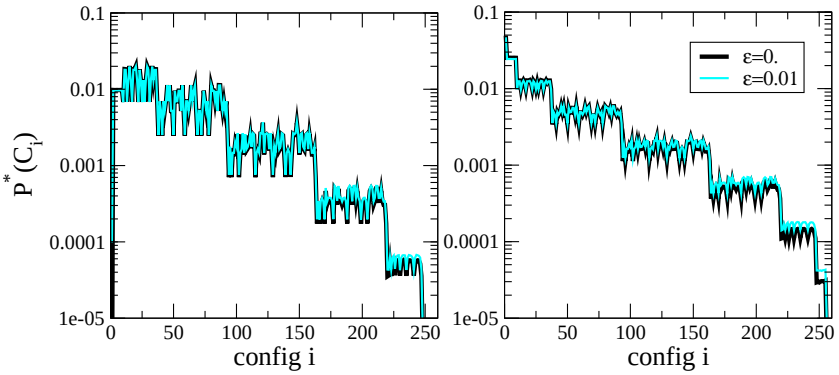

Figure 3.6: The stationary probabilities for (left) model 2 and (right) model 3 for two different values of the reversibility parameter, $\varepsilon = 0$ (black) and $\varepsilon = 0.01$ (cyan). The creation rate is set to $h = 1.0$ and the annihilation rate is set to $\lambda = 1$. The data is obtained for systems with $N = 8$ lattice sites and the diffusion constant is set to $D = 1$.

very small probability amplitudes, the influence is visible. This assures us that we are not modifying significantly the macroscopic observables as for example the mean particle density or correlation functions. Let us continue the characterization of the reaction-diffusion models with the distance from equilibrium calculated by the sum of the absolute values of the probability currents,

$$K = \sum_{i,j} \left| \omega(C_j \to C_i)\, P_s(C_j) - \omega(C_i \to C_j) P_s(C_i) \right| . \tag{3.14}$$

In figure 3.7 the current amplitudes are calculated for all four models as a function of the creation rate h and the reversibility parameter ε.

For the chosen reaction rates, we see that model 1 has a zero probability current for all values of the creation rate h. This supports our claim made in the last section, that model 1 is an equilibrium model. Model 3 and model 4 show a monotonous increase with increasing reaction rate h. Model 3 is increasing slower than model 4. Model 2 has a qualitatively different behavior. At some creation value h, the total probability current shows a maxima and for larger values of h the amplitude of K is decreasing monotonously to zero. With increasing creation rate the system becomes more and more filled with particles. In the limit

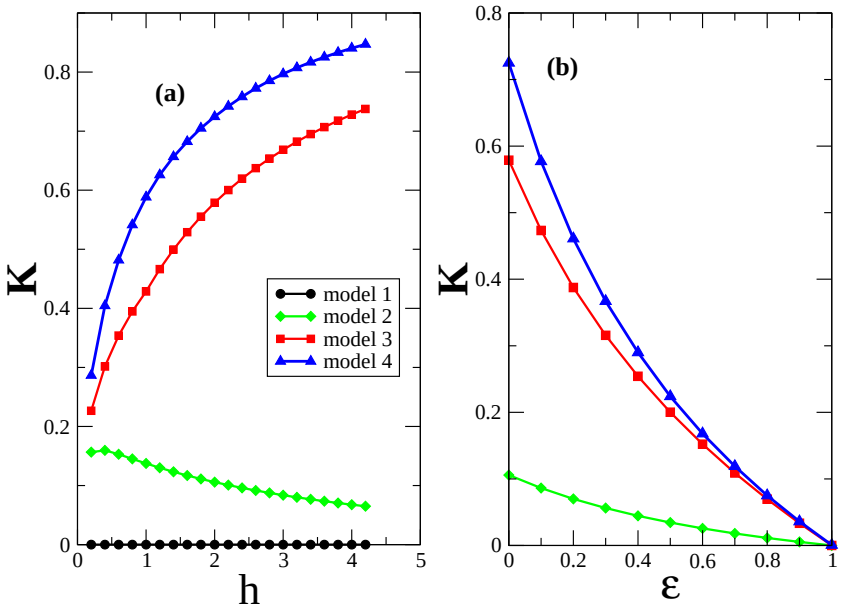

Figure 3.7: The total probability current K (a) as a function of the creation rate h for models 1, 2, 3, and 4 with a set reversibility parameter $\varepsilon = 0$ and (b) as a function of ε for models 2, 3, and 4. In all cases $\lambda = 1$ and $D = 1$. In (b) the creation rate is $h = 2$. The data are for systems with $N = 8$ lattice sites.

of infinite creation rate, the creation reaction of model 2 is equal to the creation reaction of model 1 and as a consequence model 2 satisfies detailed balance.
In figure 3.7 (right) the behavior for all three non-equilibrium models is analogous. With increasing reversibility parameter ε, the system approaches equilibrium. For $\varepsilon = 1$, by definition, all reaction-diffusion systems in table 3.2 satisfy detailed balance. In this case all stationary probabilities are equal for models 2, 3, and 4. The statement, that all configurations are equiprobable is based on the construction of closed loops in the configuration space [108].

3.4.2 Driven-Diffusive Systems

For the two different transport models, the stationary probabilities are investigated in figure 3.8 using different values of the entrance rate α and exit rate β. The results for the SSEP are displayed on the left and the results for the TASEP are on the right. The configurations are sorted first in groups of equal number of particles and for groups of configuration with equal number of particles we ranked the configurations due to their center of mass. Starting with configurations with a center of mass close to the left side to configurations with a center of mass to the right side. This helps us to understand the effect of broken symmetry due to

the boundary conditions that induces the particle current through the system. This feature was not present for reaction-diffusion systems. The stationary probabilities show a more

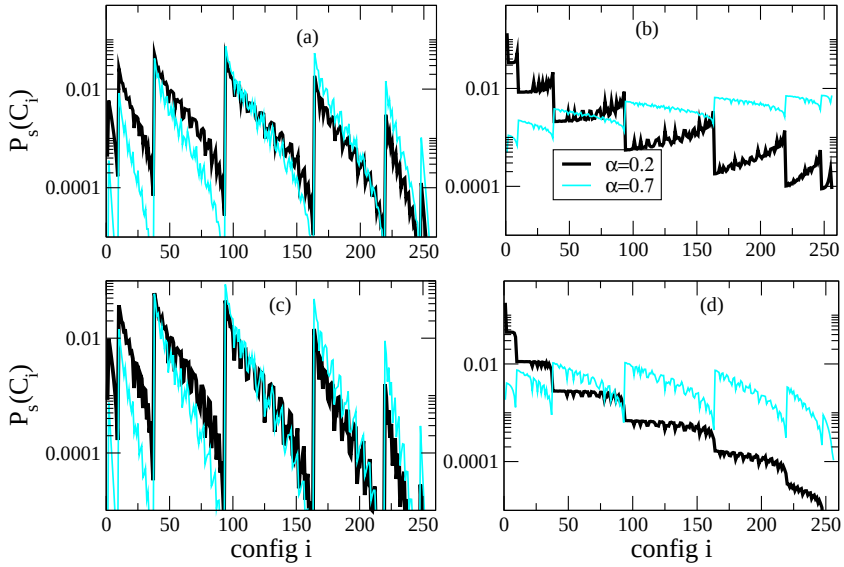

Figure 3.8: The stationary probabilities for (a) SSEP with $\beta = 0.5$, (b) TASEP with $\beta = 0.5$, (c) SSEP with $\beta = 1$, and (d) TASEP with $\beta = 1$. The entrance rate α for all cases is 0.2 (black) and 0.7 (cyan). The data is calculated for systems with $N = 8$ lattice sites. The reversibility parameter is set to $\varepsilon = 0.1$.

complex pattern than the reaction diffusion systems. In the case of symmetric bulk hopping rates, figure 3.8(a) and (c), configurations with equal number of particles vary significantly due to their center of mass. Configurations with a center of mass to the left end of the system possess a larger stationary probability than configurations with a center of mass on the right end of the system. This effect is comparable for the two different values of β. The probabilities are varying strongly with the entrance rate α. Since $\varepsilon = 0$ the particles have to cross through the system and will finally leave the system on the right but since the hopping rate inside the bulk is symmetric, particles are interacting with the boundaries over a larger distance. For this reason, the biased hopping transports the particles away from the left boundary towards the right side of the system. Correlations due to the left boundary are entering less into the system and the effect of the right boundary becomes more important. This can be seen in the results from the TASEP in figure 3.8(b) and (d). For a small entrance rate, the center of mass is located further to the right end of the system. At large entrance rate, the effect of the left boundary is still present. The influence of the right boundary is important in the case of $p = 1$. These probabilities are varying with β.

In figure 3.9 the stationary probability currents are displayed for the SSEP and the ASEP. For both models the current is presented as a function of the entrance rate α for different values of the exit rate β. For the SSEP a monotonous increase in the current as a function

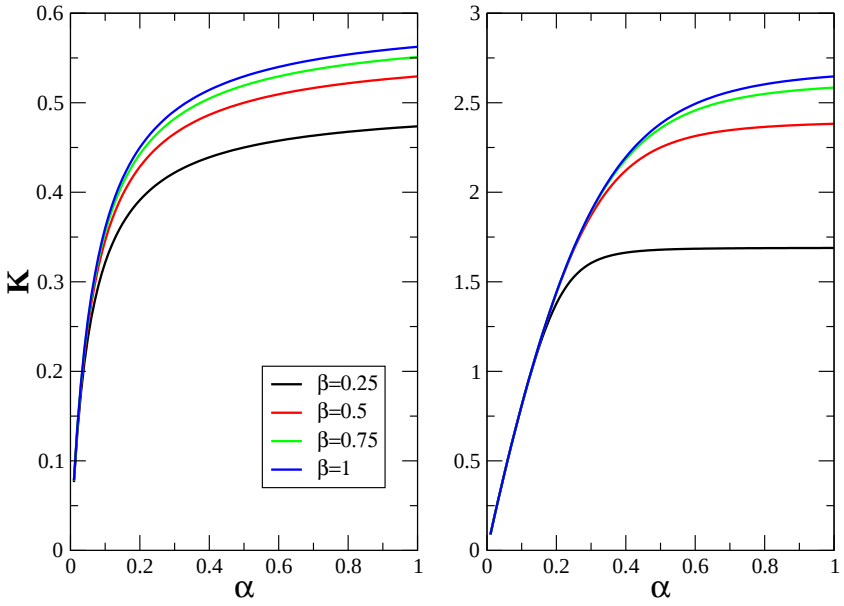

Figure 3.9: Stationary probability current of the transport model, (left) SSEP and (right) TASEP. The parameters are $N = 8$ and the reversibility parameter is set to $\varepsilon = 0.1$.

of the entrance rate exists. The final value at $\alpha = 1$ is function of the exit rate β. For larger values of β the current rises to a larger final value of the probability current. The same behavior can be seen for the TASEP but the amplitude of the current is larger by a factor of 5, compared to the SSEP.

3.5 Summary

In this chapter, the Master equation was introduced that allows us to define important observables as the stationary probabilities and the non-equilibrium currents. The time evolution was presented and the Liouville operator was defined. The stochastic models were presented and motivated because of their differences in the dynamics resulting from the reaction schemes that introduced different topological properties in configuration space. This allows us to analyze the probability current loops and their consequences for the entropy production. Transport processes were also introduced and discussed. Due to the open boundaries at both ends of the system, a net particle current is present in these systems that permits us to understand its influence on entropy production. Different models were characterized by their stationary probabilities and amplitudes of stationary probability currents.

Chapter 4

Steady State Fluctuation Relation

Ever since the discovery of steady state fluctuation relations, experiments and computer simulations were performed to analyze shapes of entropy distributions [153, 85, 75, 52, 41, 43, 32]. For a large number of systems it has been shown that the shape of the distributions are not gaussian but have complex structures that are tied to the underlying dynamics. At the same time an exponential relation involving the probability distributions of entropy change in a single steady state is satisfied. Motivated by the rich and complex distributions that were analyzed for different systems, we are going to study here the entropy distributions for the stochastic systems discussed in chapter 3. This work extends the characterization of single steady states and allows us to discuss in further detail the steady states of the stochastic systems. We have seen that the amplitude of probability current K in the steady state is non zero for models 2, 3, and 4. Non zero probability currents in the Master equation distinguish systems with general steady states from equilibrium systems, satisfying detailed balance. In both cases time translation invariance is satisfied, and for the former case an increase in entropy is observed.
The chapter is divided in two main parts. In the first part, the characteristics of the reaction-diffusion systems for short times are discussed. In the second part we are characterizing the rate function for the entropy creation which is defined in the long time limit and is time independent. Both parts provide new insights into steady state properties of interacting many particle systems.

4.1 Entropy Production at Short Time Scales

The change of entropy in a non-equilibrium steady state is on average linearly increasing with time. Given an initial configuration, the system is evolving along a trajectory in configuration space during a certain time interval τ, and along that given trajectory we are recording the change in the proposed definition of entropy, see equation (4.1). If we repeat

the measurement a large number of times for the same fixed time interval τ, we obtain the probability distribution of the entropy change. The distribution itself depends on the time interval τ and the microscopic dynamics of the model. The statement of linear growth is true for the average value of entropy change but the distribution itself shows important fluctuations for the small systems that we are investigating. The systems that are analyzed are models 2, 3 and 4. During short time intervals the distribution of the change in entropy should reveal signatures of the underlying dynamics. Indeed, as it was discussed in the previous chapter, the connectedness in configuration space is qualitatively different in the three models. This should have significant impact on the properties of the distributions of total entropy change.

4.1.1 Method

In order to obtain the distribution of entropy change $\Delta s_{\rm tot}$ in a single steady state the complete ensemble of possible trajectories is analyzed. Along each trajectory we evaluate the total entropy change,

$$\begin{aligned}\Delta s_{\rm tot} &= \ln \frac{P_s(C_0)}{P_s(C_\tau)} + \ln \prod_{\{i\}} \frac{\omega(C_i \to C_{i+1})}{\omega(C_{i+1} \to C_i)} \\ &= \ln \frac{P_s(C_0)}{P_s(C_M)} + \Delta s_m \end{aligned} \tag{4.1}$$

$\{i\}$ labels the sequence of configurations of the trajectory, and the length of the sequence grows with measurement time M. Due to the fact that we are looking at short times, we are considering the boundary term, $\ln \frac{P_s(C_0)}{P_s(C_M)}$, for finite time in addition to the medium entropy $\Delta s_{\rm m}$. The boundary term can only be neglected in the long time limit, see section 2.3.
As it was shown, a detailed fluctuation relation exists in a single steady state, as long as microscopic reversibility holds [96]:

$$\frac{P(\Delta s_{\rm tot})}{P(-\Delta s_{\rm tot})} = e^{\Delta s_{\rm tot}}. \tag{4.2}$$

The probability distribution P is the histogram of the outcome of a large number of realizations. In section 2.3 it was claimed that the fluctuation symmetry is a symmetry on the level of rate functions defined in the long time limit, when the probability distribution of entropy change can be written as

$$P(\Delta s_{\rm tot}) \cong e^{-t\chi(\sigma)} \quad t \gg 1 \tag{4.3}$$

where $h(\sigma)$ is called the rate function of entropy production. At short times the probability distribution is not simply given by an exponentiated product of time t with a time independent rate function. For this reason, we calculate in the following the entropy as the integral

over the measured time interval τ. Mathematically we define the integrated rate function as

$$X(\Delta s_{\mathrm{tot}}) = -\ln P(\Delta s_{\mathrm{tot}}). \tag{4.4}$$

We are going to discuss the integrated rate function and the average value of entropy change $\langle \Delta s_{\mathrm{tot}} \rangle$ for different measurement times M and different system sizes N. We thereby focus our analysis of the dependence of the reaction rates on prominent features. This adds to the discussion of stationary probabilities and current amplitudes in the previous chapter.

4.1.2 Variation in Time and System Size

Let us start with model 2. In figure 4.1 we are presenting for a fixed set of parameters the dependence of $X(\Delta s_{\mathrm{tot}})$ on the measurement time M and on the system size N. The

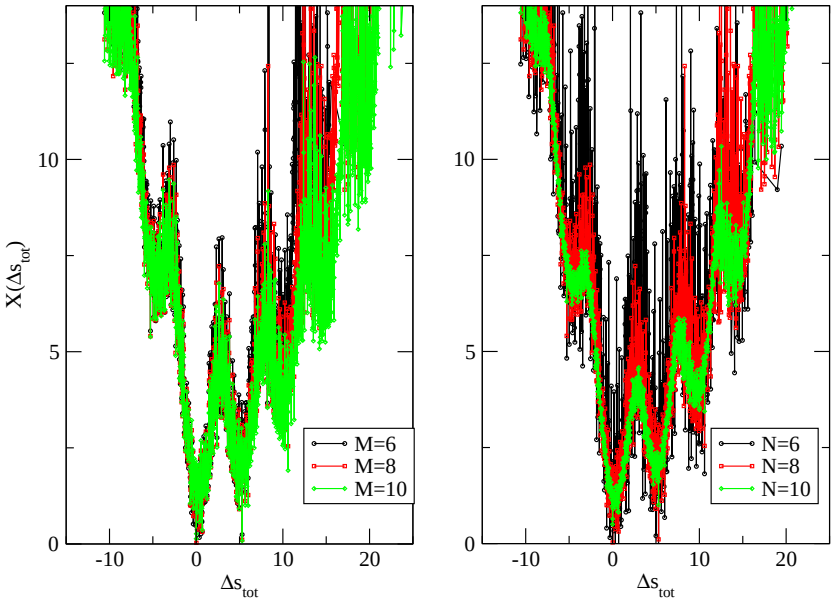

Figure 4.1: Integrated rate function of entropy increase $X(\Delta s_{\mathrm{tot}})$ in the steady state of model 2 as a function of the total measurement time M (left) and system size N (right). The parameters are $D = 1$, $h = 0.5$, $\lambda = 1$ and $\varepsilon = 0.01$. (left) $N = 8$ and (right) $M = 8$.

integrated rate functions for model 2 show modulations. The positions of the peaks neither depend on the time interval M nor on the system size N. The dependence on other system parameters is discussed in the next subsection. We also notice that the part of negative entropy change stays invariant for larger M.

Let us go on to discuss model 3, see figure 4.2. We will not display the results for model 4 as they are very similar to those obtained for model 3. Model 3 shows a very irregular distribution, mainly made up of single peaks. The same irregular shape is seen in the

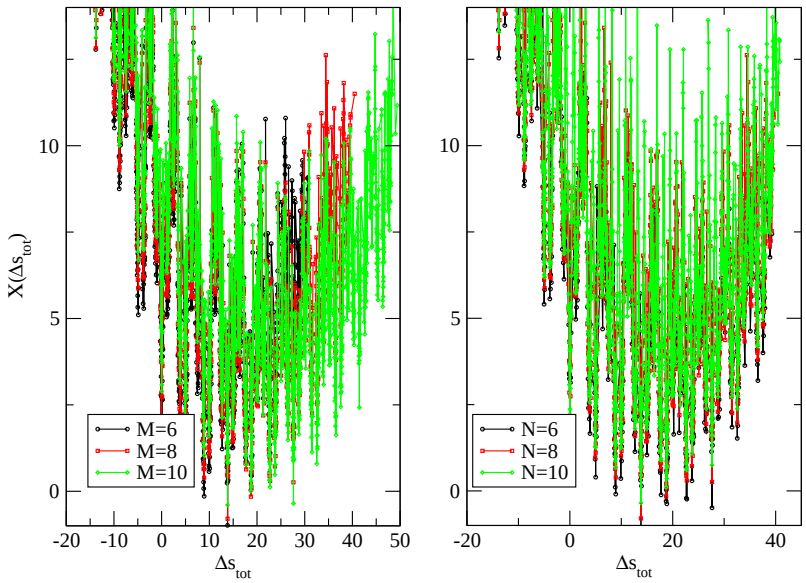

Figure 4.2: Integrated rate function of entropy increase $X(\Delta s_{\mathrm{tot}})$ in the steady state of model 3 as a function of the total measurement time M (left) and system size N (right). The parameters are $D = 1$, $h = 0.5$, $\lambda = 1$ and $\varepsilon = 0.01$. (left) $N = 8$ and and (right) $M = 8$.

distributions of model 4. We notice that the support of the rate function for model 3 (and model 4) is greater than for model 2 by a factor of two. The distances between peaks in the integrated rate function for model 3 and 4 are of comparable magnitude as for model 2 and are also independent of the time interval and the system size as it was the case for model 2. Using these distributions, we calculate the mean values of the total entropy change for all three models, see figure 4.3. Interestingly, in all three models we are already in the regime where the mean entropy change grows linear in both the system size N and the measurement time M. The slope is far greater for model 3 and model 4 than for model 2 and shows qualitatively the same hierarchy as inferred from the discussion of the probability currents.

4.1.3 Variation of the Reaction Rates

Let us go ahead and discuss the influence of the diffusion amplitude D and of the reversibility parameter ε. Both parameters should have a strong effect on the distributions. If the amplitude of diffusion exceeds the reaction rates, then trajectories with small number of reactions are favored and vice versa. The effect of varying diffusion constant D on the integrated rate function is shown in figure 4.4 for model 2 and model 3.

We see that the modulations, present in all three models, are changing with the value of the diffusion constant D. The peak at $\Delta s_{\mathrm{tot}} = 0$ is not changing its position but the neighboring peaks to the left and to the right are located at varying distances. From the data for model 2,

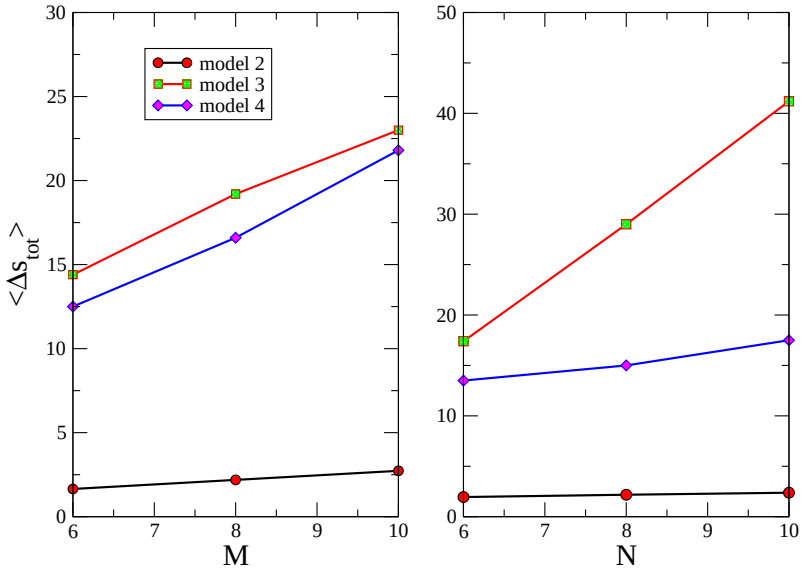

Figure 4.3: Expectation value of the mean entropy increase in the steady state as a function of the total measurement time τ (left) and system size N (right). The parameters are $D = 1$, $h = 0.5$, $\lambda = 1$ and $\varepsilon = 0.01$. (left) $N = 8$ and and (right) $M = 8$.

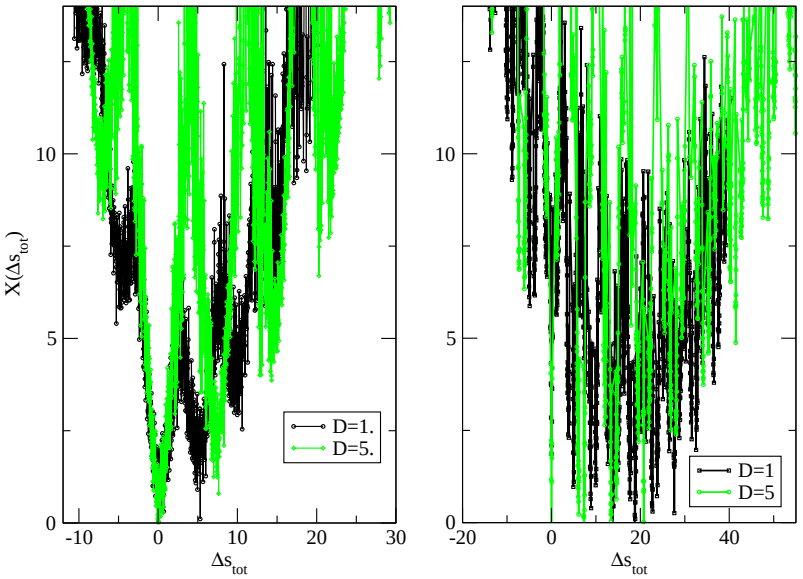

Figure 4.4: Integrated rate function of entropy increase $X(\Delta s_{\mathrm{tot}})$ in the steady state of model 2 (left) and model 3 (right) as a function of the diffusion constant D. The parameters are $N = 8$, $M = 8$, $h = 0.5$, $\lambda = 1$ and $\varepsilon = 0.001$.

see figure 4.4(left), we infer that the distance between the peaks for the values $D = 0.1, 1, 5$ does not vary monotonously with the rate of diffusion. The smallest periodicity is present in the case of $D = 1$. For the values $D = 0.1$ (not shown) and $D = 5$ the distance is larger

than for $D = 1$. A simple mathematical relation to relate the periodicity of the peaks to the changing diffusion amplitude D does not seem to exist.
In the next step the dependence on the reversibility parameter ε is investigated, see figure 4.5. The decrease in ε has two important effects. On the one hand the probability of a rare trajectory involving transitions multiplied by ε will decrease if we decrease ε. On the other hand the range of values for Δs_{tot} is increasing since information about the degree of non reversibility between the forward and the reversed trajectories enter the observable. Transitions that are proportional to ε cause either a large or a very small value for the ratio of trajectories, and the entropy change then contains a term proportional to $\ln \varepsilon$ which will cause a larger variation in the possible measured values of the entropy change Δs_{tot}, see equation 4.11 below.

This expected behavior is confirmed for model 2 and model 3, and a strong dependence of the

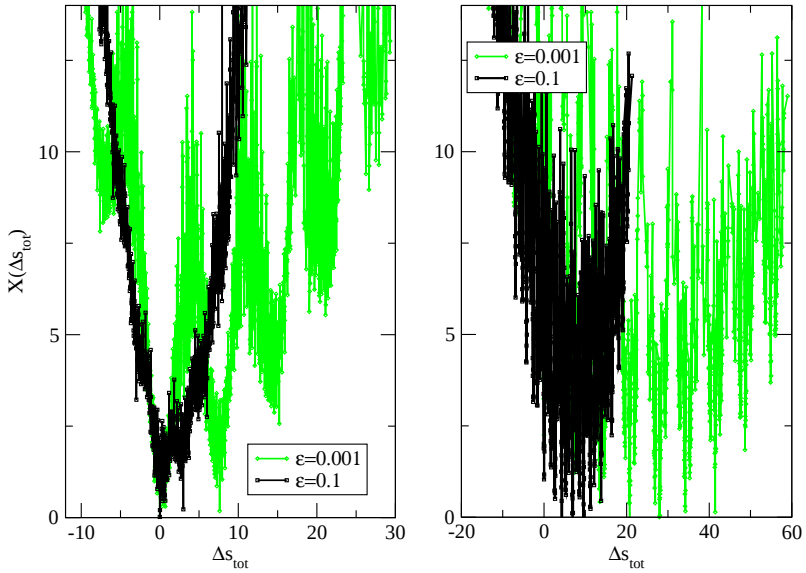

Figure 4.5: Integrated rate function of entropy increase $X(\Delta s_{\mathrm{tot}})$ in the steady state of model 2 (left) and model 3 (right) as a function of the reversibility ε. The parameters are $N = 8$, $M = 8$, $h = 0.5$, $\lambda = 1$ and $D = 1$.

modulations on the reversibility parameter ε exists. Both the amplitude of the modulations as well as the periodicity are changing with decreasing value of ε. A simple relation to superpose the distribution could not be found. The effect of ε and D is similar for all models. The discussion of the distributions as a function of the reaction rates follows.

In figure 4.6 both the creation rate h and the annihilation rate λ are discussed for model 2 whereas models 3 and 4 are discussed in figures 4.7 and 4.8. The positions of the peaks vary with the value of the reaction rates but the peaks are still equidistant. For model 2 the distances decrease for larger values of the creation rate, see figure 4.6(left), and increase for larger values of the annihilation rate, see figure 4.6(right). The parameter regime that corresponds to small values of h and large values of λ is the low density regime which for

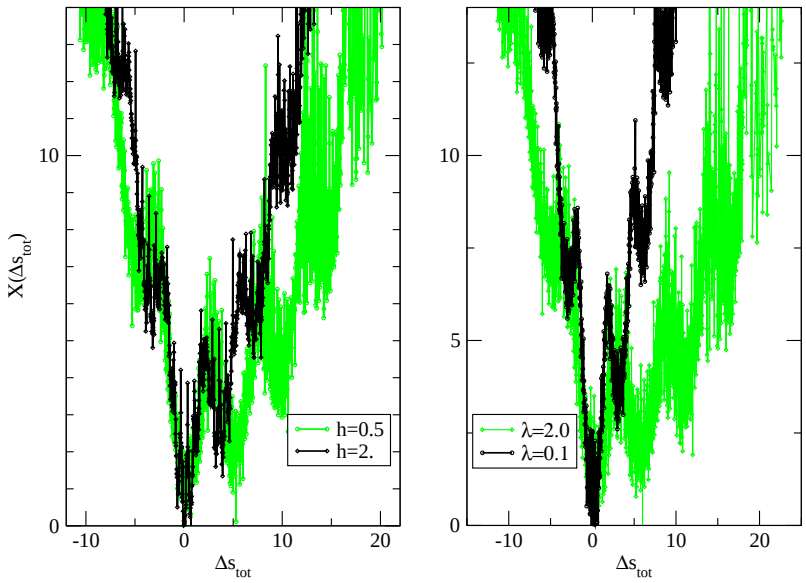

Figure 4.6: Integrated rate function of entropy increase $X(\Delta s_{\mathrm{tot}})$ in the steady state of model 2 as a function of the creation rate h (left) and annihilation rate λ (right). The common parameters are $N = 8$, $M = 6$, $D = 1$, $\varepsilon = 0.01$. The annihilation rate is $\lambda = 1$ (left) and the creation rate is $h = 1$ (right).

model 2 corresponds to the largest values of the probability current amplitude K. The extracted values for the distances are listed in table 4.1.

For models 3 and 4 the distributions are very rough. Qualitatively we see for both models that the distance between peaks is growing with increased creation rate as well as annihilation rate. This result is different than that for model 2. In table 4.1 the mean distances for different reaction rate combinations are listed, showing that in general the distances are of the same order of magnitude as for model 2. A simple relation for the periodicity as a function of the reaction parameters is difficult to obtain for models 3 and 4. Only for model 2 do the distances between neighbouring maxima in the integrated rate function have a linear dependence on the reaction rates.

To finish this first section on the total entropy change in a single steady state, we are going

Table 4.1: Mean distance of the maxima in the rate function for models 2, 3, and 4 for different values of annihilation rate λ and creation rate h with $D = 1$, $\varepsilon = 0.01$. The system size is $N = 8$ and the driving length is $M = 6$.

h	model 2	model 3	model 4	λ	model 2	model 3	model 4
0.5	4.7	3.8	4.3	0.1	2.9	2.8	3.7
1.0	4.1	4.1	4.6	1.0	3.2	3.5	4.5
2.0	3.5	4.2	4.7	2.0	3.6	4.5	4.7

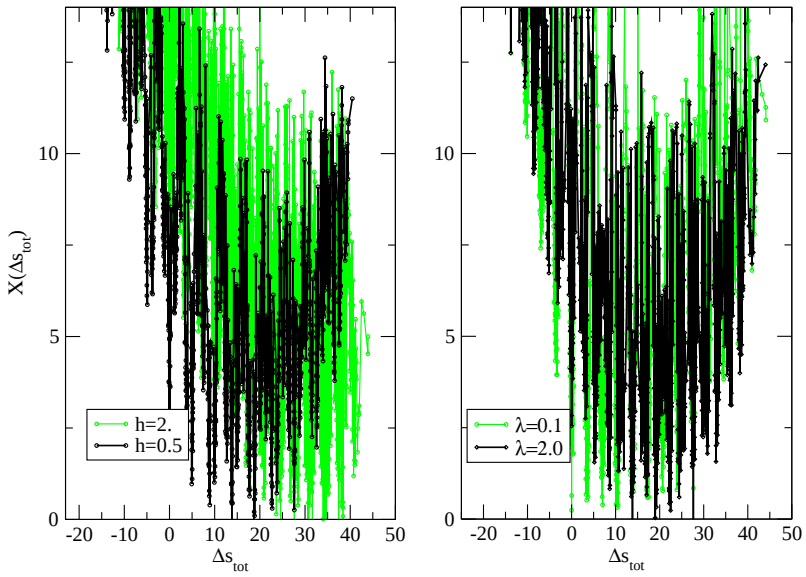

Figure 4.7: Integrated rate function of entropy increase $X(\Delta s_{\mathrm{tot}})$ in the steady state of model 3 as a function of the creation rate h (left) and annihilation rate λ (right). The common parameters are $N = 8$, $M = 6$, $D = 1$, $\varepsilon = 0.01$. The annihilation rate is $\lambda = 1$ (left) and the creation rate is $h = 1$ (right).

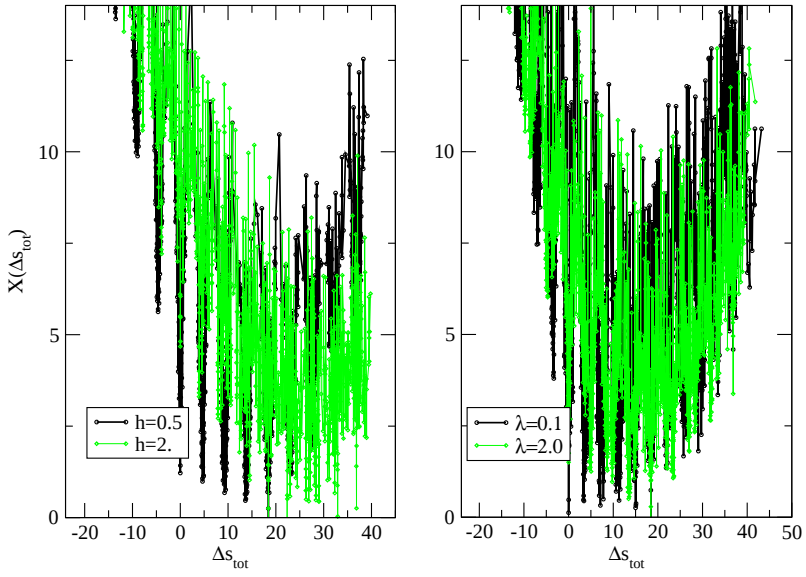

Figure 4.8: Integrated rate function of entropy increase $X(\Delta s_{\mathrm{tot}})$ in the steady state of model 4 as a function of the creation rate h (left) and annihilation rate λ (right). The common parameters are $N = 8$, $M = 6$, $D = 1$, $\varepsilon = 0.01$. The annihilation rate is $\lambda = 1$ (left) and the creation rate is $h = 1$ (right).

to present the fluctuation relation [142] for the distributions that we have just analyzed. As a result of the exact enumeration scheme of all possible trajectories, the exponential relation that relates probabilities of positive to negative changes in the entropy is also exact, see figure 4.9. The irregular distributions we were discussing in this section are difficult to

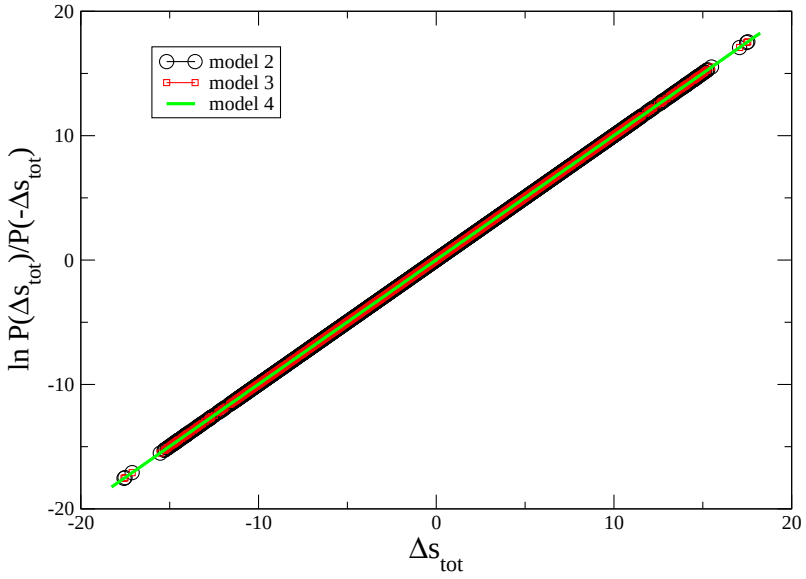

Figure 4.9: Detailed fluctuation relation of the total entropy change in a single steady state for models 2, 3, and 4. The parameters are $N = 8$, $M = 6$, $D = 1$, $\varepsilon = 0.01$, $\lambda = 1$, and $h = 0.5$.

interpret. Immediate relations between the microscopic rules of the dynamics and features in the distributions cannot be presented. The results therefore serve to complete the discussion of characterizing steady states and will allow us to compare the short term behavior to the long term behavior that is discussed in the following.

4.2 Rate Functions for Entropy Production

Large deviation functions (LDF) are of great importance in the description of equilibrium as well as non-equilibrium systems. Their mathematical structure is the basis of the modern approach to equilibrium statistical mechanics [33, 154] with the entropy of a given configuration being the large deviation function. The field in mathematics of large deviation functions was established by Ellis [50]. In the field of non-equilibrium statistical mechanics, steady state fluctuation relations are an example of large deviation functions. For non-equilibrium systems we are interested in the large deviation function in the long time limit. First explicit discussions of large deviation functions for simple systems include for example biased random walkers, overdamped particles, and the zero range process [36, 37, 38, 51, 59, 64, 96, 97, 142].

It was argued in [96, 103] that model dependent and universal features need to be discussed to extend our knowledge of non-equilibrium systems in the context of large deviation functions of total entropy production. Large deviation functions are also called rate functions of entropy production. In the next subsection we give a short review of the results presented by Mehl et al. [103].
The mathematical approach that we are exploiting is based on the work by Lebowitz and Spohn [96], already outlined in section 2.3. Our goal is to extend the findings in [103] and discuss interacting many particle systems to understand in more detail what the universal and what the model dependent features in the long time limit are. We discuss the mean entropy production rate before we present the normalized entropy production rate functions. The main emphasis is on the behavior of the kink at zero entropy production rate as pointed out in [103]. We then summarize our results.

4.2.1 Motivation and Outline

We here review the results that were obtained by Mehl et al. for the rate function of entropy production [103]. Their work discussed, for explicit examples, the shape of the rate functions. The models that have been studied in their paper are the asymmetric random walker and a single overdamped particle.The found kink at zero entropy production is related to the non reversibility of the system and trajectories of the system with negative entropy change. In the context of current distributions in driven systems' kinks were already reported in the long time limit in [97]. It was argued by the authors of [103] that the kink should be analyzed in more complex systems in order to better understand its origin.
This is the motivation of this section. For the stochastic models introduced in chapter 3 we are going to discuss as a function of the system parameters the kink at zero entropy production that we numerically obtain for the reaction-diffusion as well as the transport models. Following the demonstration of the steady state fluctuation relation in section 2.3, we determine the deformed Liouville operator L_μ,

$$\begin{aligned} L_\mu &= \sum_{C'} \omega(C' \to C) e^{-\mu \ln \frac{\omega(C' \to C)}{\omega(C \to C')}} - \sum_{C'} \omega(C \to C') \\ &= \sum_{C'} \omega(C' \to C)^{1-\mu} \omega(C \to C')^{\mu} - \sum_{C'} \omega(C \to C'). \end{aligned} \tag{4.5}$$

This operator allows us to calculate the time evolution of the change of entropy in the medium Δs_{m},

$$\Delta s_{\mathrm{m}} = \ln \prod_{\{i\}} \frac{\omega(C_i \to C_{i+1})}{\omega(C_{i+1} \to C_i)} \tag{4.6}$$

In the long time limit, the largest eigenvalue $e(\mu)$ of L_μ is allowing us to calculate the asymptotic form of the generating function. The eigenvalue $e(\mu)$, as it was demonstrated in

section 2.3, obeys the fluctuation symmetry,

$$e(\mu) = e(1-\mu). \tag{4.7}$$

Based on this relation we note that the eigenvalue is symmetric and possesses a maximum at $\mu = 0.5$ and the eigenvalue is equal to zero at $\mu = 0$ and $\mu = 1$. The next step is to calculate from the numerical data the Legendre transform [163] of the smallest eigenvalue

$$\chi(\sigma) = \max_{\mu}\{e(\mu) - \langle \dot{s_{\mathrm{m}}}\rangle \mu\sigma\}. \tag{4.8}$$

where $\sigma = \Delta s_{\mathrm{m}} / \left(t\langle \dot{s_{\mathrm{m}}}\rangle\right)$ is the normalized entropy production rate. Symmetry (4.7) translates into

$$\chi(-\sigma) = \chi(\sigma) + \langle \dot{s_{\mathrm{m}}}\rangle\sigma, \tag{4.9}$$

and translates into the following symmetry for the probability distributions $P(\sigma)$,

$$\lim_{t\to\infty} \frac{P(\sigma)}{P(-\sigma)} = e^{\langle \dot{s_{\mathrm{m}}}\rangle\sigma}. \tag{4.10}$$

4.2.2 Mean Entropy Production Rates

The variable σ is divided by the expectation value of the entropy production rate $\langle \dot{s_{\mathrm{m}}}\rangle$. Due to the normalization, the information of the mean entropy production rate is lost once we are going to discuss explicitly the function $\chi(\sigma)$. For this reason we first analyze the expectation value $\langle \dot{s_{\mathrm{m}}}\rangle$ to understand its dependence on the reaction and hopping rates. The different models are going to be discussed one after the other.

Let us start with model 2. For different fixed values of the annihilation rate λ, we calculate the expectation value of the mean entropy creation rate as a function of the creation rate h. In the limit of $h \to 0$, we expect, for all values of λ, that the mean entropy creation rate goes to zero. Entropy cannot be created if the system stays empty and no particles are added during the process. If h increases, the expectation value should increase. As we have explained in section 3.3, model 2 actually is only out of equilibrium as long as the system is at low densities. Therefore we expect that for large enough creation rates, the mean entropy creation rate decreases back to zero because of detailed balance. Due to both limiting cases at $h = 0$ and $h \gg \lambda$, a maximum has to exist at some $\lambda_c(h)$. The numerical analysis, see figure 4.10, confirms this expectation. The slope depends on the combination of h and λ and the maximum fulfills the relation $\lambda \approx 2.5h$ for the range of parameters investigated. It is interesting to analyze the impact of this maximum on the rate function $\chi(\sigma)$ in the next subsection, see figure 4.18. This maximum is a property that is inherent to model 2 and is not found for the other models studied here.

Model 3 and model 4 are not effectively reducing to an equilibrium system for large creation rates h because the change in the number of particles is not matching for individual creation and annihilation transitions. We therefore expect a monotonous increase in the expectation

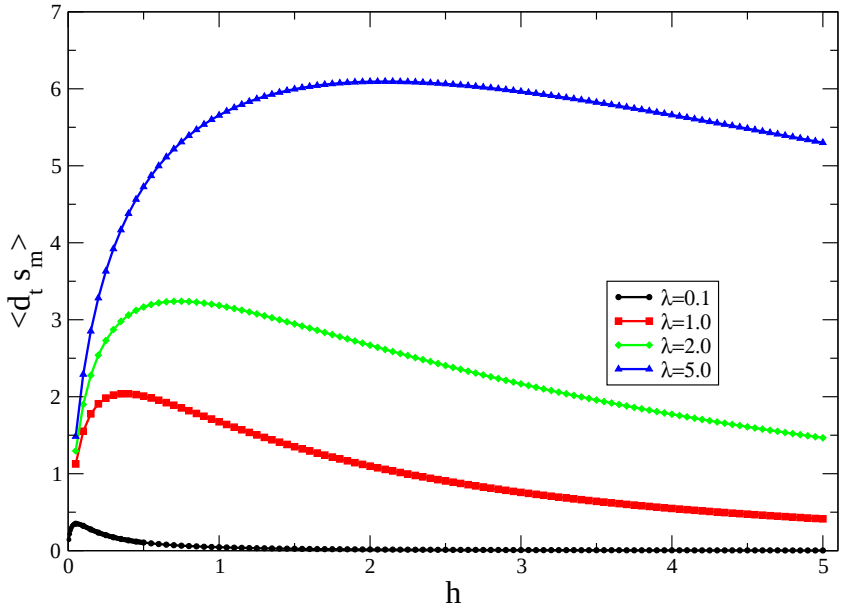

Figure 4.10: The mean entropy production rate $\langle \dot{s_{\mathrm{m}}} \rangle$ of model 2 for different values of the annihilation rate λ as a function of the creation rate h. The calculation is done for $D = 0.5$, $\varepsilon = 0.01$, and $N = 8$.

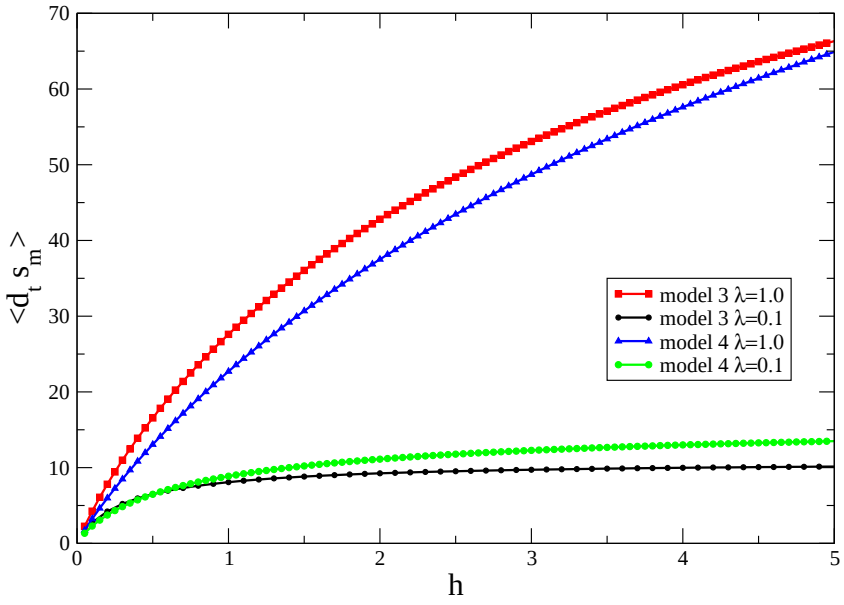

Figure 4.11: The mean entropy production rate $\langle \dot{s_{\mathrm{m}}} \rangle$ for model 3 and 4 for different values of the annihilation rate λ as a function of the creation rate h. The calculation is done for $D = 0.5$, $\varepsilon = 0.01$, and $N = 8$.

value due to the increasing probability to destroy a pair or a triplet of particles. Figure 4.11 displays the results for model 3 and model 4 for different values of the annihilation rate λ as a function of the creation rate h. For the investigated parameter range, the mean entropy production rate is indeed monotonously growing. As it was the case for model 2, the mean entropy production rate is zero at $h = 0$. For large values of h, however it converges monotonously to a plateau value at very large h as can be seen in the case of $\lambda = 0.1$ for both models. For the same values of λ model 3 converges faster to its plateau than model 4. We also notice that the two curves cross each other at $h \approx 0.6$ and that for general λ the mean value of the two models cross at $\lambda^*(h) = 0.18h$. The reason for the crossover is the nature of the annihilation process. The effectiveness of the annihilation depends on two key features, the frequency of annihilation and the change of the stationary probabilities of the two configurations before and after the transition. At very low values of the creation rate the process $2A \to 0$ happens with higher frequency than the process $3A \to 0$. Therefore model 3 has a larger mean entropy creation rate. This changes for large values of h because the frequency of annihilation is high for both models but the change of stationary probabilities along the trajectory is more important for model 4. As a consequence the mean entropy production rate is expected to be larger for model 4. In between these limiting regimes the crossover has to be expected. In the case $\lambda = 1$ the crossover cannot be seen for the parameter range of h investigated and a plateau is not yet reached. A plateau is expected for larger values of the creation rate. As we have seen from the analysis, the three reaction-diffusion models behave differently as a function of the creation rate h, resp. h/λ.
We discuss also the effect of the reversibility parameter ε for a fixed set of reaction rates. The value of the mean creation rate has to decrease to zero when the parameter ε reaches one because detailed balance is then satisfied. In contrast, it should increase with decreasing ε because of the increase of the degree of non reversibility. Let us present in figure 4.12 the results for all three models for a given set of reaction rates. We see that all three models behave qualitatively in the same way. For small enough values of ε, resp. large values of $-\ln\varepsilon$, the increase is linear in all three models. The linear increase in the expectation value is related to the logarithm of the transition rates that enter along a given trajectory. In general terms the change in entropy can be written as

$$\begin{aligned} \dot{s}_m(X) &= \lim_{\Delta t\to 0}(\Delta t)^{-1}\ln\prod_{i=0}^{\Delta t}\frac{\omega(C_i\to C_{i+1})}{\omega(C_{i+1}\to C_i)} \\ &= A(X) + B(X)\ln\varepsilon \end{aligned} \tag{4.11}$$

for each trajectory X where B is related to how many transitions occur that are weighted by ε. Since we are interested in the mean value of $\dot{s}_m$, we need to average over all possible trajectories X. The average over the trajectory dependent parameter B provides us with the mean number of trajectories that carry information about ε. For values $-\ln\varepsilon \to 0$ the linear relation does not hold anymore and a flattening towards zero is observed, with the limit $-\ln\varepsilon \to 0$ satisfying detailed balance.
For completeness, we are also analyzing mean entropy production rates for the two transport

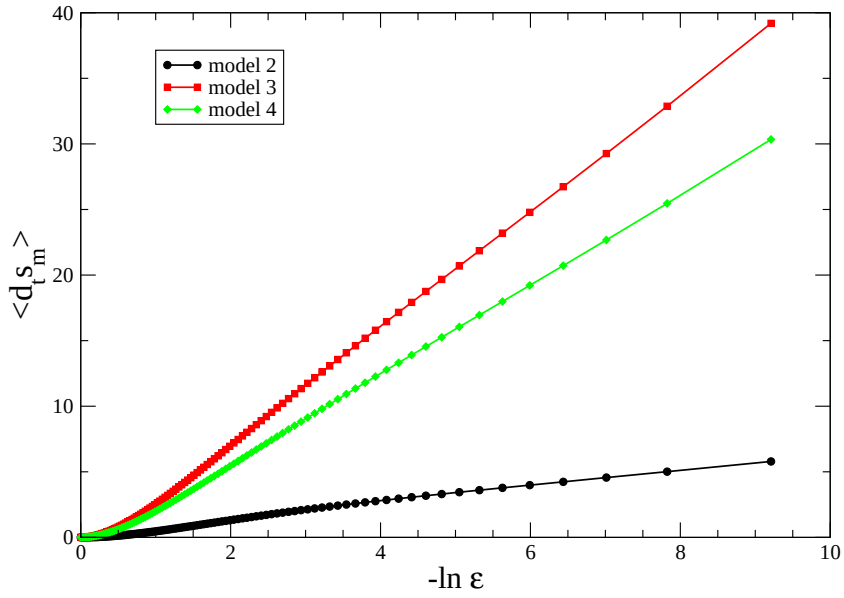

Figure 4.12: The mean entropy production rate $\langle \dot{s_{\mathrm{m}}} \rangle$ for models 2, 3, and 4 as a function of the parameter $-\ln \varepsilon$. The calculation is done for $h = 0.5$, $\lambda = 2$, $D = 0.5$, and $N = 8$.

models defined in section 3.3. The varied parameter is the entrance rate α. We calculate the expectation value for the symmetric diffusion in the bulk (SSEP), i.e. the hopping rate is $p = 0.5$, and the biased hopping to the right (ASEP) where $p = 0.95$. We expect the amplitude in the case of biased hopping to be larger than in the case of symmetric hopping. The results are presented in figure 4.13(left). Starting out from $\langle \dot{s_{\mathrm{m}}} \rangle = 0$ for the case of zero entrance rate the expectation value increases monotonously and for values $\alpha \to 1$, i.e. for large enough entrance rates, converges to a plateau. The convergence to the plateau value is slower for larger p. This convergence can be explained by the fixed exit rate β because the system becomes more and more filled with particles for larger values of α.
In figure 4.13(right) we are discussing two additional values of the exit rate β for the case of biased hopping $p = 0.95$. This permits us to discuss the parameter dependence of the crossover to the plateau. We see that this crossover is varying with respect to the exit rate β. We also see that a kink is observed for the value $\beta = 0.25$, in contrast to the two larger values of β which do not display this feature. We analyze this kink in more detail for the biased bulk hopping in figure 4.14 where we present a detailed analysis for a large number of values β. To quantify the kink, we are looking at the first and second derivatives of the expectation value with respect to the creation rate α. Since the kink is not observed for the hopping rate $p = 0.5$, we are looking at the even greater biased case of $p = 0.995$ and reversibility parameter $\varepsilon = 0.001$.

The kink in the limit of extremely biased hopping shows a second derivative with a maximum growing in amplitude for larger values of p. For a fixed value of p small values of the exit rate β show a more important peak in the second derivative. The peak is located at values $\beta \approx \alpha$ and vanishes for $\beta \to 1$. We interpret this result as a signature of the transition

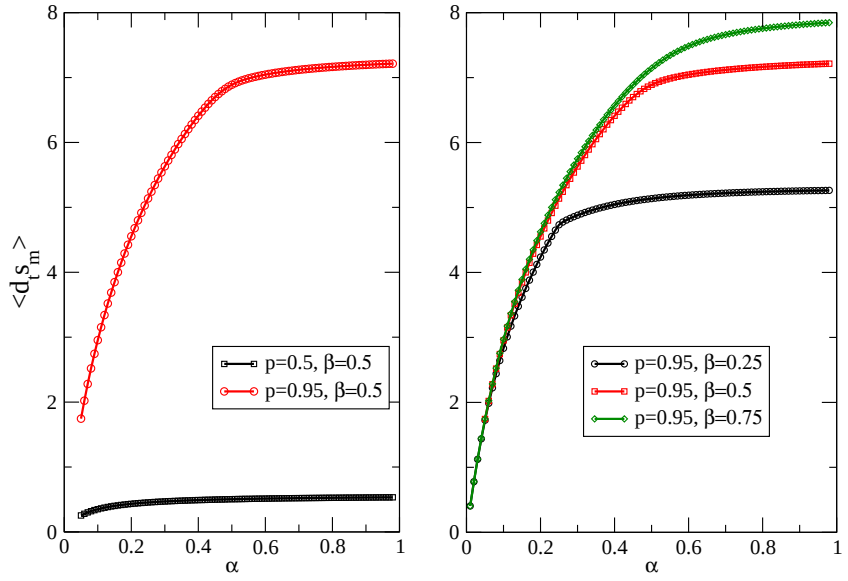

Figure 4.13: The mean entropy production rate $\langle \dot{s_{\mathrm{m}}} \rangle$ as a function of the entrance rate α for (left) two different bulk hopping rates p at constant exit rate β and (right) for different values of the exit rate β at constant hopping rate p. The calculation is done for $\varepsilon = 0.01$, and $N = 8$.

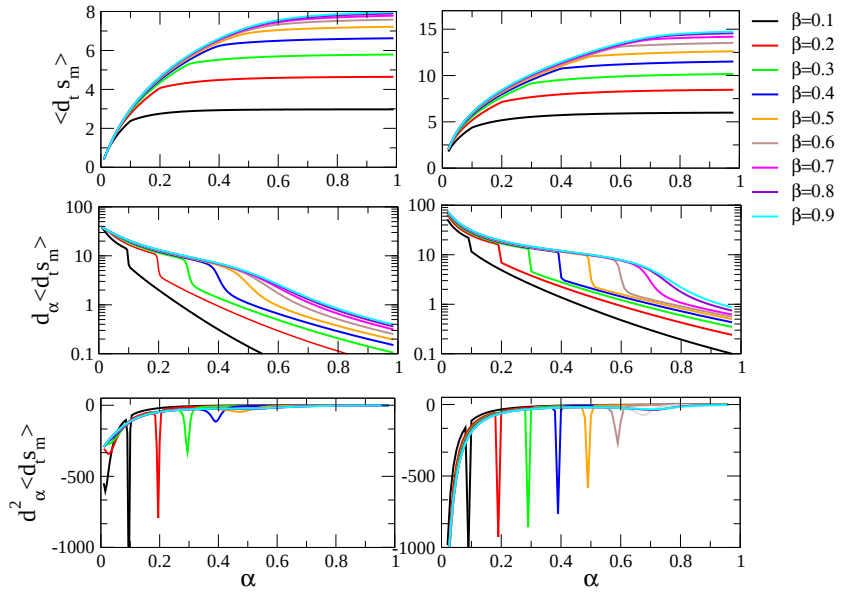

Figure 4.14: (top) The mean entropy production rate $\langle \dot{s_{\mathrm{m}}} \rangle$ as a function of the entrance rate α, (middle) its first derivative with respect to α, and (down) its second derivative. The column to the left has the parameters $p = 0.95$, $\varepsilon = 0.01$, and $N = 8$. The column on the right has the parameters $p = 0.995$, $\varepsilon = 0.001$, and $N = 8$.

line between the low density and high density phase, see illustration 3.4. This observation is investigated further in the next subsection that discusses rate functions.

4.2.3 Rate Functions

We now go ahead and analyze the normalized rate function $\chi(\sigma)$ for the different models. The presentation of the numerical results is the following in the different figures. The data for a given set of parameters is arranged in a column. On the top, we are showing the dependence of the largest eigenvalue of the Liouville operator $e(\mu)$ as a function of the parameter μ. In the middle of the column we calculate, starting from the eigenvalue $e(\mu)$, its Legendre transform $\chi(\sigma)$, the rate function of the entropy production. Generally as a result of the normalization by the expectation value, the Legendre transform always presents a minimum at $\sigma = 1$. This allows us to compare the support and the range of variation. In order to discuss in more detail the appearance of a kink at $\sigma = 0$ we calculate the derivative of the rate function $\chi(\sigma)$ at the bottom of the column. If a kink exists, its derivative at the origin should have a discontinuity. The value of the discontinuity is then quantified and analyzed in more detail.
Since we are interested in the kink at zero entropy production, we want to start out with the system size dependence. We want to see if the kink becomes more important for larger system sizes or if the kink is vanishing. The results are presented in figure 4.15 for model 3. The analysis of the numerically accessible system sizes shows the following relation for the discontinuity at $\sigma = 0$ for the reaction-diffusion models:

$$\text{model2} \quad \chi'(0^+) - \chi'(0^-) = 0.026 \cdot N \tag{4.12}$$

$$\text{model3} \quad \chi'(0^+) - \chi'(0^-) = 18.5 \cdot N \tag{4.13}$$

$$\text{model4} \quad \chi'(0^+) - \chi'(0^-) = 77 \cdot N \tag{4.14}$$

The conclusion is that in all three models the discontinuity of the derivative is increasing proportional to the system size and the factor of proportionality differs for the three models. In figure 4.16 we show our data for model 2. The dependence on the creation rate h for two different values of the annihilation rate λ is presented. In the case of $\lambda = 0.1$(left) we observe a flat plateau for the eigenvalue $e(\mu)$ that is broadening with increasing creation rate h. The maximum value at $\mu = 0.5$ is decreasing towards zero for larger values of h and the drop-off at large values of the parameter μ is constant. The rate function $\chi(\sigma)$ is increasing less steeply with increasing creation rate and the jdiscontinuity in the derivative is less pronounced. The results for the annihilation rate $\lambda = 5$ show that the dependence of the eigenvalue and rate function is not monotonous with increasing creation rate. This is based on the same arguments we were already presenting in the discussion of the mean entropy production rate. In figure 4.17 we discuss the amplitude of the discontinuity as a function of h for two values of λ. The important behavior seen in the figure is the non monotonic dependence of the strength of the kink given by the discontinuity of the first derivative of

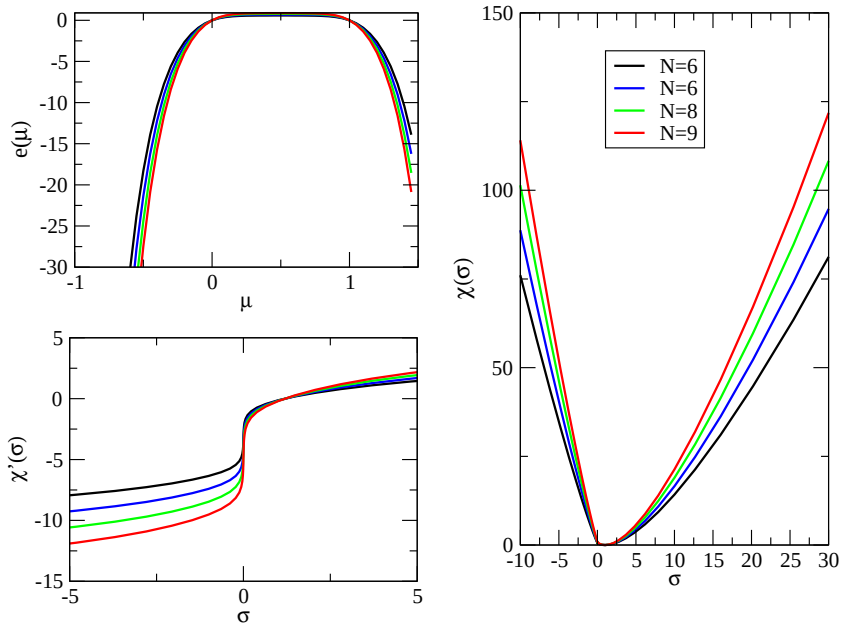

Figure 4.15: The results of model 3 show the smallest eigenvalue $e(\mu)$ of L_μ (up left), the rate function of the entropy production $\chi(\sigma)$ (right), and its derivative with respect to σ (down left) for varying system size N. The parameters in this calculation are $h = 1.0$, $\lambda = 0.1$, $D = 0.5$, and $\varepsilon = 0.01$.

the rate function. The parameter dependence on the amplitude of the kink does present a maximum for the case $\lambda = 5$ as it was already observed in the mean entropy production rate. For the case $\lambda = 0.1$ the evaluated creation rates were already too large to capture the maxima and we therefore only see the decay to zero with increasing h.

The results for model 3 resp. model 4 can be seen in figure 4.18 and 4.19. The plateau in the eigenvalue is larger for the annihilation rate $\lambda = 0.1$(left) than for the value $\lambda = 1$(right). In the latter case we notice almost a quadratic function because the quadratic function is invariant under the Legendre transformation.

To have a better understanding of the strength of the kink we are going to analyze the jump of the derivative at the origin. The results are presented in figure 4.20 for models 3 and 4 and two annihilation rates $\lambda = 0.1$ and $\lambda = 5$. For both models a strong kink is present, the amplitude is increasing monotonously for larger creation rates. The magnitude of the peak in figure 4.20 is far greater than for model 2, see figure 4.20.

Let us end this section with the analysis of the transport processes. We are going to discuss the interesting parameter combinations that showed the kink in the mean entropy production rate, see figure 4.14. We start the analysis by showing in figure 4.21 the data for the symmetric and the biased bulk hopping system for various entrance rates α. We want to understand the influence of different particle densities, directly related to the rate α, on the shape of the rate function. The symmetric hopping case 4.21(left) does not show the kink in the large density, $\alpha \to 1$, limit. Even for very small values of α, the kink is small. The

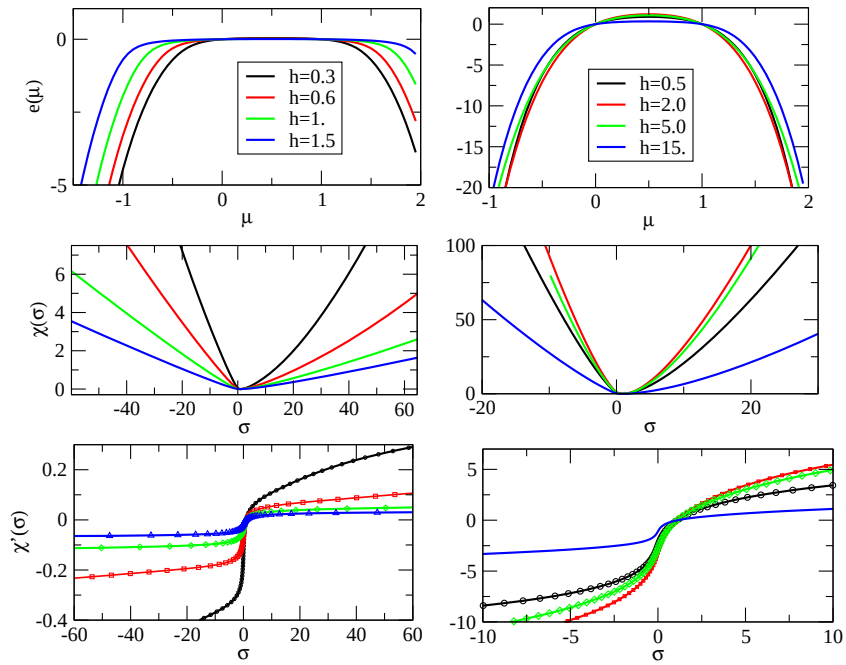

Figure 4.16: The results of model 2 show the smallest eigenvalue $e(\mu)$ of L_μ (up), the rate function of the entropy production $\chi(\sigma)$ (middle), and its derivative with respect to σ (down). Two different values of the annihilation rate $\lambda = 0.1$ (left) and $\lambda = 5.0$ (right) are evaluated for different values of the creation rate h. The other parameters in this calculation are $D = 0.5$, $\varepsilon = 0.01$, and $N = 8$.

eigenvalue function is quadratic for large α. We notice that the rate functions for the values α larger than 0.5 are similar and a superposition is attained in both cases. In the right column of figure 4.21 a kink is present and the rate functions superpose for entrance rates α larger than 0.5. The derivative of the rate function shows that a kink is present for all values of α. We discuss the biased hopping for $p = 0.95$ and $p = 0.995$, the same values as for the mean entropy production rate. Different pairs of the exit rate β and entrance rate α are chosen that correspond to the kinks in the mean entropy creation rate.

The amplitude of the kink is growing for larger values of $\alpha = \beta$. To understand the limit of vanishing jump amplitude of the first derivative of the rate function, we are discussing the case of changing bias in the hopping rate as well as the case of decreased reversibility at the boundaries, see figure 4.23. Since the degree of non reversibility in the bulk is determined by p we are studying the limit $p \to 1$ and analyze the amplitude of the discontinuity, see figure 4.23(left). In figure 4.23 (right) we study in more detail the jump of the first derivative of the rate function as a function of the reversibility at the boundaries with homogeneous hopping in the bulk.

We see that the amplitude in both cases increases as a function of decreased reversibility in the bulk and at the boundaries. From the derivative of the rate function we are obtaining

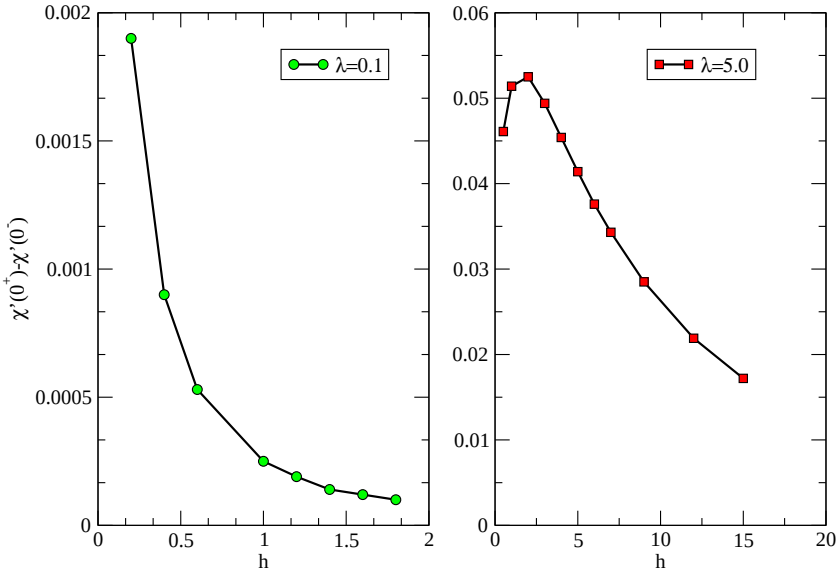

Figure 4.17: The amplitude of the discontinuity of the first derivative of the rate function of model 2 as a function of the creation rate h. (left) the annihilation rate is set to $\lambda = 0.1$ and (right) the annihilation rate is set to $\lambda = 5$. The other parameters in this calculation are $D = 0.5$, $\varepsilon = 0.01$, and $N = 8$.

the following relation for the discontinuity at $\sigma = 0$,

$$\chi'(0, \varepsilon) = 0.82 + 0.16 \ln \varepsilon. \tag{4.15}$$

The amplitude of the discontinuity as a function of the bulk hopping rate does not have a simple relation. The amplitude is increasing rapidly and diverges for $p \to 1$ but a theoretical prediction can not be presented.

4.3 Summary

In chapter 4 we discussed the distributions of total entropy change for reaction-diffusion models and transport models in their non-equilibrium steady states. Important signatures of the dynamics were present in the distributions at short times. We are able to identify modulations in all three reaction diffusion systems. Even though the distributions are very irregular, the steady state fluctuation relation was exact because of the exact enumeration of all possible trajectories. In addition, already at short times we were able to show numerically that the expectation value of the total entropy change is proportional to the system size and measurement time.
In the second part, we showed that rate functions in the long time limit do not display

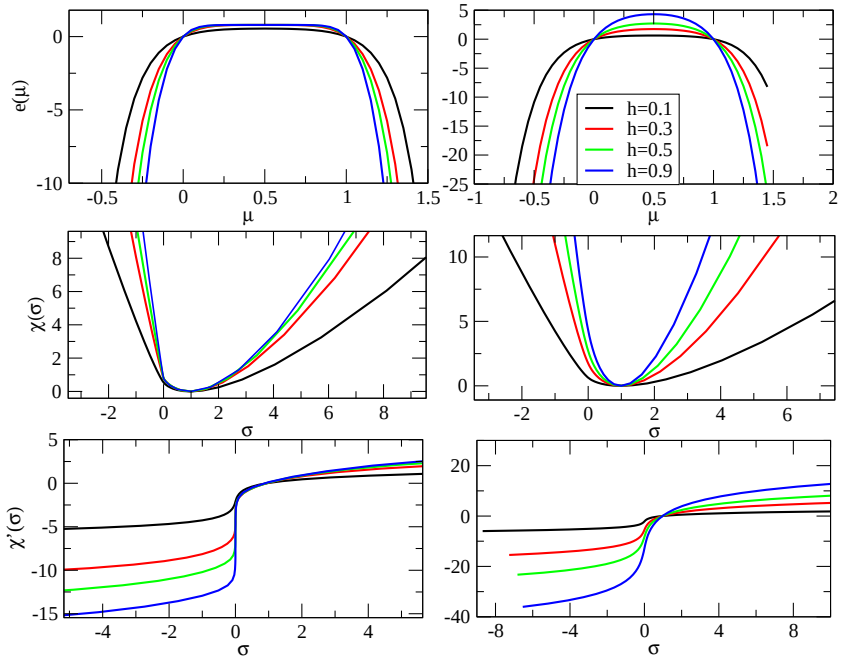

Figure 4.18: The results of model 3 show the smallest eigenvalue $e(\mu)$ of L_μ (up), the rate function of the entropy production $\chi(\sigma)$ (middle), and its derivative with respect to σ (down) for different values of the creation rate h. The other parameters in this calculation are $D = 0.5$, $\varepsilon = 0.01$, and $N = 8$.

modulations. All details of the underlying dynamics are reduced to a kink at zero entropy change. The discontinuity of the first derivative of the rate function showed the same behavior as a function of the system parameters as the probability current amplitude and the mean entropy production rate. The parameter ε allowed us to manipulate the strength of the kink. This confirms that the existence of the kink is model independent and follows even for interacting many particle systems with boundary induced currents and chemical reactions. At this point no thorough understanding of the presence of the kink except that a qualitative behavior related to the mean entropy production exists. The reaction diffusion models will be investigated further in the future and analytical aspects for related models can be added.

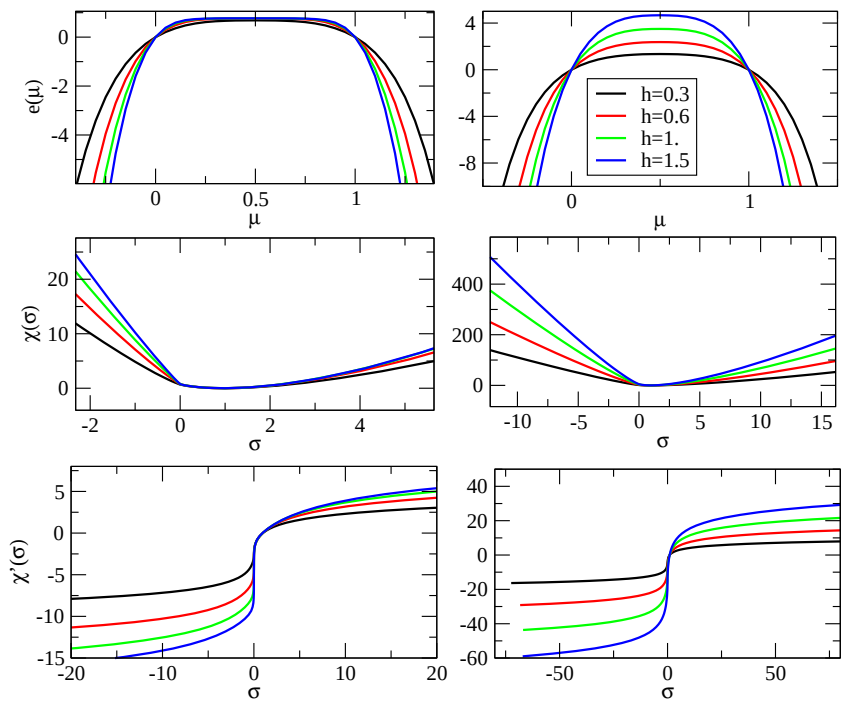

Figure 4.19: The results of model 4 show the smallest eigenvalue $e(\mu)$ of L_μ (up), the rate function of the entropy production $\chi(\sigma)$ (middle), and its derivative with respect to σ (down) for different values of the creation rate h. The other parameters in this calculation are $D = 0.5$, $\varepsilon = 0.01$, and $N = 8$.

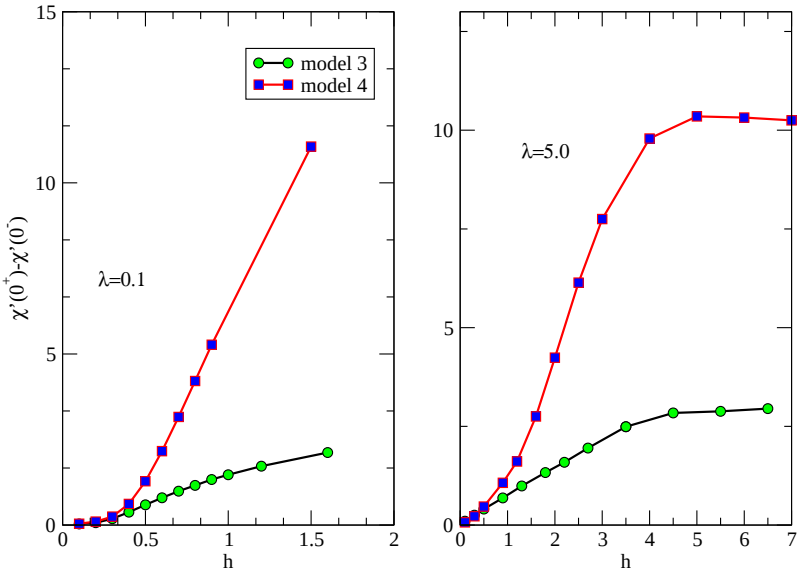

Figure 4.20: The amplitude of the discontinuity of the first derivative of the rate function of model 3 and model 4 as a function of the creation rate h. (left) The annihilation rate is set to $\lambda = 0.1$ and (right) the annihilation rate is set to $\lambda = 5$. The other parameters in this calculation are $D = 0.5$, $\varepsilon = 0.01$, and $N = 8$.

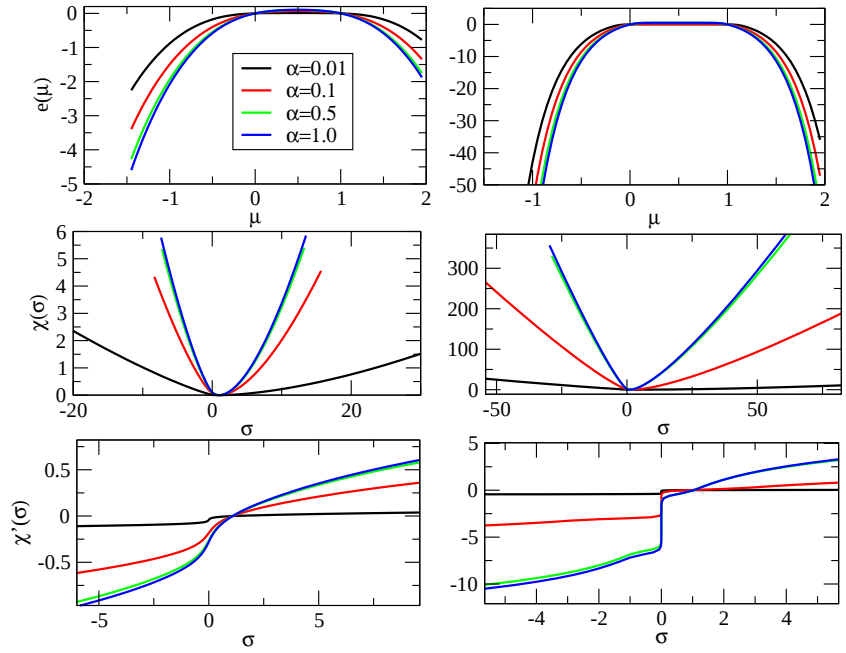

Figure 4.21: The smallest eigenvalue $e(\mu)$ of L_μ (up), the rate function of the entropy production $\chi(\sigma)$ (middle), and its derivative with respect to σ (down) for different values of the entrance rate α for two different bulk hopping rates $p = 0.5$ (left) and $p = 0.95$ (right). The exit rate is $\beta = 0.5$, $N = 8$, and $\varepsilon = 0.01$.

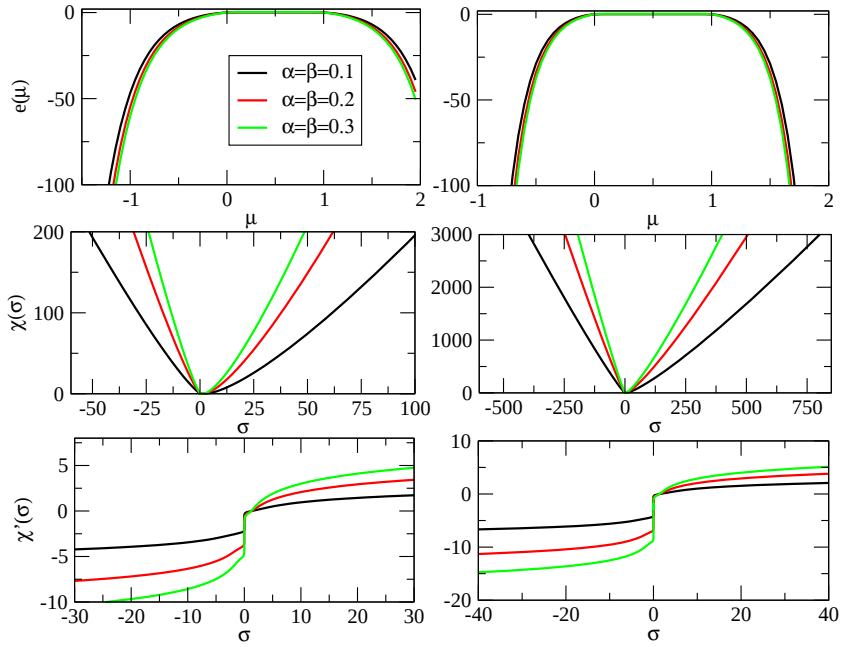

Figure 4.22: The results for the transport models show the smallest eigenvalue $e(\mu)$ of L_μ (up), the rate function of the entropy production $\chi(\sigma)$ (middle), and its derivative with respect to σ (down) for different values of the exit rate β and entrance rate α for two different bulk hopping rates and reversibility parameters $p = 0.95$ and $\varepsilon = 0.01$ (left) and $p = 0.995$ and $\varepsilon = 0.001$ (right). The system size is $N = 8$.

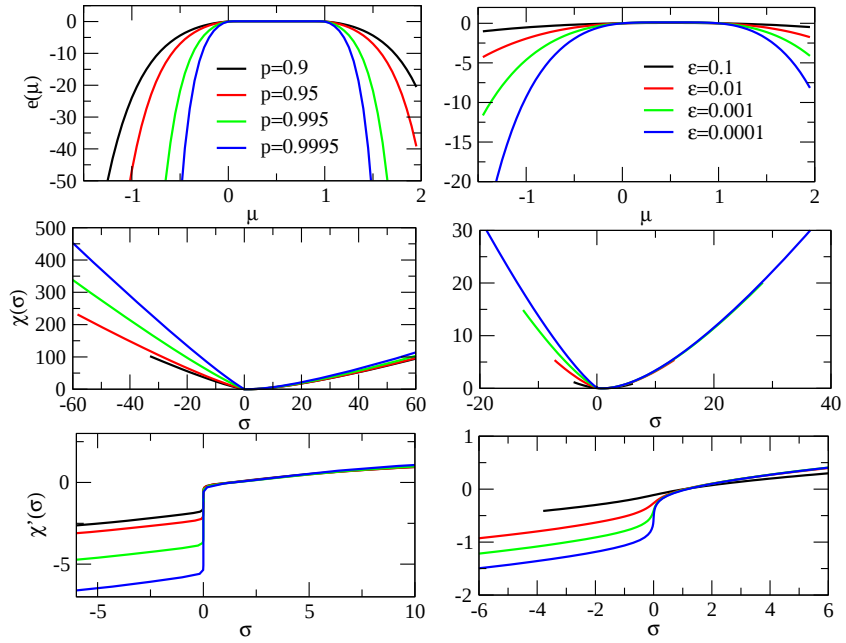

Figure 4.23: The smallest eigenvalue $e(\mu)$ of L_μ (up), the rate function of the entropy production $\chi(\sigma)$ (middle), and its derivative with respect to σ (down) for different (left) values of the bulk hopping rate and (right) different values of the reversibility parameters ε. The parameters are (left) $\alpha = \beta = 0.5$, $\varepsilon = 0.001$, and (right) $\alpha = \beta = 0.5$ and $p = 0.5$. The system size is $N = 8$.

Chapter 5

Evaluating the Work Observable

In chapter 4 we evaluated the steady state entropy production for the stochastic models defined in chapter 3. The prominent features of the entropy distribution were shown to characterize non-equilibrium steady states. In the definition of the dynamics of the models a small parameter ε was introduced to ensure reversibility of all reactions. This was a necessary condition for the change of entropy to be well defined. In this chapter, time dependent processes are analyzed by varying one of the reaction rates in a finite time interval. This is done for the observable R which reduces to the Seifert entropy, Δs_{tot} in the case of a single steady state. If $\varepsilon = 0$, the observable R is not well defined, as we would measure an infinite change in the change in entropy R. The observable that is finite even in the case of non reversible reactions is the observable ϕ obeying an integral fluctuation theorem, shown in [66].
In this chapter these two different observables are discussed and analyzed for the different reaction-diffusion systems. As long as the reversibility parameter is non zero, the observable R, resulting from the comparison of forward and reversed trajectory, is analyzed. We show exact detailed fluctution relations for the different models and discuss their probability distributions. The second observable we study is the work observable ϕ, whose distribution is analyzed for all four models. Based on the distribution we can verify the Jarzynski [77] and Crooks relations [29] for model 1, resp. the Hatano Sasa [66] and Seifert entropy relation [142] for the non-equilibrium systems. Recalling that for systems satisfying detailed balance we have the identity $\phi = W_d$, where $W_d = W - \Delta F$ is the dissipated heat of the process, it is tempting to ask whether for ϕ an exact detailed fluctuation theorem like (2.12) can also be encountered for a system initially in a non-equilibrium steady state. In fact, this is not the case: the absence of detailed balance in a non-equilibrium steady state entails non-zero probability currents, and no simple relation like the relation (2.12) exists for ϕ in this case. As we shall discuss below, the corresponding fluctuation ratios yield *systematic* deviations from the simple behavior encountered in systems with detailed balance. These deviations containing non-trivial information on the non-equilibrium system at hand.
The chapter is organized in the following way. We first define the transient process, its time

reversed process, and the observables ϕ and R. We then examine the relation between the two observables and discuss exact fluctuation relations. In the next step, we motivate the calculation of distributions for the work observable even though detailed balance is broken. We discuss the probability distributions obtained and relate them to intrinsic properties of the dynamics. The last section is devoted to fluctuation ratios for the distributions of ϕ. We discuss the arising modulations on top of an exponential relation and summarize our results.

5.1 Motivation and Setup

In this chapter transient processes are analyzed for the reaction-diffusion systems, models 1- 4. The system under consideration is prepared in its stationary state. During the time interval τ one of the reaction rates is varied in time. The stationary probabilities and non-equilibrium currents carry therefore a time index that parametrizes the process. We are no longer analyzing the system through its properties in a steady state but we are rather analyzing how the system responds to arbitrary fast external driving protocol.
Experimentally, a change of rates of chemical reactions can be achieved by changing the temperature, for example. In our protocol we change one of the rates r from an initial value r_0 to a final value r_M in M equidistant steps of length Δr, yielding for the reaction rate the values $r_i = r_0 + i\Delta r$ with $i = 0, \cdots, M$. We assume that at every step only one reaction or diffusion process takes place.
Respecting the varying time index, we state here the observable R that relates the forward to the reversed trajectory. Starting from a configuration C_0, the system is in the configuration C_i at step i, such that after M steps the system has performed the following path in configuration space:

$$\mathbf{X} = C_0 \longrightarrow C_1 \longrightarrow \cdots \longrightarrow C_{M-1} \longrightarrow C_M. \tag{5.1}$$

The probability for this path is given by

$$P(\mathbf{X}) = P_s(C_0) \prod_{i=0}^{M-1} \omega(C_i \longrightarrow C_{i+1}) \ , \tag{5.2}$$

where $\omega(C_i \to C_{i+1})$ is the transition probability from configuration C_i to configuration C_{i+1}. Denoting the reversed path by

$$\tilde{\mathbf{X}} = C_M \longrightarrow C_{M-1} \longrightarrow \cdots \longrightarrow C_1 \longrightarrow C_0, \tag{5.3}$$

one defines, for Markovian systems, the quantity

$$R = \ln \frac{P_s(C_0, r_0)}{P_s(C_M, r_M)} + \sum_{i=0}^{M-1} \ln \frac{\omega(C_i \to C_{i+1}, r_{i+1})}{\omega(C_{i+1} \to C_i, r_i)} \tag{5.4}$$

where $P_s(C_i, r_i)$ is the probability to find the configuration C_i in the stationary state corresponding to the value r_i of the reaction rate r and $\omega(C_i \to C_{i+1}, r_{i+1})$ is the transition probability from C_i to C_{i+1} at step $i+1$. The observable R in a single steady state equals the Seifert entropy [139] as well as the finite time action functional W in [96]

$$R_{ss} = \ln \frac{P(\mathbf{X})}{P(\tilde{\mathbf{X}})} = \ln \frac{P_s(C_0)}{P_s(C_M)} + \sum_{i=0}^{M-1} \ln \frac{\omega(C_i \to C_{i+1})}{\omega(C_{i+1} \to C_i)} \; . \tag{5.5}$$

The index ss indicates the entropy change in a single steady state. A closer look at the observable R reveals that its definition requires that if $\omega(C_i \to C_{i+1}, r_{i+1}) > 0$ then $\omega(C_{i+1} \to C_i, r_i)$ also has to be non zero. However, in some of our reaction-diffusion models this condition is not fulfilled as microscopic reversibility is broken. We install reversibility in the reaction schemes by the parameter $\varepsilon > 0$, see chapter 3. If $\varepsilon = 0$, we cannot use R to study these systems. Hatano and Sasa [66] have proposed a different quantity, called ϕ in the following, that is closely related to R. ϕ does not require microscopic reversibility in order to be well defined.
By the definition of the models 2, 3, and 4, irreversible trajectories appear if $\varepsilon = 0$. Actually all trajectories that involve a change in the number of particles would be non reversible for model 3 and model 4. Irreversible dynamics can be realized in an experiment of chemical reactions through a fast evacuation of some of the reaction products. This makes plausible a possible future verification of the intriguing features that are revealed in this study. A brief account of some of our results has been given previously [45] and a more detailed discussion with additional analysis of the complete entropy observable in the case of transient processes can be found in [44]. The observable ϕ is defined as

$$\phi = \sum_{i=0}^{M-1} \ln \left[\frac{P_s(C_i, r_i)}{P_s(C_i, r_{i+1})} \right] \; . \tag{5.6}$$

The only information that enters the observable ϕ is the stationary probabilities that are well defined even in the limit of irreversible reactions. The quantity ϕ has been called the driving entropy production in [63].

For a system with microscopic reversibility we can derive a relation between R and ϕ. With the help of the probability current

$$K_s(C_i, C_{i+1}, r_{i+1}) = \omega(C_{i+1} \to C_i, r_{i+1}) P_s(C_{i+1}, r_{i+1}) - \omega(C_i \to C_{i+1}, r_{i+1}) P_s(C_i, r_{i+1}) \; , \tag{5.7}$$

we can write Eq. (5.6) for ϕ in the following form:

$$\phi = R - \sum_{i=0}^{M-1} \ln \left[-\frac{K_s(C_i, C_{i+1}, r_{i+1})}{P_s(C_{i+1}, r_{i+1})\, \omega(C_{i+1} \to C_i, r_i)} + \frac{\omega(C_{i+1} \to C_i, r_{i+1})}{\omega(C_{i+1} \to C_i, r_i)} \right] , \tag{5.8}$$

which reveals that the difference between R and ϕ is composed of terms which have very different physical origins. The first term in the ln in equation (5.8) is due to non-vanishing

probability currents between different configurations and is therefore characteristic for non-equilibrium states. The second term is non-trivial only in transient processes as it accounts for a shift in the reversed transition probability. This term reduces to the trivial value 1 in case one remains in a given steady state, with $r_{i+1} = r_i = r_0$ for all i. If this steady state is in addition an equilibrium state, the probability currents are all vanishing, and one has $R = \phi = 0$.
It is easy to show [66, 139, 63] that for transient processes both quantities fulfill an integral fluctuation theorem. We demonstrate in both cases the integral fluctuation relation, $\langle e^{-R}\rangle = 1$ and $\langle e^{-\phi}\rangle = 1$, where the average is taken over all possible histories when driving the system out of a general steady state:

$$\begin{aligned}
\langle e^{-R}\rangle &= \sum_{C_0,\dots C_M} P_s(C_0,0)\prod_{i=0}^{M-1}\omega(C_i\to C_{i+1},i+1)\frac{P_s(C_M,M)}{P_s(C_0,0)}\prod_{k=0}^{M-1}\frac{\omega(C_{k+1}\to C_k,k)}{\omega(C_k\to C_{k+1},k+1)}\\
&= \sum_{C_0,\dots C_M} P_s(C_M,M)\prod_{i=0}^{M-1}\omega(C_{i+1}\to C_i,i)\\
&= \sum_{C_M} P_s(C_M,M)\prod_{i=0}^{M-1}\sum_{C_i}\omega(C_{i+1}\to C_i,i)\\
&= \sum_{C_M} P_s(C_M,M) = 1. \qquad (5.9)
\end{aligned}$$

The expectation value for the observable $e^{-\phi}$ is calculated to be

$$\begin{aligned}
\langle e^{-\phi}\rangle &= \sum_{C_0,\dots C_M} P_s(C_0,0)\prod_{i=0}^{M-1}\omega(C_i\to C_{i+1},i+1)\prod_{k=0}^{M-1}\frac{P_s(C_k,k)}{P_s(C_k,k+1)}\\
&= \sum_{C_1,\dots C_M}\left(\sum_{C_0} P_s(C_0,1)\omega(C_0\to C_1,1)\right)\prod_{i=1}^{M-1}\omega(C_i\to C_{i+1},i+1)\prod_{k=1}^{M-1}\frac{P_s(C_k,k)}{P_s(C_k,k+1)}\\
&= \sum_{C_2,\dots C_M}\left(\sum_{C_1} P_s(C_1,2)\omega(C_1\to C_2,2)\right)\prod_{i=2}^{M-1}\omega(C_i\to C_{i+1},i+1)\prod_{k=2}^{M-1}\frac{P_s(C_k,k)}{P_s(C_k,k+1)}\\
&= \dots\\
&= \sum_{C_M}\left(\sum_{C_{M-1}} P_s(C_{M-1},M)\omega(C_{M-1}\to C_M,M)\right)\\
&= \sum_{C_M} P_s(C_M,M) = 1, \qquad (5.10)
\end{aligned}$$

where at every step we need the relation $\sum_{C_i} P_s(C_i,j)\omega(C_i\to C_j,j) = P_s(C_j,j)$.
The average value, $\langle e^{-\phi}\rangle = 1$, is the Hatano Sasa relation in the case of discrete dynamics [66]. For a system that is initially in an equilibrium steady state the relation $\langle e^{-\phi}\rangle = 1$

reduces to the Jarzynski relation [77] because $\phi = \beta(W - \Delta F)$, where W is the work done on the system, ΔF is the free energy difference between initial and final states, and β is the inverse temperature. The difference $W_d = W - \Delta F$ is the dissipative work.
In the following we discuss mainly numerically exact results for small one-dimensional systems. This numerical exact approach is rather straightforward and is summarized in the Appendix A. Larger systems can be studied along the same lines through numerical simulations, but this must be done with some care in order to guarantee a sufficient sampling of rare events [44].

5.2 Probability Distributions

We shall first discuss the probability distributions themselves. Figures 5.2-5.4 show typical examples for the probability distributions of R and ϕ when changing the creation rate from an initial value h_0 to a final value h_M in M steps. We only show the case of a varying creation rate h, but the following discussion can be made along similar lines when changing the value of the annihilation rate λ. A important range of values in the observable ϕ and R can be obtained by varying significantly the stationary probabilities during the process. This is done by changing the creation parameter h or the annihilation parameter λ.

Figure 5.2 shows the probability distributions of R for three cases that fulfill microscopic

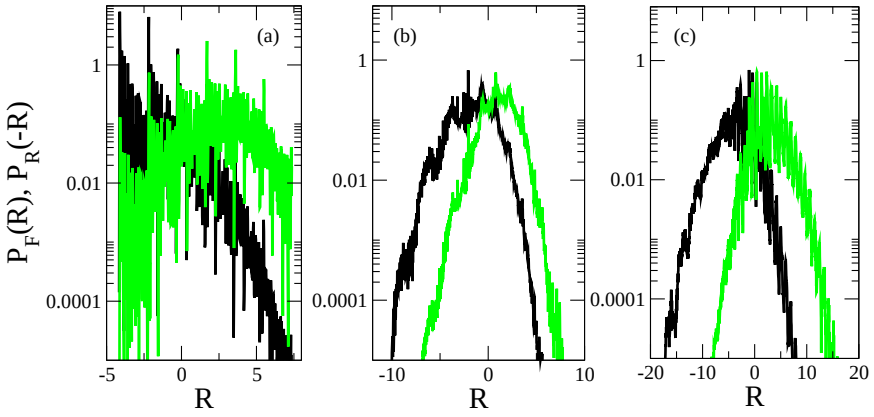

Figure 5.1: Probability distributions for the quantity R when the creation rate is changed in M=6 equidistant steps from 0.2 to 1.4 ($P_F(R)$, black curve) or from 1.4 to 0.2 ($P_R(-R)$, green (gray) curve). The data is obtained for a system with $N = 8$ sites, with $D = 5$ and $\lambda = 1$. (a) Model 1, (b) model 2 with $\varepsilon = 0.01$, and (c) model 3 with $\varepsilon = 0.1$. Reprinted with permission from S. Dorosz and M. Pleimling. Characterizing steady-state and transient properties of reaction-diffusion systems. Phys. Rev. E, 80(6):061114, Dec 2009. Copyright 2009, American Physical Society.

reversibility: models 1, 2, and 3 with $\varepsilon = 0.01$. As already mentioned in the previous section, the quantity R is ill defined in absence of this reversibility parameter ε. These

different probability distributions are not Gaussian and are characterized by a rather irregular structure. Their shape depends on the dynamics of the different models, expressed by the different reaction schemes. It is, however, not straightforward to relate specific features of the probability distributions to the different reactions. It is important to note that the peaks dominating these distributions do not have their origin in the noisiness of the numerical data, but are real as we are using a numerically exact method. In addition, our numerically exact method also allows us to circumvent any issues that might appear due to an insufficient sampling of rare events. This is of importance in the next section when we discuss the ratios of the forward and reversed probability distributions.

The probability distributions show a strong dependence on the system parameters. This is

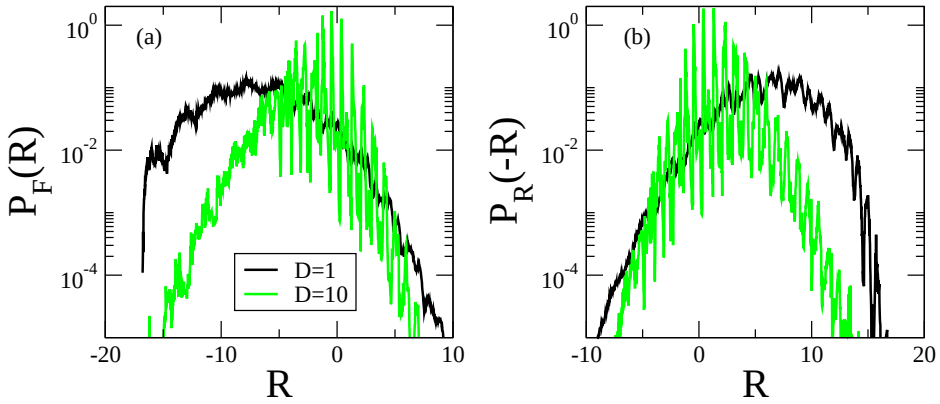

Figure 5.2: Probability distributions for the quantity R for model 3 for two different values of the diffusion rate. (a) $P_F(R)$ from the forward process and (b) $P_R(-R)$ from the reversed process. Reprinted with permission from S. Dorosz and M. Pleimling. Characterizing steady-state and transient properties of reaction-diffusion systems. Phys. Rev. E, 80(6):061114, Dec 2009. Copyright 2009, American Physical Society.

illustrated in figure 5.2 where we compare the distributions for model 3 obtained for different values of the diffusion rate D. When we increase the diffusion rate, the general shape of the probability distribution changes and, in addition, a large number of distinct peaks appear.

The probability distributions for ϕ differ markedly from those for R for model 2, 3, and 4, see figure 5.3. This was expected as the main difference between both quantities are the probability currents which are non-zero for a system that is out of equilibrium. It is only for the equilibrium model 1 that the distributions for both quantities match. Interestingly, the probability distributions for ϕ for both the forward and reversed processes are characterized by the presence of prominent peaks. An increase of the diffusion constant strongly amplifies these peaks but does not change the overall shape of the probability distributions. The fact that the heights of the peaks depend on the value of the diffusion constant indicates that these peaks are related to trajectories in configuration space that are dominated by diffusion steps and not by reactions.

In figure 5.4 we verify for model 3 that the main contributions to the peaks for a drive of

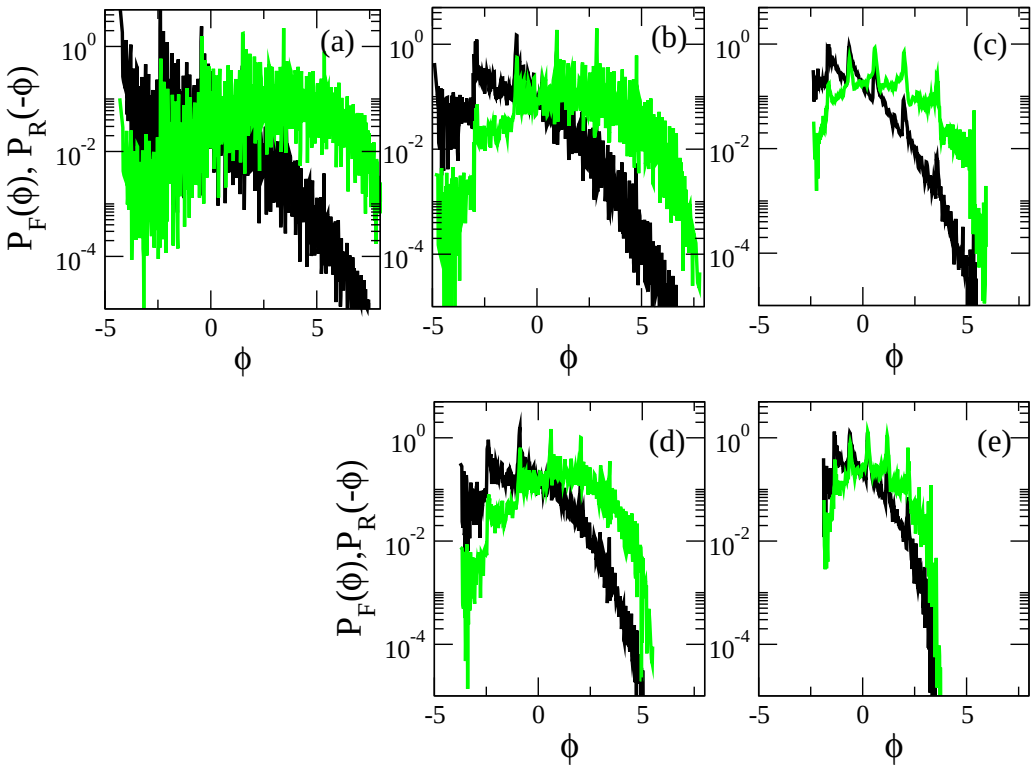

Figure 5.3: Probability distributions for the quantity ϕ when the creation rate h is changed in M=6 steps from 0.2 to 1.4 ($P_F(\phi)$, black curve) or from 1.4 to 0.2 ($P_R(-\phi)$, green curve). The data has been obtained for a system with $N = 8$ sites, with $D = 5$ and $\lambda = 1$. (a) Model 1, (b) model 2, (c) model 3, (d) model 2 with $\varepsilon = 0.1$, and (e) model 3 with $\varepsilon = 0.1$. Reprinted with permission from S. Dorosz and M. Pleimling. Characterizing steady-state and transient properties of reaction-diffusion systems. Phys. Rev. E, 80(6):061114, Dec 2009. Copyright 2009, American Physical Society.

length $M = 6$ indeed come from the trajectories where only diffusion takes place such that the number of particles is constant along these trajectories. The subleading contribution, also shown in figure 5.4, comes from the trajectories where a single reaction takes place which changes the number of particles in the system. Because the peaks are dominated by trajectories with pure diffusion, the positions of the peaks are the same for the forward and reversed processes, we are able to identify the leftmost peak as a result from the diffusion of a single particle in the system, whereas the rightmost peak is due to the diffusion of a single empty site in the system.

Before closing this section, we remark that in [63] similar peaks have been observed in the probability distributions of the driving entropy production as well as of other related quantities in a model for electron transport through a single level quantum dot because the underlying dynamics is a stochastic counting process of events.

5.3 Fluctuation Ratios

After the discussion the probability distributions of the quantities R and ϕ, we move on and study the fluctuation ratios formed by these probability distributions. For a system driven out of an initial equilibrium state and fulfilling detailed balance, Crooks has shown the exact relation (2.12) to exist between the probability distributions of the dissipative work measured in the forward and time-reversed processes. This remarkable result can be extended to systems that are still reversible microscopically but that do not fulfill detailed balance any more [64]. As illustrated in figure 5.5 for models 2 and 3, the ratios of the probability distributions for R show a simple exponential dependence on R. The perfect exponential obtained from our data nicely validates our numerical exact approach. Obtaining a plot of similar quality through Monte Carlo simulations is difficult as rare events are then hard to measure.

Even though in the absence of microscopic reversibility R is ill defined, this is different for ϕ as this quantity exclusively involves the steady-state probabilities, see equation (5.6). For an equilibrium system ϕ fulfills an exact fluctuation theorem as it then reduces exactly to the dissipative work. As shown in figure 5.6 for model 1, an exponential relation is indeed obtained for all parameter values as well as for different driving processes $h(t)$.

However, for a system with non-equilibrium steady states no exponential detailed fluctuation relation is expected for ϕ as this quantity does not contain the information on non-equilibrium currents, see equation (5.8). We show in figure 5.7 ratios of the probability distributions of ϕ for models 2 and 3. For model 2 the deviations from the exponential are random and no pronounced dependence on system parameters, as for example the diffusion rate D, is observed. For model 3, however, a qualitatively different behavior is encountered and *systematic* deviations in the form of oscillations are observed. Similar oscillations are also observed for model 4 where three neighboring particles are destroyed in the annihilation process.

Interestingly, the amplitudes of these oscillations increase for increasing diffusion rates. At first one might think that this increase in peak height when increasing D should be related to the increase of the peaks in the probability distributions themselves, see the discussion in the previous section. However this is too simplistic, as an increase of peak heights in the probability distributions is also observed for models 1 and 2 for which we do not observe in the corresponding behavior in the fluctuation ratios. There is a qualitative difference in the dynamics between models 1 and 2 on the one hand and models 3 and 4 on the other hand. For the former models any change in the forward and reversed probability distributions is compensated when forming the ratio (this compensation is exact for model 1 and approximate for model 2), whereas for the latter models this compensation is only partial, such giving rise to peaks also in the fluctuation ratios.

Before discussing the origin of this difference, let us first have for model 3 a closer look at the peaks in the fluctuation ratio. We first note that the positions of these peaks are *not* identical to the positions of the extrema in the probability distributions (see for example figure 5.7). In table 5.1 we compare the positions of the maxima and minima in the fluctuation ratio

with the peak positions in the probability distributions. The observed offset means that the peaks in the probability distributions for the forward and reversed processes compensate each other when forming the ratio, but that the compensation is only partial away from the peaks. Recalling that the peaks result from trajectories in configuration space with only diffusion steps and that trajectories with reactions make up the part between the peaks, we can conclude that reactions are responsible for the peaks in the fluctuation ratios.
In order to verify this assumption we analyzed the contributions to the fluctuation ratio coming from the different types of trajectories. We show in figure 5.8 that the observed minima and maxima are indeed mainly due to the trajectories with a single reaction process. For this we compare the fluctuation ratio with the quantity $\Pi_F(\phi)/\Pi_R(-\phi)$ where $\Pi(\phi)$ is the probability distribution for all trajectories having (a) only diffusion steps or (b) exactly one reaction process. Obviously, the peaks in the latter ratio coincide with the peaks in the fluctuation ratio. As a second interesting observation we note that the oscillations in the

PD maxima	FR maxima	FR minima
-1.63	-1.78	-1.5
-0.61	-0.72	-0.38
0.60	0.50	0.82
2.02	1.89	2.25
3.64	3.44	3.84

Table 5.1: Positions of the maxima in the probability distributions (PD) and of the maxima and minima in the fluctuation ratio (FR) for model 3, with $D = 5$, $h_0 = 0.2$, $\Delta h = 1.2$, and $\lambda = 1$. The system size is $N = 8$ and the driving length is $M = 6$.

fluctuation ratios are not restricted to cases where microscopic reversibility is broken but are much more widespread. As is shown in figure 5.9 for model 3 with $\varepsilon > 0$ (the same holds for model 4 with $\varepsilon > 0$) peaks in the fluctuation ratios also show up in some systems where all reactions are reversible.

In order to understand the origin of these oscillations we need to go back to the different reaction schemes summarized in table 3.2. The configuration space of a reaction-diffusion system can be thought to be composed of smaller units formed by the configurations with a common number n of particles. A diffusion step conserves the number of particles, thereby connecting two configurations in the same unit. A passage from one unit to another always involves a change of particle number and is therefore exclusively due to a reaction process. This is sketched in figure 3.2.
Keeping this in mind, a fundamental difference emerges between models 1 and 2 on the one hand and models 3 and 4 on the other hand. In the former systems every reaction changes the particle number by 1, $\Delta n = \pm 1$. In the latter systems, however, also larger changes in the particle number happen in the annihilation process, with $\Delta n = -2$ for model 3 and $\Delta n = -3$ for model 4. As a consequence, loops in configuration space that connect a unit with constant n with itself and that involve reactions display an asymmetry in the number

of creation and annihilation processes. Thus for model 3 the smallest loop contains two creation processes and one annihilation. This effect is still present, even though in a weaker form, when we add the backreactions and end up with a microscopically reversible model like model 3 with $\varepsilon > 0$ with a variable number of particles added or subtracted in the different reactions. It is this difference in the number of particles created in a creation process or destroyed in an annihilation event that yields contributions to the probability distributions which are not compensated in the fluctuation ratio.

5.4 Summary

In chapter 5 transient processes were analyzed for reaction diffusion models. We identified two observables that were investigated in a numerical exact method and with Monte Carlo simulations. The relationship between the two observables were presented. Whereas the observable R reduces to the Seifert entropy that was analyzed in chapter 3 for single steady states, the observable ϕ is equal to the work observable in the Jarzynski relation if detailed balance is satisfied. The latter has the advantage that it is well defined even in the extreme case of irreversible transitions that are present if $\varepsilon = 0$.
The probability distributions for a linear increasing creation rate were analyzed. None of the distributions had a gaussian like shape. The distributions were irregular with peaks arising if trajectories become far more probable than others. In our case this was achieved with an increased diffusion constant. Whereas a one to one correspondence was possible between the amplified peaks and the number of particles for the observable ϕ, this was not possible for the complex shape of the distributions for the observable R.
We went on and confirmed for reversible reactions that the observable R fulfills an exact detailed fluctuation for all parameter values. For the observable ϕ we also showed for model 1 that the Crooks relation holds exactly. This was also tested for different ways of changing the creation rate in time. For models 2, 3 and 4 we then calculated the ratio of the forward and reversed distributions. In this case deviations from the exponential relation were expected. We found that in addition to an irregular pattern of scattering around the exponential for model 2, regular patterns exist for model 3 and model 4. These patterns were modulations. They are rooted in the unsuccesful compensation of peaks in the forward and reversed distributions. For larger values of D, model 3 and model 4 had increased modulations. We identified the main contribution coming from trajectories having the majority of transitions due to diffusion and one or two reactions. The topology in configuration space is the reason for this. Model 2 is not showing signatures in the ratio because only subgroups with a difference of one particle are connected by reactions, whereas for model 3 and model 4 larger changes in the total number of particles exist for a single reaction. Therefore we can see in the ratio of the distributions the underlying reaction schemes by analyzing the work observable ϕ.

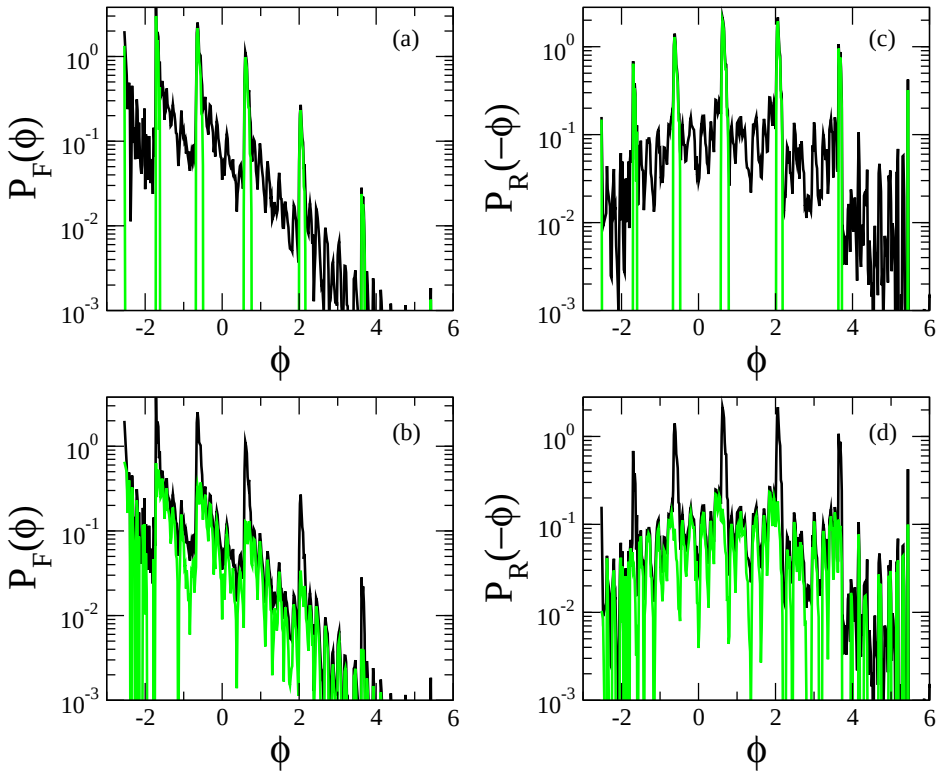

Figure 5.4: Main contributions to the probability distributions for ϕ in the forward and reversed processes. The black lines show the full probability distributions whereas the gray lines show the contributions coming from (a,c) trajectories in configuration space with only diffusion steps and no reactions and (b,d) from trajectories where exactly one reaction takes place that changes the number of particles in the system. The data are for model 3 with $D = 10$, $h_0 = 0.2$, $\Delta h = 1.2$, and $\lambda = 1$. The system size is $N = 8$ and the driving length is $M = 6$. Reprinted with permission from S. Dorosz and M. Pleimling. Characterizing steady-state and transient properties of reaction-diffusion systems. Phys. Rev. E, 80(6):061114, Dec 2009. Copyright 2009, American Physical Society.

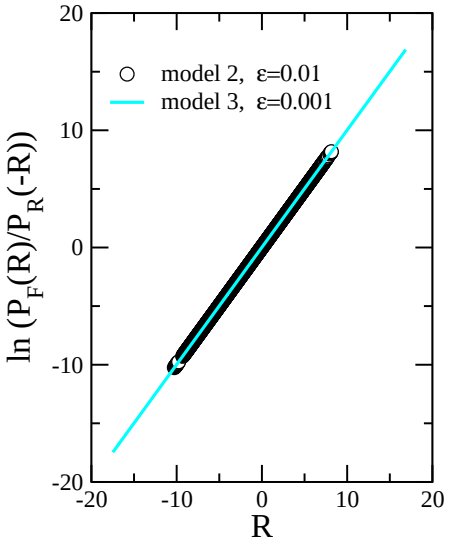

Figure 5.5: Fluctuation relation for the observable R for model 2 and model 3 for different values of the parameter ε. The parameters in this calculation are $h_0 = 0.2$, $\Delta h = 1.2$, $\lambda = 1$, and $D = 5$. The system size is $N = 8$ and the driving length is $M = 6$. Reprinted with permission from S. Dorosz and M. Pleimling. Characterizing steady-state and transient properties of reaction-diffusion systems. Phys. Rev. E, 80(6):061114, Dec 2009. Copyright 2009, American Physical Society.

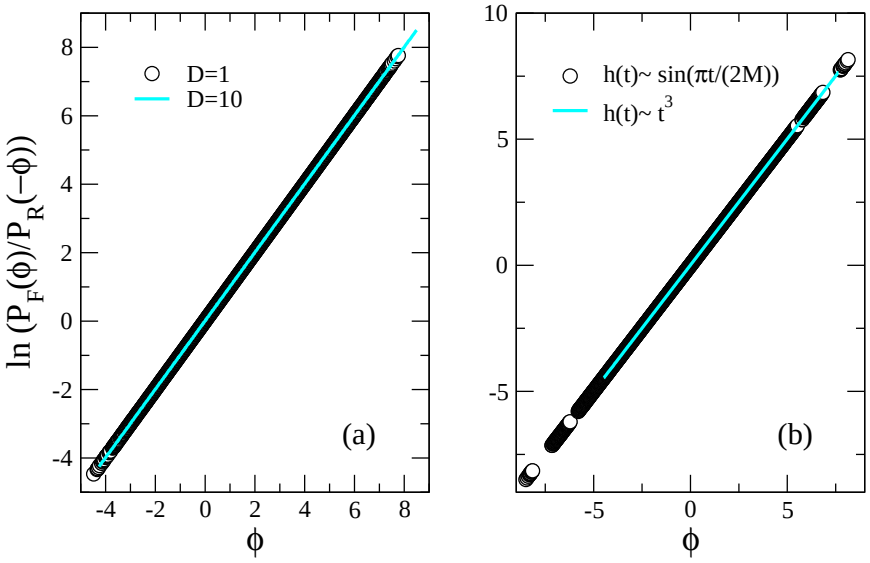

Figure 5.6: Fluctuation relation for the observable ϕ for model 1 with (a) different values of D and (b) different ways of changing the parameter $h(t)$ with $D = 1$. The driving process usually studied in this paper and which yields the data shown in (a) is $h(t) \sim t$. The parameters used in these calculations are $h_0 = 0.2$, $\Delta h = 1.2$, and $\lambda = 1$. The system size is $N = 8$ and the driving length is $M = 6$. Reprinted with permission from S. Dorosz and M. Pleimling. Characterizing steady-state and transient properties of reaction-diffusion systems. Phys. Rev. E, 80(6):061114, Dec 2009. Copyright 2009, American Physical Society.

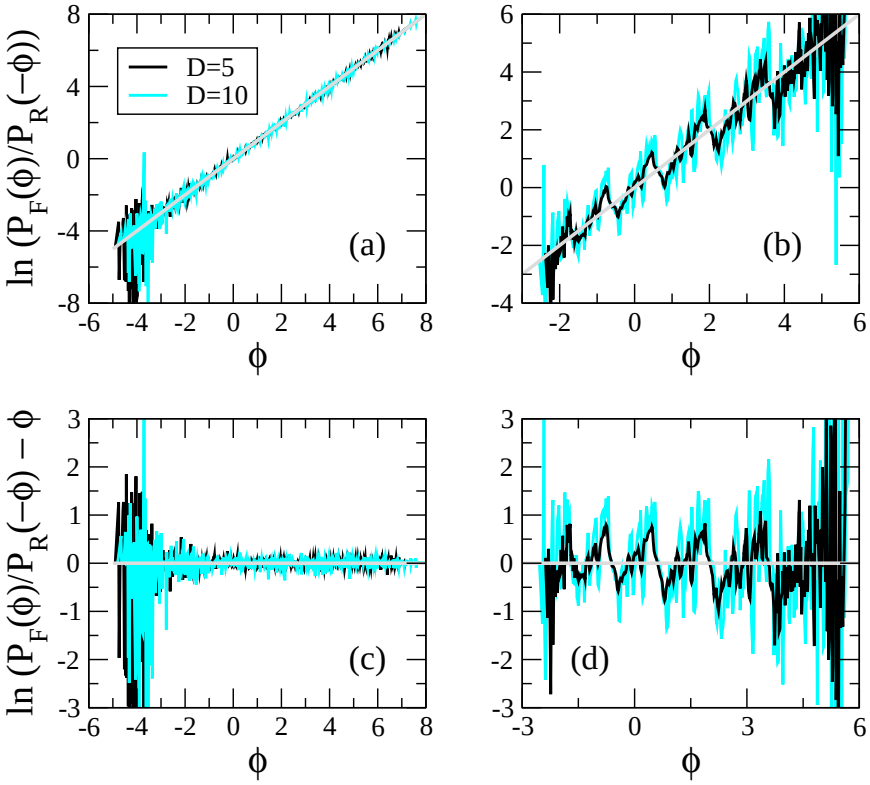

Figure 5.7: Fluctuation ratios for the observable ϕ for (a) model 2 and (b) model 3 and different values of the diffusion constant D. Whereas in model 2 only random deviations from a simple exponential behavior are observed, systematic deviations show up for model 3. This is highlighted in (c) and (d) where we subtract ϕ from the logarithm of the fluctuation ratio. The light gray lines indicate a simple exponential dependence. The parameters used in this calculation are $h_0 = 0.2$, $\Delta h = 1.2$, and $\lambda = 1$. The system size is $N = 8$ and the driving length is $M = 6$. Reprinted with permission from S. Dorosz and M. Pleimling. Characterizing steady-state and transient properties of reaction-diffusion systems. Phys. Rev. E, 80(6):061114, Dec 2009. Copyright 2009, American Physical Society.

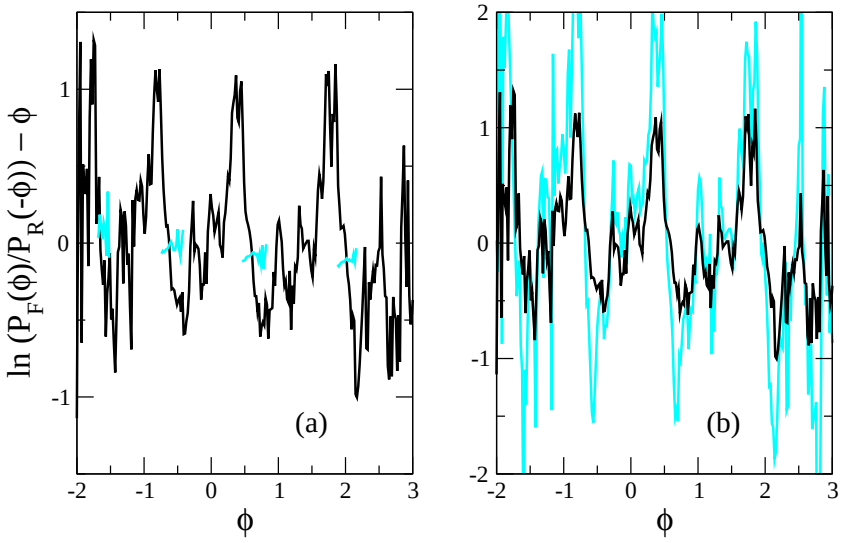

Figure 5.8: Comparison for model 3 of the fluctuation ratio (black line) with the ratio $\Pi_F(\phi)/\Pi_R(-\phi)$ (cyan line) where $\Pi(\phi)$ is the probability distribution of ϕ for all trajectories with (a) only diffusion steps and (b) exactly one reaction process. Note that for trajectories with only diffusion few values of ϕ can be realized. The common parameters are $h = 0.2$, $\lambda = 1.$, $M = 6$ and $N = 8$ and $D = 5$. Reprinted with permission from S. Dorosz and M. Pleimling. Characterizing steady-state and transient properties of reaction-diffusion systems. Phys. Rev. E, 80(6):061114, Dec 2009. Copyright 2009, American Physical Society.

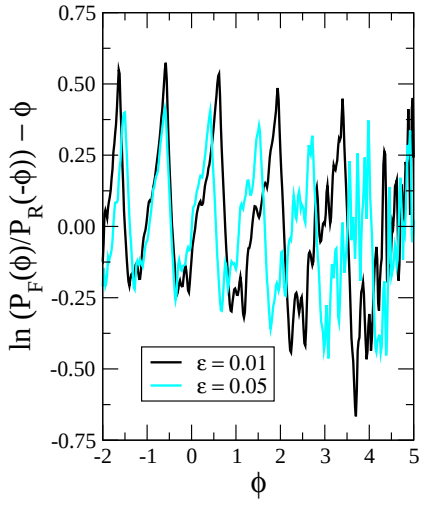

Figure 5.9: Fluctuation relations for model 3 and different values of ε. The values of the parameters are $D = 5$, $h_0 = 0.2$, $\Delta h = 1.2$, and $\lambda = 1$. The system size here is $L = 10$ and the driving length is $M = 10$. These data have been obtained through Monte Carlo simulations. Reprinted with permission from S. Dorosz and M. Pleimling. Characterizing steady-state and transient properties of reaction-diffusion systems. Phys. Rev. E, 80(6):061114, Dec 2009. Copyright 2009, American Physical Society.

Chapter 6

Conclusion

Characterizing the out-of-equilibrium properties of interacting many-body systems remains one of the most challenging tasks in contemporary physics. The recent advent of exact fluctuation and work theorems yielded some excitement in the community as it indicated a possible way of characterizing large classes of non-equilibrium systems.
In our work we try to characterize diffusion-limited reactions both in their non-equilibrium steady state and in the transient state when the systems are driven out of stationarity. For systems in their steady state we confirm the expectation that probability currents allow to distinguish between equilibrium and non-equilibrium steady states. In addition, non-equilibrium currents across bonds connecting two configurations allow to define a metric that quantifies the distance to equilibrium. The probability current amplitude K was shown to grow linearly with the system size and to approach zero in the case of detailed balance.
We were able to identify with the help of K the qualitative differences between the different non-equilibrium reaction-diffusion models. This discussion showed that non-equilibrium currents are needed in order to describe the stationary states of stochastic systems far from equilibrium. It was further shown for transport models how the particle current running through the system affects the stationary probabilities and the amplitude K. This way of characterizing non-equilibrium steady systems remains valid even when microscopic reversibility is broken.
We further analyzed the steady states of the different reaction-diffusion models for different system parameters. The reversibility parameter ε has to be greater than zero in this case because the definition of entropy would otherwise not be well defined. For short measurement times we saw important modulations in the logarithm of the probability distributions of total entropy change. These modulations are present for all values of the system parameters and remain constant for different system sizes and measurement times. The distributions themselves are irregular even though the algorithm used is exact. Even though the distributions are very irregular, we find that the expectation values for the mean entropy change is already growing linearly with system size and measurement time. The periodicity of the modulations depends on the reaction rates, but a general relation to predict the positions of

the maxima could not be obtained.
In the second part of the analysis of entropy production in single steady states we investigated the long time limit. In this limit the rate function of entropy change is time independent and a function of the normalized variable σ. Previous results of asymmetric random walks and overdamped particles were extended in this work to many particle systems in order to understand the origin of a characteristic kink at zero entropy production. With the help of the different reaction-diffusion and transport models we characterized the discontinuity in the first derivative of the rate function. We find the same qualitative behavior as we have seen for the amplitude of the probability current. The existence of the kink is therefore not a model dependent feature but rather expresses the non-equilibrium properties of the system.
The calculation of the entropy production allowed us also to investigate the parameter dependence of the mean entropy production rate $\langle \dot{s_{\mathrm{m}}} \rangle$. A general statement for reaction-diffusion processes could not be made. For the transport models we saw a kink when the entrance rate α is equal to the exit rate β. Since the peak is decreasing in magnitude when $\alpha \to 1$ we interpret this anomaly as a signature of the coexistence line between the high and low density phases of the irreversible TASEP model.
In chapter 5 we analyzed the stationary properties of the reaction-diffusion models by driving the system out of the stationary state. One of the reaction rates was varied in a finite time interval and the change in entropy was recorded. Two observables were analyzed. The observable R, see eq. (5.4), relies on the reversibility of the dynamics. As long as the reversibility parameter $\varepsilon > 0$, all models satisfy an exponential relation between forward and reversed process. The distributions are non gaussian and have amplified peaks if the rate of diffusion increases. A simple relation between the details of the distributions and the system parameters does not seem to exist.
Since many of the reaction-diffusion models are irreversible, we focused on the analysis of the observable ϕ, called the driving entropy production, see eq. (5.6), initially introduced in [66, 63]. This quantity exclusively uses stationary probabilities and therefore remains well defined even in the absence of microscopic reversibility. In the case of an equilibrium reaction-diffusion model, satisfying detailed balance, the work observable ϕ shows an exact exponential relation between the forward and reversed process. This allowed us to verify the Crooks and Jarzynski relation for different protocols.
Whereas the driving entropy production always fulfills a global fluctuation theorem [66, 63], it only fulfills a detailed fluctuation theorem for systems with equilibrium steady states. At first look, this seems to strongly reduce the usefulness of his quantity for the characterization of systems with non-equilibrium steady states. However, as we showed, the deviations of the fluctuation ratios for ϕ from a simple exponential behavior do contain non-trivial information on the trajectories in configuration space. Indeed, in cases where the change in the number of particles is different for different reactions, we observe systematic deviations from a simple exponential behavior. These deviations, which take the form of peaks superimposed on an exponential, mainly result from trajectories in configuration space where exactly one reaction takes place.
Based on the reaction schemes discussed in this work and given in Table 3.2, we expect the

peaks to appear in the fluctuation ratios for ϕ for any reaction-diffusion system that allows for a variable number of particles to be created or destroyed in the different reactions. This also encompasses more complicated systems with two or more particle types. In addition, signatures of the same type should also be observed for other system classes with a configuration space topology that is similar to that of the the reaction-diffusion systems (i.e., composed by groups of configurations that are only connected in a very specific way) and with a similar asymmetry in the configuration space trajectories.

Bibliography

[1] D. A. Adams, R. K. P. Zia, and B. Schmittmann. Power spectra of the total occupancy in the totally asymmetric simple exclusion process. *Phys. Rev. Lett.*, 99(2):020601, Jul 2007.

[2] A. E. Allahverdyan and Th. M. Nieuwenhuizen. Fluctuations of work from quantum subensembles: The case against quantum work-fluctuation theorems. *Phys. Rev. E*, 71(6):066102, Jun 2005.

[3] D. Andrieux and P. Gaspard. Fluctuation theorem and onsager reciprocity relations. *The Journal of Chemical Physics*, 121(13):6167–6174, 2004.

[4] D. Andrieux and P. Gaspard. Fluctuation theorems and the nonequilibrium thermodynamics of molecular motors. *Phys. Rev. E*, 74(1):011906, Jul 2006.

[5] D. Andrieux and P. Gaspard. Fluctuation theorem for currents and schnakenberg network theory. *Journal of Statistical Physics*, 127(1):107–131, 04 2007.

[6] D. Andrieux and P. Gaspard. Temporal disorder and fluctuation theorem in chemical reactions. *Phys. Rev. E*, 77(3):031137, Mar 2008.

[7] D. Andrieux, P. Gaspard, S. Ciliberto, N. Garnier, S. Joubaud, and A. Petrosyan. Thermodynamic time asymmetry in non-equilibrium fluctuations. *Journal of Statistical Mechanics: Theory and Experiment*, 2008(01):P01002, 2008.

[8] D. Andrieux, P. Gaspard, T. Monnai, and S. Tasaki. The fluctuation theorem for currents in open quantum systems. *New Journal of Physics*, 11(4):043014 (25pp), 2009.

[9] J. Berg. Out-of-equilibrium dynamics of gene expression and the Jarzynski equality. *Physical Review Letters*, 100(18):188101, 2008.

[10] J. T. Berryman and T. Schilling. A general algorithm for sampling rare events in non-equilibrium and non-stationary systems, 2010.

[11] V. Blickle, Y. Speck, L. Helden, U. Seifert, and C. Bechinger. Thermodynamics of a colloidal particle in a time-dependent nonharmonic potential. *Phys. Rev. Lett.*, 96(7):070603, Feb 2006.

[12] G. N. Bochkov and Y. E. Kuzovlev. Nonlinear fluctuation-dissipation relations and stochastic models in nonequilibrium thermodynamics : I. generalized fluctuation-dissipation theorem. *Physica A: Statistical and Theoretical Physics*, 106(3):443 – 479, 1981.

[13] G. N. Bochkov and Y. E. Kuzovlev. Nonlinear fluctuation-dissipation relations and stochastic models in nonequilibrium thermodynamics : Ii. kinetic potential and variational principles for nonlinear irreversible processes. *Physica A: Statistical and Theoretical Physics*, 106(3):480 – 520, 1981.

[14] F. Bonetto, G. Gallavotti, A. Giuliani, and F. Zamponi. Chaotic hypothesis, fluctuation theorem and singularities. *Journal of Statistical Physics*, 123(1):39–54, 04 2006.

[15] A. B. Bortz, M. H. Kalos, and J. L. Lebowitz. A new algorithm for monte carlo simulation of ising spin systems. *Journal of Computational Physics*, 17(1):10 – 18, 1975.

[16] J. Braga, J. G. McNally, and M. Carmo-Fonseca. A reaction-diffusion model to study rna motion by quantitative fluorescence recovery after photobleaching. *Biophysical Journal*, 92(8):2694–2703, 04 2007.

[17] C. Bustamante, J. Liphardt, and F. Ritort. The nonequilibrium thermodynamics of small systems. *Physics Today*, 58(7):43–48, 2005.

[18] M. Campisi, P. Talkner, and P. Hänggi. Fluctuation theorem for arbitrary open quantum systems. *Phys. Rev. Lett.*, 102(21):210401, May 2009.

[19] D. M. Carberry, J. C. Reid, G. M. Wang, E. M. Sevick, D. J. Searles, and D.J. Evans. Fluctuations and irreversibility: An experimental demonstration of a second-law-like theorem using a colloidal particle held in an optical trap. *Phys. Rev. Lett.*, 92(14):140601, Apr 2004.

[20] J. L. Cardy and P. Grassberger. Epidemic models and percolation. *Journal of Physics A: Mathematical and General*, 18(6):L267–L271, 1985.

[21] V. Y. Chernyak, M. Chertkov, and C. Jarzynski. Path-integral analysis of fluctuation theorems for general langevin processes. *Journal of Statistical Mechanics: Theory and Experiment*, 2006(08):P08001, 2006.

[22] R. Chetrite. Fluctuation relations for diffusion that is thermally driven by a nonstationary bath. *Phys. Rev. E*, 80(5):051107, Nov 2009.

[23] R. Chetrite, G. Falkovich, and K. Gawedzki. Fluctuation relations in simple examples of non-equilibrium steady states. *Journal of Statistical Mechanics: Theory and Experiment*, 2008(08):P08005 (25pp), 2008.

[24] R. Chetrite and K. Gawędzki. Fluctuation relations for diffusion processes. *Communications in Mathematical Physics*, 282(2):469–518, 09 2008.

[25] R. Chetrite and K. Mallick. Fluctuation relations for quantum markovian dynamical system. *arXiv:1002.0950v1 [cond-mat.stat-mech]*, 2010.

[26] S. Ciliberto and C. Laroche. An experimental test of the gallavotti-cohen fluctuation theorem. *J. Phys. IV France*, 08(6):Pr6–215–Pr6–219, oct 1998.

[27] D. Collin, F. Ritort, C. Jarzynski, S.B. Smith, I. Tinoco Jr, and C. Bustamante. Verification of the crooks fluctuation theorem and recovery of rna folding free energies. *Nature*, 437(7056):231–4, Sep 2005.

[28] J. L. Cook and R. K. P. Zia. Feedback and fluctuations in a totally asymmetric simple exclusion process with finite resources. *Journal of Statistical Mechanics: Theory and Experiment*, 2009(02):P02012 (12pp), 2009.

[29] G. E. Crooks. Nonequilibrium measurements of free energy differences for microscopically reversible markovian systems. *Journal of Statistical Physics*, 90(5):1481–1487, March 1998.

[30] G. E. Crooks. Entropy production fluctuation theorem and the nonequilibrium work relation for free energy differences. *Phys. Rev. E*, 60(3):2721–2726, Sep 1999.

[31] G. E. Crooks. Path-ensemble averages in systems driven far from equilibrium. *Phys. Rev. E*, 61(3):2361–2366, Mar 2000.

[32] S. Deffner and E. Lutz. Nonequilibrium work distribution of a quantum harmonic oscillator. *Phys. Rev. E*, 77(2):021128, Feb 2008.

[33] A. Dembo and O. Zeitouni. *Large Deviation Techniques and Applications*. Berlin Springer, 1998.

[34] B. Derrida. An exactly soluble non-equilibrium system: The asymmetric simple exclusion process - probabilites et statistiques. *Physics Reports*, 301:65–83(19), 1998.

[35] B. Derrida, M. R. Evans, V. Hakim, and V. Pasquier. Exact solution of a 1d asymmetric exclusion model using a matrix formulation. *Journal of Physics A: Mathematical and General*, 26(7):1493–1517, 1993.

[36] B. Derrida and J. L. Lebowitz. Exact large deviation function in the asymmetric exclusion process. *Phys. Rev. Lett.*, 80(2):209–213, Jan 1998.

[37] B. Derrida, J. L. Lebowitz, and E. R. Speer. Large deviation of the density profile in the steady state of the open symmetric simple exclusion process. *Journal of Statistical Physics*, 107(3):599–634, 05 2002.

[38] B. Derrida, J. L. Lebowitz, and E. R. Speer. Exact large deviation functional of a stationary open driven diffusive system: The asymmetric exclusion process. *Journal of Statistical Physics*, 110(3):775–810, 03 2003.

[39] U. Dobramysl and U. C. Täuber. Spatial Variability Enhances Species Fitness in Stochastic Predator-Prey Interactions. *Physical Review Letters*, 101(25):258102, December 2008.

[40] J. J. Dong, B. Schmittmann, and R. K. Z. Zia. Inhomogeneous exclusion processes with extended objects: The effect of defect locations. *Phys. Rev. E*, 76(5):051113, Nov 2007.

[41] S Dorosz. Work relations in quantum spin chains. Master's thesis, University Henri Poincare, Nancy I, May 2006.

[42] S. Dorosz, S. Mukherjee, and T. Platini. Dynamical phase transition of a 1d transport process including death. http://arxiv.org/abs/0912.1290, 2009.

[43] S. Dorosz, T. Platini, and D. Karevski. Work fluctuations in quantum spin chains. *Phys. Rev. E*, 77(5):051120, May 2008.

[44] S. Dorosz and M. Pleimling. Characterizing steady-state and transient properties of reaction-diffusion systems. *Phys. Rev. E*, 80(6):061114, Dec 2009.

[45] S. Dorosz and M. Pleimling. Fluctuation ratios in the absence of microscopic time reversibility. *Phys. Rev. E*, 79(3):030102, Mar 2009.

[46] S. Dorosz and M. Pleimling. Steady-state and transient properties of reaction-diffusion systems. In *Physics Procedia*, number in print, 2010.

[47] F. Douarche, S. Ciliberto, A. Petrosyan, and I. Rabbiosi. An experimental test of the jarzynski equality in a mechanical experiment. *EPL (Europhysics Letters)*, 70(5):593–599, 2005.

[48] M. Ebbinghaus and L. Santen. A model for bidirectional traffic of cytoskeletal motors. *Journal of Statistical Mechanics: Theory and Experiment*, 2009(03):P03030 (19pp), 2009.

[49] V. Elgart and M. Pleimling. Aging processes in reversible reaction-diffusion systems. *Phys. Rev. E*, 77(5):051134, May 2008.

[50] R. S. Ellis. *Entropy, Large Deviations, and Statistical Mechanics*. Berlin Springer, 1985.

[51] C. Enaud and B. Derrida. Large deviation functional of the weakly asymmetric exclusion process. *Journal of Statistical Physics*, 114(3):537–562, 02 2004.

[52] A. Engel. Asymptotics of work distributions in nonequilibrium systems. *Phys. Rev. E*, 80(2):021120, Aug 2009.

[53] M. Esposito and S. Mukamel. Fluctuation theorems for quantum master equations. *Phys. Rev. E*, 73(4):046129, Apr 2006.

[54] D. J. Evans, E. G. D. Cohen, and G. P. Morriss. Probability of second law violations in shearing steady states. *Phys. Rev. Lett.*, 71(15):2401–2404, Oct 1993.

[55] D. J. Evans and D. J. Searles. Equilibrium microstates which generate second law violating steady states. *Phys. Rev. E*, 50(2):1645–1648, Aug 1994.

[56] G Frobenius. Ueber matrizen aus nicht negativen elementen. *Sitzungsber. Preuss. Akad. Wiss. Berlin*, page 456, 1912.

[57] G. Gallavotti and E. G. D. Cohen. Dynamical ensembles in nonequilibrium statistical mechanics. *Phys. Rev. Lett.*, 74(14):2694–2697, Apr 1995.

[58] P. Gaspard. Fluctuation theorem for nonequilibrium reactions. *The Journal of Chemical Physics*, 120(19):8898–8905, 2004.

[59] C. Giardinà, J. Kurchan, and L. Peliti. Direct evaluation of large-deviation functions. *Phys. Rev. Lett.*, 96(12):120603, Mar 2006.

[60] D. T. Gillespie. A general method for numerically simulating the stochastic time evolution of coupled chemical reactions. *Journal of Computational Physics*, 22(4):403 – 434, 1976.

[61] J. Gore, F. Ritort, and C. Bustamante. Bias and error in estimates of equilibrium free-energy differences from nonequilibrium measurements. *Proceedings of the National Academy of Sciences of the United States of America*, 100(22):12564–12569, 2003.

[62] M. S. Green. Markoff random processes and the statistical mechanics of time-dependent phenomena. ii. irreversible processes in fluids. *The Journal of Chemical Physics*, 22(3):398–413, 1954.

[63] U. Harbola, M. Esposito, and S. Mukamel. Statistics and fluctuation theorem for boson and fermion transport through mesoscopic junctions. *Phys. Rev. B*, 76(8):085408, Aug 2007.

[64] R. J. Harris and G. M. Schutz. Fluctuation theorems for stochastic dynamics. *Journal of Statistical Mechanics: Theory and Experiment*, 2007(07):P07020, 2007.

[65] R. J. Harris and R. B. Stinchcombe. Disordered asymmetric simple exclusion process: Mean-field treatment. *Phys. Rev. E*, 70(1):016108, Jul 2004.

[66] T. Hatano and S. Sasa. Steady-state thermodynamics of langevin systems. *Phys. Rev. Lett.*, 86(16):3463–3466, Apr 2001.

[67] M. Henkel and H. Hinrichsen. The non-equilibrium phase transition of the pair-contact process with diffusion. *Journal of Physics A: Mathematical and General*, 37(28):R117–R159, 2004.

[68] M. Henkel, H. Hinrichsen, and S. Lübeck. *Non-Equilibrium Phase Transitions. Volume 1: Absorbing Phase Transitions*. Springer, 2009.

[69] H. Hinrichsen. Non-equilibrium critical phenomena and phase transitions into absorbing states. *Advances in Physics*, 49(7):815–958, November 2000.

[70] R. A. Horn and C. R. Johnson. *Matrix Analysis*. Cambridge University Press, 1990.

[71] J. Horowitz and C. Jarzynski. Comparison of work fluctuation relations. *Journal of Statistical Mechanics: Theory and Experiment*, 2007(11):P11002, 2007.

[72] R. Howard. *Dynamic Probabilistic Systems*. John Wiley and Sons, 1971.

[73] G. Hummer and A. Szabo. Free energy reconstruction from nonequilibrium single-molecule pulling experiments. *Proceedings of the National Academy of Sciences of the United States of America*, 98(7):3658–3661, 2001.

[74] A. Imparato and L. Peliti. The distribution function of entropy flow in stochastic systems. *Journal of Statistical Mechanics: Theory and Experiment*, 2007(02):L02001, 2007.

[75] A. Imparato and L. Peliti. Work and heat probability distributions in out-of-equilibrium systems. *Comptes Rendus Physique*, 8(5-6):556 – 566, 2007. Work, dissipation, and fluctuations in nonequilibrium physics.

[76] C. Jarzynski. Equilibrium free-energy differences from nonequilibrium measurements: A master-equation approach. *Phys. Rev. E*, 56(5):5018–5035, Nov 1997.

[77] C. Jarzynski. Nonequilibrium equality for free energy differences. *Phys. Rev. Lett.*, 78(14):2690–2693, Apr 1997.

[78] C. Jarzynski. Hamiltonian derivation of a detailed fluctuation theorem. *Journal of Statistical Physics*, 98(1):77–102, 01 2000.

[79] C. Jarzynski. Rare events and the convergence of exponentially averaged work values. *Phys. Rev. E*, 73(4):046105, Apr 2006.

[80] C. Jarzynski. Comparison of far-from-equilibrium work relations. *Comptes Rendus Physique*, 8(5-6):495 – 506, 2007. Work, dissipation, and fluctuations in nonequilibrium physics.

[81] C. Jarzynski. Nonequilibrium work relations: foundations and applications. *The European Physical Journal B - Condensed Matter and Complex Systems*, 64(3):331–340, 08 2008.

[82] C. Jarzynski. Nonequilibrium work relations. *Boulder Lecture Notes-Nonequilibrium Statistical Mechanics: Fundamental Problems and Applications*, 2009.

[83] J. Jensen. Sur les fonctions convexes et les inégalités entre les valeurs moyennes. *Acta Mathematica*, 30(1):175–193, 12 1906.

[84] P. Jop, A. Petrosyan, and S. Ciliberto. Work and dissipation fluctuations near the stochastic resonance of a colloidal particle. *EPL (Europhysics Letters)*, 81(5):50005 (6pp), 2008.

[85] S. Joubaud, N. B. Garnier, and S. Ciliberto. Fluctuations of the total entropy production in stochastic systems. *EPL (Europhysics Letters)*, 82(3):30007 (4pp), 2008.

[86] R. Kawai, J. M. R. Parrondo, and C. Van den Broeck. Dissipation: The phase-space perspective. *Phys. Rev. Lett.*, 98(8):080602, Feb 2007.

[87] C.-H. Kiang. Single molecule manipulation: Experiments of biological molecules. *Boulder Lecture Notes-Nonequilibrium Statistical Mechanics: Fundamental Problems and Applications*, 2009.

[88] A. N. Kolmogorov. Zur Theorie der Markoffschen Ketten. *Math. Ann.*, 112(155), 1936.

[89] R. Kubo. Statistical-mechanical theory of irreversible processes. i. general theory and simple applications to magnetic and conduction problems. *Journal of the Physical Society of Japan*, 12(6):570–586, 1957.

[90] J. Kurchan. Fluctuation theorem for stochastic dynamics. *J. Phys. A: Math. Gen*, 31:3719–3729, 1998.

[91] J. Kurchan. A quantum fluctuation theorem. cond-mat/0007360, 2000.

[92] J. Kurchan. Non-equilibrium work relations. *Journal of Statistical Mechanics: Theory and Experiment*, 2007(07):P07005, 2007.

[93] G. Lakatos and T. Chou. Totally asymmetric exclusion processes with particles of arbitrary size. *Journal of Physics A: Mathematical and General*, 36(8):2027–2041, 2003.

[94] D. P. Landau and K. Binder. *A guide to monte carlo simulations in statistical physics*. Cambridge; New York Cambidge University Press, 2000.

[95] J. L. Lebowitz. Microscopic origins of irreversible macroscopic behavior. *Physica A: Statistical Mechanics and its Applications*, 263(1-4):516 – 527, 1999. Proceedings of the 20th IUPAP International Conference on Statistical Physics.

[96] J. L. Lebowitz and H. Spohn. A Gallavotti–Cohen-type symmetry in the large deviation functional for stochastic dynamics. *Journal of Statistical Physics*, 95(1):333–365, 04 1999.

[97] V. Lecomte, U. C. Täuber, and F. van Wijland. Current distribution in systems with anomalous diffusion: renormalization group approach. *Journal of Physics A: Mathematical and Theoretical*, 40(7):1447–1465, 2007.

[98] J. Liphardt, S. Dumont, S. B. Smith, I. Tinoco JR, and C. Bustamante. Equilibrium Information from Nonequilibrium Measurements in an Experimental Test of Jarzynski's Equality. *Science*, 296(5574):1832–1835, 2002.

[99] C. MacDonald, J. Gibbs, and A. Pipken. *Biopolymers*, 6, 1968.

[100] C. Maes. The fluctuation theorem as a gibbs property. *Journal of Statistical Physics*, 95(1):367–392, 04 1999.

[101] C. Maes. On the origin and the use of fluctuation relations for the entropy. *Seminaire Poincare*, 2:29–62, 2003.

[102] P. K. Maini, D. L. Benson, and J. A. Sherratt. Pattern formation in reaction-diffusion models with spatially inhomogeneous diffusion coefficients. *Mathematical Medicine and Biology*, 9(3):197–213, 1992.

[103] J. Mehl, T. Speck, and U. Seifert. Large deviation function for entropy production in driven one-dimensional systems. *Phys. Rev. E*, 78(1):011123, Jul 2008.

[104] N. Metropolis, A. W. Rosenbluth, M. N. Rosenbluth, A. H. Teller, and E. Teller. Equation of state calculations by fast computing machines. *The Journal of Chemical Physics*, 21(6):1087–1092, 1953.

[105] C. Michael. Fast heat-bath algorithm for the ising model. *Phys. Rev. B*, 33(11):7861–7862, Jun 1986.

[106] M. Mobilia, I. Georgiev, and U. Täuber. Phase transitions and spatio-temporal fluctuations in stochastic lattice Lotka–Volterra models. *Journal of Statistical Physics*, 128(1):447–483, 07 2007.

[107] T. Monnai. Fluctuation theorem in rachet system. *Journal of Physics A: Mathematical and General*, 37(6):L75–L79, 2004.

[108] D. Mukamel. *Phase Transitions in Non equilibrium Systems in Soft and Fragile Matter: Nonequilibrium Dynamics, Metastatbility and Flow, ed. M. E. Cates and M. R. Evans.* IOP Publishing, Bristol, 2000.

[109] S. Mukamel. Quantum extension of the Jarzynski relation: Analogy with stochastic dephasing. *Phys. Rev. Lett.*, 90(17):170604, May 2003.

[110] S. A. Nowak, P.-W. Fok, and T. Chou. Dynamic boundaries in asymmetric exclusion processes. *Phys. Rev. E*, 76(3):031135, Sep 2007.

[111] H. Oberhofer and C. Dellago. Efficient extraction of free energy profiles from nonequilibrium experiments. *J Comput Chem*, 30(11):1726–36, Aug 2009.

[112] G. Ódor. *Universality in Nonequilibrium Lattice Systems: Theoretical Foundations.* World Scientific/Singapore, 2008.

[113] J. Ohkubo. Posterior probability and fluctuation theorem in stochastic processes. *Journal of the Physical Society of Japan*, 78(12):123001, 2009.

[114] L. Onsager. Reciprocal relations in irreversible processes. i. *Phys. Rev.*, 37(4):405–426, Feb 1931.

[115] Y. Oono and M. Paniconi. Steady state thermodynamics. *Progress of Theoretical Physics Supplement*, 130:29–44, 1998.

[116] A. Pérez-Madrid and I. Santamaría-Holek. Fluctuation theorems for systems under fokker-planck dynamics. *Phys. Rev. E*, 79(1):011101, Jan 2009.

[117] O. Perron. Zur theorie der matrices. *Mathematische Annalen*, 64(2):248–263, 06 1907.

[118] T. Platini and R. K. P. Zia. private communication.

[119] V. Popkov, L. Santen, A. Schadschneider, and G. M. Schutz. Empirical evidence for a boundary-induced nonequilibrium phase transition. *Journal of Physics A: Mathematical and General*, 34(6):L45–L52, 2001.

[120] A. Prados, J. Brey, and B. Sánchez-Rey. A dynamical monte carlo algorithm for master equations with time-dependent transition rates. *Journal of Statistical Physics*, 89(3):709–734, 11 1997.

[121] W. H. Press, S. A. Teukolsky, B. P. Flannery, and W. T.Vetterling. *Numerical Recipes in FORTRAN: The Art of Scientific Computing.* Cambridge University Press, New York, NY, USA, 1992.

[122] H. Qian. Open-system nonequilibrium steady state: Statistical thermodynamics, fluctuations, and chemical oscillations. *The Journal of Physical Chemistry B*, 110(31):15063–15074, 07 2006.

[123] H Risken. *The Fokker–Planck Equation: Methods of Solutions and Applications*, volume 2nd of *Springer Series in Synergetics*. Springer, 1989.

[124] F. Ritort. Single-molecule experiments in biological physics: methods and applications. *Journal of Physics: Condensed Matter*, 18(32):R531–R583, 2006.

[125] D. Ruelle. A measure associated with axiom-a attractors. *American Journal of Mathematics*, 98(3):619–654, 1976.

[126] D. Ruelle. Positivity of entropy production in nonequilibrium statistical mechanics. *Journal of Statistical Physics*, 85(1):1–23, 10 1996.

[127] D. Ruelle. Entropy production in nonequilibrium statistical mechanics. *Communications in Mathematical Physics*, 189(2):365–371, 11 1997.

[128] S. Sandow. Partially asymmetric exclusion process with open boundaries. *Phys. Rev. E*, 50(4):2660–2667, Oct 1994.

[129] T. Schmiedl and U. Seifert. Stochastic thermodynamics of chemical reaction networks. *The Journal of Chemical Physics*, 126(4):044101, 2007.

[130] T. Schmiedl, T. Speck, and U. Seifert. Entropy production for mechanically or chemically driven biomolecules. *Journal of Statistical Physics*, 128(1):77–93, 07 2007.

[131] B. Schmittmann and R. K. P. Zia. *Phase Transition and Critical Phenomena*, volume 17. New York Academic, 1995.

[132] J. Schnakenberg. Network theory of microscopic and macroscopic behavior of master equation systems. *Rev. Mod. Phys.*, 48(4):571–585, Oct 1976.

[133] S. Schuler, T. Speck, C. Tietz, J. Wrachtrup, and U. Seifert. Experimental test of the fluctuation theorem for a driven two-level system with time-dependent rates. *Phys. Rev. Lett.*, 94(18):180602, May 2005.

[134] S. Schuler, T. Speck, C. Tietz, J. Wrachtrup, and U. Seifert. Experimental test of the fluctuation theorem for a driven two-level system with time-dependent rates. *Phys. Rev. Lett.*, 94(18):180602, May 2005.

[135] G. Schütz and E. Domany. Phase transitions in an exactly soluble one-dimensional exclusion process. *Journal of Statistical Physics*, 72(1):277–296, 07 1993.

[136] G. M. Schütz. *Phase Transition and Critical Phenomena*, volume 19. London Academic, 2001.

[137] D. J. Searles and D. J. Evans. Fluctuation theorem for stochastic systems. *Phys. Rev. E*, 60(1):159–164, Jul 1999.

[138] U. Seifert. Fluctuation theorem for birth and death for chemical master equations with time-dependent rates. *Journal of Physics A: Mathematical and General*, 37(42):L517–L521, 2004.

[139] U. Seifert. Entropy production along a stochastic trajectory and an integral fluctuation theorem. *Phys. Rev. Lett.*, 95(4):040602, Jul 2005.

[140] U. Seifert. Fluctuation theorem for a single enzym or molecular motor. *EPL (Europhysics Letters)*, 70(1):36–41, 2005.

[141] U. Seifert. Stochastic thermodynamics. *Lecture Notes: 'Soft Matter, From Synthetic to Biological Materials'. 39th IFF Spring School, Institut of Solid State Research Centre Jülich*, 2008.

[142] U. Seifert. Stochastic thermodynamics: principles and perspectives. *The European Physical Journal B - Condensed Matter and Complex Systems*, 64(3):423–431, 08 2008.

[143] L. B. Shaw, R.K.P. Zia, and K. H. Lee. Totally asymmetric exclusion process with extended objects: A model for protein synthesis. *Phys. Rev. E*, 68(2):021910, Aug 2003.

[144] M. R. Shirts, E. Bair, G. Hooker, and V. S. Pande. Equilibrium free energies from nonequilibrium measurements using maximum-likelihood methods. *Phys. Rev. Lett.*, 91(14):140601, Oct 2003.

[145] T. Speck and U. Seifert. Distribution of work in isothermal nonequilibrium processes. *Phys. Rev. E*, 70(6):066112, Dec 2004.

[146] T. Speck and U. Seifert. Integral fluctuation theorem for the housekeeping heat. *Journal of Physics A: Mathematical and General*, 38(34):L581–L588, 2005.

[147] F. Spitzer. Interaction of markov processes. *Adv. in Math.*, 5(2):246 – 290, 1970.

[148] H. Spohn. Long range correlations for stochastic lattice gases in a non-equilibrium steady state. *Journal of Physics A Mathematical General*, 16:4275–4291, December 1983.

[149] K. E. P. Sugden and M. R. Evans. A dynamically extending exclusion process. *Journal of Statistical Mechanics: Theory and Experiment*, 2007(11):P11013, 2007.

[150] J. Tailleur, M. R. Evans, and Y. Kafri. Nonequilibrium phase transitions in the extraction of membrane tubes by molecular motors. *Phys. Rev. Lett.*, 102(11):118109, Mar 2009.

[151] U. Täuber. Scale invariance and dynamic phase transitions in diffusion-limited reactions. *Advances in Solid State Physics*, pages 19–53, 2003.

[152] J. Teifel and G. Mahler. Model studies on the quantum jarzynski relation. *Phys. Rev. E*, 76(5):051126, Nov 2007.

[153] C. Tietz, S. Schuler, T. Speck, U. Seifert, and J. Wrachtrup. Measurement of stochastic entropy production. *Physical Review Letters*, 97:050602, 2006.

[154] H. Touchette. The large deviation approach to statistical mechanics. *Physics Reports*, 478(1-3):1 – 69, 2009.

[155] E. H. Trepagnier, C. Jarzynski, F. Ritort, G. E. Crooks, C. J. Bustamante, and J. Liphardt. Experimental test of Hatano and Sasa's nonequilibrium steady-state equality. *Proceedings of the National Academy of Sciences of the United States of America*, 101(42):15038–15041, 2004.

[156] N. G. van Kampen. *Stochastic processes in physics and chemistry*. Amsterdam - New York - Oxford: North-Holland Publishing Company. XIV, 1981.

[157] P. Visco. Work fluctuations for a brownian particle between two thermostats. *Journal of Statistical Mechanics: Theory and Experiment*, 2006(06):P06006, 2006.

[158] J. Vollmer. Chaos, spatial extension, transport, and non-equilibrium thermodynamics. *Physics Reports*, 372(2):131 – 267, 2002.

[159] G. M. Wang, E. M. Sevick, Emil Mittag, Debra J. Searles, and Denis J. Evans. Experimental demonstration of violations of the second law of thermodynamics for small systems and short time scales. *Phys. Rev. Lett.*, 89(5):050601, Jul 2002.

[160] J.-S. Wang and R. H. Swendsen. Cluster monte carlo algorithms. *Physica A: Statistical and Theoretical Physics*, 167(3):565–579, 1990.

[161] R. Wanga, M. Liua, and R. Jiangb. Local inhomogeneity in two-lane asymmetric simple exclusion processes coupled with langmuir kinetics. *Physica A: Statistical Mechanics and its Applications*, 387(2-3):457–466, 2008.

[162] U. Wolff. Comparison between cluster monte carlo algorithms in the ising model. *Physics Letters B*, 228(3):379–382, 1989.

[163] R. K. P. Zia, E. F. Redish, and S. R. McKay. Making sense of the legendre transform. *American Journal of Physics*, 77(7):614–622, 2009.

[164] R. K. P. Zia and B. Schmittmann. A possible classification of nonequilibrium steady states. *Journal of Physics A: Mathematical and General*, 39(24):L407–L413, 2006.

[165] R. K. P. Zia and B. Schmittmann. Probability currents as principal characteristics in the statistical mechanics of non-equilibrium steady states. *Journal of Statistical Mechanics: Theory and Experiment*, 2007(07):P07012, 2007.

[166] D. M. Zuckerman and T. B. Woolf. Theory of a systematic computational error in free energy differences. *Phys. Rev. Lett.*, 89(18):180602, Oct 2002.

Appendix A

Numerical Algorithm

We discuss the numerical algorithm that was exploited in chapter 4 and 5. In chapter 4 the distributions for total entropy production in a steady state were evaluated. For short times all possible trajectories were individually generated and the corresponding change in entropy was recorded in a histogramm. The analog procedure was applied in chapter 5. The reaction rates were now changing of time. Nevertheless the complete set of possible trajectories, this time for a transient process, were analyzed one by one and the distribution was obtained. We discuss in the following the calculation of these probability distributions in the case of time dependent reaction rates. This includes the time independent case of chapter 4.
During the time dependent process one of the reaction rates r is varied from its initial value r_0 to the final value r_M in M time steps. In the case of a linear variation in time, intermediate reaction rates are calculated as $r_i = r_0 + \frac{i}{M}(r_M - r_i)$, $i = 0, \cdots M$. The definition of the observables ϕ requires the stationary probabilities for any value r_i. This is easily done by determining the unique eigenvector corresponding to the eigenvalue zero of the Liouville matrix by standard numerical routines [121] for every time step. We then need to generate all possible sequences of configurations (*paths* in configuration space) $\mathbf{X} = C_0 \longrightarrow C_1 \longrightarrow \cdots \longrightarrow C_{M-1} \longrightarrow C_M$, where only one reaction or diffusion takes place at every step. This allows us to enumerate all possible trajectories and to obtain an exact exponential relation between the forward and reversed processes. Starting form every possible initial configuration, we have to built up a tree structure to all the configurations that can be reached in M steps with non-zero probability. This is done recursively by a standard depth-first search algorithm that ends when we reach the M^{th} step. We now have to attach a probability to every one of these generated paths. For this we are multiplying the probability, $P_s(C_0, r_0)$, to select the initial configuration C_0 with the product of the M transition probabilities $\omega(C_i \longrightarrow C_{i+1}, r_{i+1})$:

$$P_F(\mathbf{X}) = P_s(C_0, r_0) \prod_{i=0}^{M-1} \omega(C_i \longrightarrow C_{i+1}, r_{i+1}) \ . \tag{A.1}$$

Having now determined every path and its probability, we need in addition the values of ϕ along these different paths, which we obtain through the equation

$$\widetilde{\phi}\,(\mathbf{X}) = \sum_{i=0}^{M-1} \left(\ln P_s(C_i, r_{i+1}) - \ln P_s(C_i, r_i)\right) \ , \tag{A.2}$$

where $P_s(C_i, r_i)$ is the stationary probability to find the configuration C_i at the value r_i of the rate r. Putting everything together, the probability distribution is finally obtained by summing over all trajectories, respecting the delta constraint, through the expression

$$P_F(\phi) = \sum_{\mathbf{X}} P_F\,(\mathbf{X})\ \delta\left(\widetilde{\phi}\,(\mathbf{X}) - \phi\right) \ . \tag{A.3}$$

In addition to this forward process we also study the reversed process where we start in the configuration C_M with the rate r_M before changing the reaction rate in M steps to its final value r_0. The probability distribution for this process is

$$P_R(\phi) = \sum_{\mathbf{X}} P_R\,(\mathbf{X})\ \delta\left(\widetilde{\phi}\,(\mathbf{X}) - \phi\right) \tag{A.4}$$

with

$$P_R\,(\mathbf{X}) = P_s(C_M, r_M) \prod_{i=0}^{M-1} \omega(C_{M-i} \longrightarrow C_{M-i-1}, r_{M-i-1}) \ . \tag{A.5}$$

In chapter 5 we discuss not only the quantity ϕ but also the quantity R defined by Eq. (5.4). For this second quantity the procedure is exactly the same, only the calculation of the values of ϕ for the different paths has to be replaced by the values of R. This numerical exact approach is limited to small system sizes N and few time steps M, as the number of paths grows exponentially with both N and M, see figure A. For example, for $N = 6$ the number of paths increases from 404 for $M = 2$ to $8.6 \cdot 10^8$ for $M = 9$. As an alternative, one can study larger systems with more steps through Monte Carlo simulations, which, however, does yield rather noisy data. In order to discuss the probability distributions obtained from Monte Carlo simulations, we compare in figure A.2 the exact results and the results obtained from simulation both for the probability distribution, figure A.2(left), and the corresponding fluctuation ratio, figure A.2(right). For model 3 the distributions are overlapping. In contrast the fluctuation ratio shows deviations for the extreme values of R that correspond to very unlikely events. The magnitude of the deviations are of comparable size as for model 2 in the case of the observable ϕ, see figure 5.7. This fact would have hidden the observation of scattered points around the exponential that were due to non-equilibrium currents and are a result of the exact calculations. For that reason we are relying in the discussion of fluctuation ratios on the numerical exact results.

We want to address one more fact about the generation of trajectories. As we outlined, we assume that in every time step one transition occurs. The external parameter is varied in discrete time steps, and therefore only contributions to the observable ϕ enter if the reaction

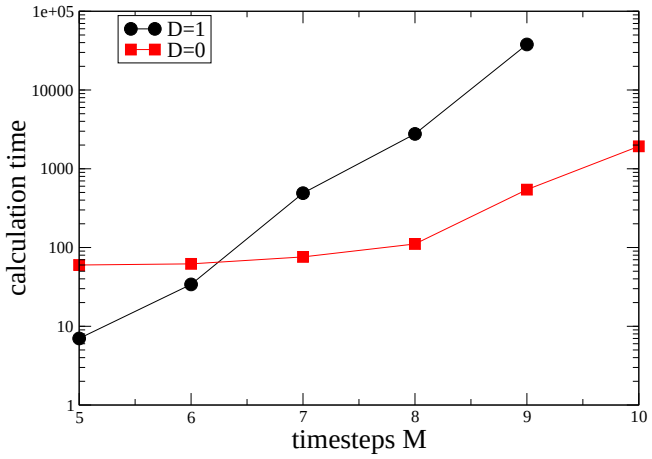

Figure A.1: Exponential growth of the calculation time in function of the number of steps for model 1, see chapter 3, with $N = 6$ sites where the creation rate h was changed between $h_0 = 0.2$ and $h_M = 1.4$. For this calculation we set $\lambda = 1.0$ and considered both vanishing ($D = 0$) and non-vanishing ($D = 1$) diffusion rates.

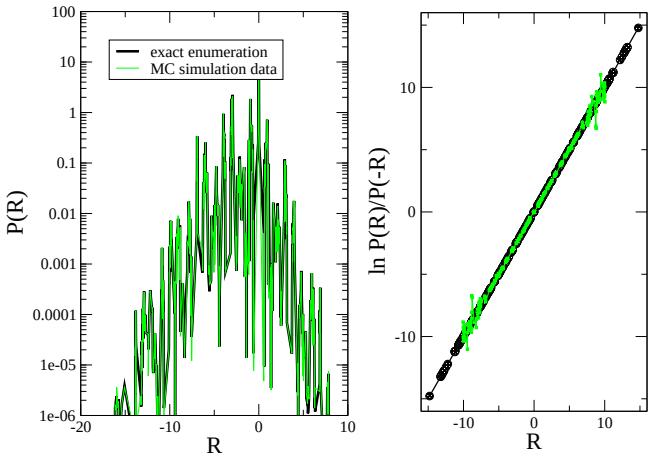

Figure A.2: Comparison of the numerical results obtained by exact enumeration and Monte Carlo simulations. The calculation is done for model 3, see chapter 3, with $N = 6$ sites where the creation rate h is kept constant for $M = 6$ time steps. For this calculation we set $\lambda = 1.0$ and $D = 5$.

rates are changing in time. The kinetic Monte Carlo algorithm that could be used as an alternative in this analysis would produce a larger number of trajectories that would vary in the number of configurations that were visited [15, 60, 120]. Since an exact enumeration would not be possible we choose to work with an exact enumeration scheme.